

**University of Alberta**

**Study of Polymer Adhesion Using Atomic Force Microscopy**

by

**Seung-ju Park**



A thesis submitted to the Faculty of Graduate Studies and Research in partial  
fulfillment of the requirements for the degree of  
Master of Science

in

Chemical Engineering

Department of Chemical & Materials Engineering

Edmonton, Alberta  
Fall 2005



Library and  
Archives Canada

Bibliothèque et  
Archives Canada

Published Heritage  
Branch

Direction du  
Patrimoine de l'édition

395 Wellington Street  
Ottawa ON K1A 0N4  
Canada

395, rue Wellington  
Ottawa ON K1A 0N4  
Canada

*Your file* *Votre référence*

*ISBN: 0-494-09256-4*

*Our file* *Notre référence*

*ISBN: 0-494-09256-4*

#### NOTICE:

The author has granted a non-exclusive license allowing Library and Archives Canada to reproduce, publish, archive, preserve, conserve, communicate to the public by telecommunication or on the Internet, loan, distribute and sell theses worldwide, for commercial or non-commercial purposes, in microform, paper, electronic and/or any other formats.

The author retains copyright ownership and moral rights in this thesis. Neither the thesis nor substantial extracts from it may be printed or otherwise reproduced without the author's permission.

#### AVIS:

L'auteur a accordé une licence non exclusive permettant à la Bibliothèque et Archives Canada de reproduire, publier, archiver, sauvegarder, conserver, transmettre au public par télécommunication ou par l'Internet, prêter, distribuer et vendre des thèses partout dans le monde, à des fins commerciales ou autres, sur support microforme, papier, électronique et/ou autres formats.

L'auteur conserve la propriété du droit d'auteur et des droits moraux qui protègent cette thèse. Ni la thèse ni des extraits substantiels de celle-ci ne doivent être imprimés ou autrement reproduits sans son autorisation.

---

In compliance with the Canadian Privacy Act some supporting forms may have been removed from this thesis.

Conformément à la loi canadienne sur la protection de la vie privée, quelques formulaires secondaires ont été enlevés de cette thèse.

While these forms may be included in the document page count, their removal does not represent any loss of content from the thesis.

Bien que ces formulaires aient inclus dans la pagination, il n'y aura aucun contenu manquant.

  
**Canada**

# University of Alberta

## Library Release Form

**Name of Author:** Seung-ju Park

**Title of Thesis:** Study of Polymer Adhesion Using Atomic Force Microscopy

**Degree:** Master of Science

**Year this Degree Granted:** 2005

Permission is hereby granted to the University of Alberta Library to reproduce single copies of this thesis and to lend or sell such copies for private, scholarly or scientific research purpose only.

The author reserves all other publication and other rights in association with the copyright in the thesis, and except as herein before provided, neither the thesis nor any substantial portion thereof may be printed or otherwise reproduced in any material form whatsoever without the author's prior written permission.

---

*Signature*

## ABSTRACT

Polymer blends are being used in an increasingly wider range of applications in industry. It is required to understand the surface characteristics of polymers with emphasis on polymer adhesion because most applications of polymer blends depend on the critical interactions at the interface between homopolymers in the blend.

The DCB test was performed for measurement of interfacial fracture energy between two kinds of polymer-polymer systems. In PS/PMMA system, fracture energy was found to be 12-13 J/m<sup>2</sup>. The interfacial fracture energy of PS/PP system was zero due to a large difference in thermal expansion coefficient. Another measurement for determining adhesion force between polymer particle and polymer surface were carried out using atomic force microscope (AFM). We found normalized pull-off forces in a range of 21-48 mN/m for the PP/PS system and 34-43 mN/m for PS/PMMA system. In last, the effect of interfacial adhesion on impact property of polymer blend was studied.

## ACKNOWLEDGEMENT

First, I would like to express my sincere gratitude and appreciation to my two supervisors, Prof. Uttandaraman Sundararaj and Prof. Zhenghe Xu, for their support, encouragement and academic guidance through the course of this thesis.

I would like to acknowledge Dr. Jianjun Liu and Dr. Liyan Zhang for teaching experimental techniques used in Atomic Force Microscope (AFM) and for helping my research work using AFM in Chapter 4. I would like to thank Dr. Hongbin Chen, who helped me in operating the twin-screw extruder for polymer blends preparation in Chapter 5. My thanks also go to Dr. Bin Lin and Mr. Baoliang Shi for SEM and TEM sample preparation and SEM and TEM images analysis with helpful discussions. Particularly, I owe much appreciation to Dr. Bin Lin for her assistances and suggestions in most experiments of this thesis. I would also like to thank my colleagues in polymer processing group who gave me personal and academic helping during my research.

I have also been helped tremendously from many people outside our department. I would like to thank Dr. Pean-Yue Ben Jar and Dr. Takashi Kuboki in the Dept. of Mechanical Engineering, who helped me in performing the drop-weight impact test in Chapter 5. My thanks are extended to Dr. Daniel Y. Kwok for providing me the opportunity to use the spectroscopic ellipsometer. I would also like to appreciate Ms. Stephanie Bozic in the NanoFab for teaching and allowing me to use the Profilometer. I am grateful to Dr. Dong-Chan Lee in the Dept. of Earth and Atmospheric Sciences for helping me in obtaining SEM images in Chapter 4 and 5. I am also grateful to Mr. Randy Mandryk in the Dept. of Biological Sciences, who assisted me in using the microtome.

I acknowledge with gratitude my thesis committee members: Dr. Anthony Yeung and Dr. Pean-Yue Ben Jar for their criticism, advice and comments in reviewing my thesis.

Finally, I would like to thank my family and friends for their unconditional encouragement, support and love throughout my life.

## TABLE OF CONTENTS

<b>Chapter 1</b>	<b>Introduction</b>	<b>1</b>
1.1	General	1
1.2	Objective	3
<b>Chapter 2</b>	<b>Literature Review</b>	<b>7</b>
2.1	Introduction	7
2.2	Polymer Adhesion	7
2.2.1	Surface and Interfacial Energy	10
2.2.1.1	Surface Energy and Surface Tension	10
2.2.1.2	Interfacial Tension: Classical Thermodynamics of Interface	12
2.2.2	Work of Adhesion and Wettability	14
2.2.2.1	Dispersion Interactions (Non-Polar system)	17
2.2.2.2	Non-dispersion Interactions (Polar system)	18
2.2.3	Mechanism of Adhesion	19
2.2.3.1	Mechanical Interlocking	21
2.2.3.2	Adsorption	22
2.2.3.3	Chemical Bonding Theory	23
2.2.3.4	Electrostatic Theory	23
2.2.3.5	Diffusion Theory	24
2.2.4	Polymer Particle-Surface Adhesion	25
2.2.4.1	Elastic Contact Mechanics	26
2.2.4.2	van der Waals Forces between Surfaces	31
<b>Chapter 3</b>	<b>The Double Cantilever Beam Test</b>	<b>37</b>
3.1	Introduction	37
3.2	Fracture Energy	38
3.2.1	Mechanical Properties of Polymer Interface	38

3.3	Experimental Procedure	46
3.3.1	DCB test	46
3.3.2	Sample Preparation	47
3.4	Results and Discussions	49
3.4.1	Fracture Energy of PS/PS and PS/PMMA	49
3.4.2	Temperature Dependence of $G_c$ of PS-PMMA Interface	51
3.4.3	Effect of Annealing Time on PS/PMMA Interface	53
3.4.4	Effect of Surface Roughness on PS/PMMA Interface	55
3.4.5	Contributions of Diblock Copolymer on Adhesion of PS/PMMA	56
3.5	Conclusions	58
<b>Chapter 4 Study of Polymer Adhesion Using Atomic Force Microscopy</b>		<b>63</b>
4.1	Introduction	63
4.2	Background	64
4.2.1	Atomic Force Microscopy	64
4.2.1.1	Contact Mode	66
4.2.1.2	Tapping Mode	67
4.2.1.3	Force-Distance Curve	68
4.2.2	Colloid Probe AFM	69
4.3	Experimental Procedure	72
4.3.1	Materials and Sample Preparation	72
4.3.2	Surface Imaging and Pull-off Force Measurements	75
4.4	Results and Discussions	77
4.4.1	Determination of Polymer Film Thickness	77
4.4.2	Distribution of Measured Pull-off Force	79
4.4.3	Determination of Surface Energy of Polymer Using AFM	83
4.4.3.1	Discrepancies in Adhesion Measurement	84



4.4.4	The Effect of Film Thickness on Pull-off Force of Polymers	85
4.4.4.1	T-test of Pull-off Force	87
4.4.5	The Effect of Surface Roughness on Pull-off Force of Polymers	87
4.4.5.1	Surface Roughness Analysis for Polymer Surfaces	89
4.4.5.2	Comparison of Measured Pull-off Forces to Rabinovich Model	90
4.5	Conclusions	93
<b>Chapter 5</b>	<b>Influence of Interfacial Adhesion on Impact Properties of Polymers</b>	<b>97</b>
5.1	Introduction	97
5.2	Toughened Polymers	98
5.3	Experiments	103
5.3.1	Materials and Blends Preparation	103
5.3.2	Impact Test	105
5.3.3	Analysis of Interfacial Adhesion	106
5.3.4	Scanning Electron Microscopy (SEM) and Images Analysis	107
5.3.5	Transmission Electron Microscopy	108
5.4	Results and Discussions	109
5.4.1	Morphology study of Polymer Blends	109
5.4.2	Mechanical Compatibilization of Polymer Blends	117
5.4.3.	Analysis of Particle Size and Interfacial Adhesion	117
5.4.3.1	Interfacial Adhesion	124
5.4.3.2	Effect of Particle Size on Impact Property in PS/PP Blends	126
5.5	Conclusions	129

<b>Chapter 6</b>	<b>Conclusions and Future Work</b>	<b>135</b>
6.1	General Conclusions	135
6.2	Future Work	139
6.2.1	Investigation of Effect of Molecular Weight on Polymer Adhesion	139
6.2.2	Measurement of Nanomechanical Properties of Polymer Surfaces Using AFM	139
6.2.3	The Effect of Different Compatibilizers on Interfacial Adhesion	140
6.2.4	Experimental Improvement	140
6.2.4.1	The Automated DCB Test	140
6.2.4.2	Improvement in Polymer Particles Preparation	141
6.2.4.3	Improvement for Accuracy in Film Thickness Measurement	142
6.2.4.4	Improvement in Specimen Preparation for Impact Test	142
Appendix I	Comparing Two Means of Measured Adhesion Forces	144
Appendix II	Saturation Concentration	148

## List of Tables

<b>Table 2-1</b>	Comparison between cohesive fracture energy $G$ and surface tension $\gamma$ for some materials	20
<b>Table 2-2</b>	van der Waals interaction free energies between bodies with different geometries.	33
<b>Table 3-1</b>	Polymers used in the DCB test	49
<b>Table 4-1</b>	Physical properties of used polymers in this study	75
<b>Table 4-2</b>	Thicknesses of polymer film measured by; first row: scratching method using AFM; second row: Alpha-step 200 Profiler.	79
<b>Table 4-3</b>	Surface energies of polymers determined by Pull-off force measurements and Literature values	84
<b>Table 5-1</b>	Properties of used polymers in this study	104
<b>Table 5-2</b>	The average values of impact test results for uncompatibilized PS/PP blends	118
<b>Table 5-3</b>	The average values of impact test results for compatibilized PS/PP blends	119
<b>Table 5-4</b>	The average values of impact test results for compatibilized PS/PP blends	120

## List of Figures

<b>Fig. 1-1</b>	Work of adhesion. For two identical media ( $1=2$ ), this work becomes the work of cohesion $W_{11}$ ]	2
<b>Fig. 1-2</b>	(a) The MultiMode Scanning Probe Microscope (SPM), (b) Silicon nitride probe, and (c) Silicon probe used in Atomic Force Microscopy. Cantilever lengths of probes are 100-200 $\mu\text{m}$	3
<b>Fig. 2-1</b>	Intermolecular net forces in the liquid in contact with the air	11
<b>Fig. 2-2</b>	A liquid drop at equilibrium on a solid surface	15
<b>Fig. 2-3</b>	A schematic diagram of mechanical interlocking	21
<b>Fig. 2-4</b>	A schematic diagram of interdiffusion across the interface	25
<b>Fig. 2-5</b>	Geometry of a contact between a rigid particle and compliant substrate (a) and a compliant particle and a rigid substrate (b)	26
<b>Fig. 2-6</b>	Schematic of the formation of a neck between the particle and surface in the JKR theory	30
<b>Fig. 3-1</b>	Three basic fracture modes; (a) Opening mode, (b) Sliding mode, and (c) Tearing	39
<b>Fig. 3-2</b>	Schematic of the DCB fracture test	42
<b>Fig. 3-3</b>	Failure of the PS/PMMA interface by the phenomenon of crazing	43
<b>Fig. 3-4</b>	$G_c$ of PS/PMMA samples with different beam thicknesses at 120 $^{\circ}\text{C}$ for 1hr	50
<b>Fig. 3-5</b>	$G_c$ of PS/PMMA samples annealed at four different temperatures between 100 and 130 $^{\circ}\text{C}$ for 1hr	52
<b>Fig. 3-6</b>	$G_c$ of PS/PMMA samples annealed for different times at the fixed temperature 120 $^{\circ}\text{C}$	54
<b>Fig. 3-7</b>	Comparison $G_c$ of PS/PMMA samples annealed at temperature 120 $^{\circ}\text{C}$ between pre-treated surfaces using sand paper and silicon wafer	55

<b>Fig. 3-8</b>	Fracture energy ratio of the modified PS/PMMA interface over the unmodified interface at the fixed temperature 120°C for 1hr.	57
<b>Fig. 4-1</b>	A basic schematic of AFM; Feedback loop maintains a constant deflection between the cantilever and the sample or a constant oscillation amplitude of the cantilever	65
<b>Fig.4-2</b>	The force-distance curve and different regimes of the tip-surface contact: A: Jump-in contact (contact repulsive mode), B: Loading part (force modulation mode), C: Attrition (contact attraction mode). D: Pull-off point (adhesion), E: Dynamic, non-contact mode; F: Maximum loading, the indentation point	68
<b>Fig. 4-3</b>	The interaction force $F_i = F_s + F_d$ is a sum of many interactions, where $F_s$ is the surface force and $F_d$ is the sample deformation. The interaction force is balanced by force $F_c$	70
<b>Fig. 4-4</b>	Alberta Polymer Asymmetric Minimixer (APAM)	73
<b>Fig. 4-5</b>	(a) SEM micrographs of morphology of PP/PS (20/80 wt. %) blend, (b) PP particle obtained from the solution of PP/C <sub>6</sub> H <sub>4</sub> (CH <sub>3</sub> ) <sub>2</sub> , (c) A SEM micrograph of isolated PP particles using the syringe driven filter & (d) A picture of the filter surface using the Zeiss optical microscope	74
<b>Fig. 4-6</b>	SEM images of polymer particles on the AFM cantilever glued by epoxy glue a) PP particle (R=5μm) & b) PS particle (R=2.75μm)	76
<b>Fig. 4-7</b>	Fig. 4-8. Image of the scratch and its cross-section of PS film from 0.2 wt.-% solution. The average film thickness is 14.1nm.	78
<b>Fig. 4-8</b>	Variation of thickness of the PS and PMMA films with concentration of cast solution. The film thickness increases with concentration.	78
<b>Fig. 4-9</b>	Cumulative distribution versus pull-off force of Polymer particle-surface (a) a PP particle on the PS surface (b) a PS particle on the PMMA surface	81
<b>Fig. 4-10</b>	Pull-off force vs. applied loading force during contact between a PP particle and the PS surface (b) a PS particle and the PMMA surface (◇ 0.2 wt.%; □ 0.5 wt.%; △ 0.8 wt.%; × 1 wt.%; ○ 2wt.%)	82

<b>Fig. 4-11</b>	Graph of the normalized pull-off force versus film thickness	86
<b>Fig. 4-12</b>	A surface roughness profile of PS film with about 230 nm thickness; in all polymer films used in this study, the parameters of $rms_1$ and $\lambda_1$ can be regarded as zero. (Height data scale: 10 nm)	90
<b>Fig. 4-13</b>	Comparison of measured pull-off forces with values predicted by the modified Rumpf model and the Rabinovich model. The surface roughness affects the dramatic decrease.	91
<b>Fig. 5-1</b>	Structure of poly(styrene)-block-poly(ethylene-butylene)-block-poly(styrene) (SEBS). The polymer used in this work contains 30% of PS and 70 % of PEB copolymer	101
<b>Fig. 5-2</b>	Free radical reaction in polystyrene and vinyl acetate group. The phenyl group releases the electrons and the vinyl acetate group withdraws the electrons.	101
<b>Fig. 5-3</b>	Drop weight impact tester	102
<b>Fig. 5-4</b>	Morphology of PS/PP blends with different weight ratios. (a) 50/50, (b) 70/30, (c) 80/20, (d) 90/10 PS/PP blends	111
<b>Fig. 5-5</b>	Morphology of PS/PP blends with addition of 6.7% wt.% SEBS as a compatibilizer (a) 50/50, (b) 70/30, (c) 80/20, (d) 90/10 PS/PP blends	111
<b>Fig. 5-6</b>	The enlarged micrographs of PS/PP blends with addition of 6.7% wt.% SEBS (a) 50/50, (b) 70/30, (c) 80/20, (d) 90/10 PS/PP blends. The dispersed PP particles connected to the matrix PS are observed in circles.	112
<b>Fig. 5-7</b>	Morphology of PS/PP (80/20) blend containing (a) 1 wt.% (b) 2 wt.% (c) 5 wt.% (d) 6.7 wt.% (e) 12.5 wt.% and (f) 17.6 wt.% of SEBS. The fibrils connecting the matrix and the dispersed particles, was observed in PS/PP blend with addition of 1 wt.% and 2 wt.% SEBS.	116
<b>Fig. 5-8</b>	Load-time trace for uncompatibilized PS/PP blends	118
<b>Fig. 5-9</b>	Load-time trace for compatibilized PS/PP blends	119
<b>Fig. 5-10</b>	Load-time trace for PS/PP blends with addition of different concentrations of SEBS	120

<b>Fig. 5-11</b>	Comparison of the absorbed impact energy between compatibilized and uncompatibilized PS/PP blends. The impact property is improved by the reduction of particle size and the interface modification.	122
<b>Fig. 5-12</b>	Comparison of the absorbed impact energy as a function of SEBS content. The impact property is improved by the increase of interfacial adhesion and the dispersion of excessive compatibilizer in the bulk polymer.	124
<b>Fig. 5-13</b>	(a) Height image of 124 nm thickness PS film (b) Height image of PS film covered by a SEBS layer (scan size: 10 $\mu\text{m}$ $\times$ 10 $\mu\text{m}$ , and data scale: (a) 10 nm and (b) 50 nm)	125
<b>Fig. 5-14</b>	Pull-off force vs. applied loading force between a PP particle and the PS surface. ( $\diamond$ : 124 nm thickness PS film with a SEBS layer; $\square$ : 226 nm thickness PS film with a SEBS layer; $\circ$ : 226 nm thickness PS film; $\triangle$ : 124 nm thickness PS film)	126
<b>Fig. 5-15</b>	(a) Number average diameter and (b) Polydispersity of PP particle with different blend compositions. The block copolymer (SEBS) used has a molecular weight of 75,000 g/mol.	127
<b>Fig. 5-16</b>	Dependence of the dispersed PP particle size for PS/PP (80/20) blend as a function of the wt.% of SEBS	128

# CHAPTER 1

## Introduction

### 1.1 General

A polymer is a chemical compound of a large molecule made of many smaller repeating units of monomer. Polymers include plastics, thermosets, and rubbers. The use of polymeric materials is increasing rapidly and they are replacing conventional materials such as metals, wood, and natural fibers in many applications.

In today's polymer industry, pure polymers have limited use. In general, a variety of products are made by combining or blending two or more polymers. Blending two or more polymers is a widely accepted method for producing new materials because it can provide a new material having better properties than its components. Nevertheless, most polymers are inherently incompatible with each other and each component in a blend exists in its own phase. Consequently, there is an interface between the phases. The properties of the materials are influenced by the interactions at the interface between the polymers. These interactions are attributed to the nature of mechanical, chemical, and electrostatic forces. The strength of the contact interactions is termed of "*adhesion*".

As for adhesion, Israelachvili stated that adhesion is defined as the free energy change, or reversible work done to separate unit areas of two media from contact to infinity in vacuum [1]. This definition emphasizes on the thermodynamic reversibility and intermolecular interactions at interfaces. On the other hand, Wu defines adhesion as the state in which two dissimilar bodies are held together by intimate interfacial contact such that mechanical force or work can be transferred across interface [2]. This definition



indicates that practical adhesion (experimental adhesion) is determined not only by the interfacial interactions, but also by the mechanical strength of interfacial zone or the bulk phases.

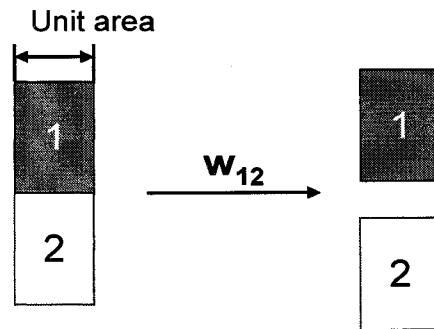


**Fig. 1-1.** Work of adhesion. For two identical media ( $1=2$ ), this work becomes the work of cohesion  $W_{11}$  [1].

Adhesion is a very complex concept, involving several mechanisms governed simultaneously by chemical and mechanical properties. In spite of a number of studies on polymer adhesion, fundamental knowledge of adhesion is still lacking. This is because adhesion embraces a large number of phenomena, which can vary depending on whether the phenomenon is observed at molecular or macroscopic level in nature. Thus, study of polymer adhesion is multidisciplinary in nature and requires understanding aspects of surface chemistry, surface physics, fracture mechanisms, strength of materials, polymer chemistry, and rheology.

Direct measurement of adhesion force between polymer surfaces or polymer particle-polymer surface has been reported. Surface energy and surface properties play an importantly critical role in polymer adhesion. Thus, a precise surface characterization is required for developing proper polymer blends of desired properties. Atomic Force Microscopy (AFM) was introduced by Binnig et al. in 1986 [3]. AFM is a new

experimental technique for the investigation of surface phenomena and properties on the micron or nanometer scale. The widespread utilization of AFM is due to its ease of use, the molecular-level information that it provides, and the variety of surfaces that can be studied in various environments. The first AFM images of polymeric materials were published in 1988-1991 by Patil et al., Drake et al., and Stocker et al. [4, 5, 6]. Since then, this emerging new technique has been of a great interest and an attraction. In addition, the most important advantage of using AFM is that it can directly measure the interactions (the adhesion force) between a sample surface and a colloidal particle. The use of AFM to study adhesion and mechanics of polymer surfaces was first reported by Meyers et al. [7]. AFM is now widely been used to study polymer adhesion.

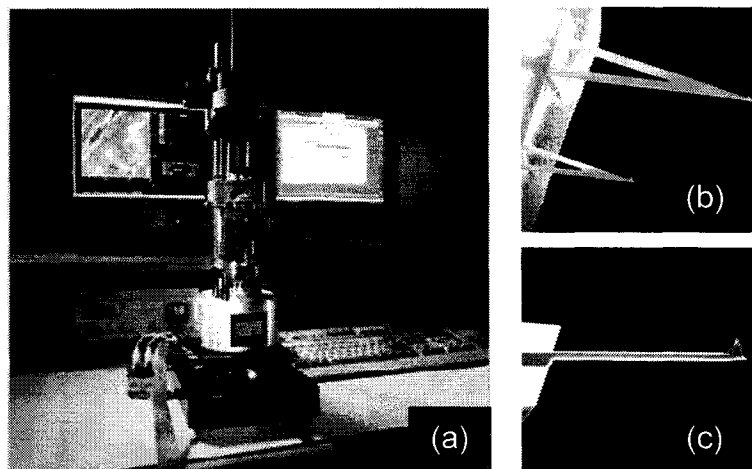


**Fig. 1-2.** (a) The MultiMode Scanning Probe Microscope (SPM), (b) Silicon nitride probe, and (c) Silicon probe used in Atomic Force Microscopy. Cantilever lengths of probes are 100-200  $\mu\text{m}$  [8]

## 1.2 Objective

The aim of this thesis is to review the current understanding of polymer adhesion and study the adhesion at the interface in a polymer-polymer system. Most applications of polymer blends depend on the compatibility and interfacial adhesion between the

components in the blend. With conventional mechanical tests, adhesion has been evaluated using the strain energy released by the failure of the interface. These tests are not suitable to properly determine intrinsic polymer adhesion at the interface; especially when considering the interfacial adhesion of polymer blends. Thus, our interests in this study are:

- (i) To measure polymer adhesion using a newly developed technique (pull-off force measurement using atomic force microscopy), which is more acceptable for interfacial adhesion in polymer blends
- (ii) To compare the results obtained using AFM with interfacial fracture energy measured by a mechanical test (double cantilever beam test).
- (iii) To establish the relation between the interfacial adhesion and mechanical properties, particularly impact strength in polymer blends.

The organization of the thesis is as follows: Chapter 2 reviews the nature of interactions, the mechanism of adhesion, and polymer adhesion. In chapter 3, the double cantilever beam (DCB) test is performed to study the interfacial fracture energy in a polymer-polymer system. Chapter 4 shows the measurement of polymer adhesion using atomic force microscopy (AFM). Chapter 5 describes the effect of interfacial adhesion on the mechanical properties of polymers. In chapter 6, conclusions are shown and future works are proposed. Chapters 3, 4, and 5 have its own literature survey for that particular area.

The first mechanical fracture energy test that will be studied is the DCB test since there is an abundance of literatures on this subject. The DCB test is well adapted for measurement of interfacial fracture energy between two solid polymer pairs. It is based

on a balance between the stored elastic energy in a beam and the energy necessary to propagate a crack at the interface between the two polymers. The test consists of creating an initial crack by inserting a razor blade, and then following the propagation of the crack with time [9]. The driving force for the propagation of crack results primarily from the stiffness of the beams separated by the razor blade and this driving force decreases as the crack propagates. A more detailed discussion on this subject is given in Chapter 3.

To study interfacial interactions of polymers, polymer particle-polymer surface interactions are measured with AFM, which enables measurement the adhesion force at micron level. The values of work of adhesion determined by the pull-off force measurement are compared with those calculated by elastic contact theories. More details and experimental results are given in Chapter 4.

Impact strength is one of the most important mechanical properties of polymer blends since it determines the utility of these materials. It is generally believed that the effect of interfacial adhesion between the dispersed particles and the matrix on the impact strength has been of great interest over last decades. For a constant interfacial adhesion, it has been widely reported that the impact strength is influenced by morphological parameters. The effects of the size, size distribution and volume fraction of dispersed particles on the impact strength of a blend have been studied. The results are presented in Chapter 5.

## **REFERENCE**

- [1] J. Israelachvili, *Intermolecular and Surface forces (2nd ed.)*, Academic Press: London (1992)
- [2] S. Wu, *Polymer interface and Adhesion*, Marcel Dekker: New York (1982)
- [3] G. Binnig, C. F. Quate, and C. Gerber, *Phys. Rev. Lett.*, **56**, pp 930-933 (1986)
- [4] R. Patil, S.J. Kim, E. Smith, D. H. Reneker, and A. L. Weishnhorn, *Polym. Comm.*, **31**, pp 455-457 (1990)
- [5] B. Drake, C. B. Prater, A. L. Weisenhorn, S. A. Gould, T. R. Albrecht, C. Quate, D. S. Cannell, H. G. Gansma, and P. K. Hansma, *Science*, **243**, pp 1586-1588 (1988)
- [6] W. Stocker, G. Bar, M. Kunz, M. Moller, S. N. Magonve, and H. J. Cantow, *Polym. Bull.*, **26**, pp 215-222 (1991)
- [7] G. F. Meyers, B. M. DeKoven, and J. T. Seitz, *Langmuir*, **9**, pp 2330-2335 (1992)
- [8] Retrieved April 10, 2005 from the website: [www.veeco.com](http://www.veeco.com)
- [9] J. G. Williams, *Polymer Eng. Sci.*, **17**, No.3, pp 144-149 (1977)

# CHAPTER 2

## Literature Review

### 2.1 Introduction

Polymers are being used in an increasingly wider range of applications in industry. A number of products are made by blending or joining two or more different polymers. Thus, it is required to understand the surface characteristics of polymers with emphasis on polymer adhesion because many critical interactions between the polymer and its environment occur at the surface or interface. In general, adhesion is a phenomenon that occurs due to the intermolecular forces (physical/chemical) between two materials that occur at the interface when atoms or molecules at both sides come in contact with each other. Such intermolecular forces result in the source of the surface energy or intrinsic adhesion. Adhesion strength is governed by the intrinsic adhesion from the intermolecular forces. However, when considering polymer adhesion it is important to recognize that the bulk mechanical properties of the polymer greatly influence interfacial forces required for adhesion. Therefore, to better understand the adhesion in polymers, it is required to study both the molecular level interactions that occur at the interface and the energy dissipation process that occur in the bulk materials adjacent to the interface.

### 2.2 Polymer Adhesion

Regarding the intrinsic adhesion in polymeric system, it is caused by any one or a combination of the following mechanisms [1]:

- (i) intermolecular forces such as van der Waals interactions
- (ii) interdiffusion and entanglement of polymer chains across the interface

(iii) formation of chemical bonds between molecules across the interfaces

In the absence of mechanisms (ii) and (iii), the intrinsic adhesion is given by the thermodynamic work of adhesion, which depends on the surface energies and the interfacial energy between the surfaces in contact. To date, there is little knowledge of the intrinsic adhesion energy because a direct experimental measurement of the intrinsic adhesion values is difficult to perform. Thus, most values reported are experimentally measured using a mechanical test. However, the experimental value determined using mechanical tests is usually greater than the calculated adhesion value, because the tests in most cases are carried out under conditions very far from thermodynamic reversibility.

A close or intimate contact at a molecular scale between both materials is needed for interfacial interactions to occur. Good wetting, i.e., well spreading of a material onto another, is necessary to obtain this close contact. In previous study, the thermodynamic work of adhesion was approached with wettability [2]. For adhesion between materials in contact, the formation of the interfacial interactions is due to different nature of forces such as van der Waals interactions, acid–base interactions, and/or others. More details of these forces will be reviewed later in this chapter.

For polymer adhesion, good wetting is first required for formation of physical interfacial interactions. For a system using an adhesive joint, a sufficiently low adhesive viscosity and sometimes the application of pressure on the joint are necessary to ensure good wetting. Furthermore, a high substrate roughness, i.e. a substance that contains more pores, holes, and other irregularities is an important factor that increases the interfacial strength.

The adhesion energy is also increased by formation of strong interfacial bonds, such as acid–base or chemical interactions, which are more energetic compared with van der Waals interactions. Acid–base interactions require the presence of polar sites (acidic or basic) on both materials in contact for high adhesion energy. In most previous studies where adhesion values between a polymeric adhesive and substrates were determined using a mechanical test, it has demonstrated that the formation of acid–base interactions includes the use of polar polymers (or polymer grafted with polar groups) and also polar substrates. Polarity of substrate can be increased by using surface treatments, leading to an oxidized surface (possibly also by grafting polar molecules onto the substrate surface). In addition, in some cases, the adhesive is able to exchange chemical (or covalent) bonds with the substrate, making a stronger interfacial bond. Polar groups such as carboxylic acid (or anhydride), amine, hydroxyle, epoxyde, isocyanate, and grafted polymer, copolymer, or monomer (directly polymerized on the substrate) are able to exchange chemical bonds with the reactive sites of the substrate surface [3]. Many mechanical tests have shown that there is a dramatic increase in the interfacial strength due to placing a grafted polymer or copolymer sheet between two bonding adherends.

Interdiffusion is also possible in polymer–polymer adhesion if chains interpenetration is able to occur from both phases at the interface. This phenomenon is called the interdiffusion theory of adhesion and occurs only if both polymers are compatible and their chains are sufficiently mobile. Consequently, interdiffusion leads to the formation of an interphase, and the properties of this interphase differs from the properties of bonding materials.



As mentioned earlier, the term of adhesion is ambiguous since it can be described in two manners:

- (i) The work of adhesion is thermodynamically defined as the free energy change or reversible work to separate phases 1 and 2 from contact to infinity. This is simply the only sum of all intermolecular interactions at the interface
- (ii) Experimental adhesion (practical adhesion) is measured by the energy required to break the bond formed between adhering phases.

In practice, therefore, both interfacial forces and mechanical properties of adhering phases in interfacial zone and in the bulk affect on the mechanical response of the bonding phases. If adhesion was the work needed for separation, the value would be close to the surface energies of materials in contact, which are typically  $10^{-2}$  to  $10^{-1}$  J/m<sup>2</sup>. However, practical work of separation can be 10 up to  $10^6$  greater than this. For this reason, it seems useful to know the basic aspects of adhesion at both the fundamental and practical levels; especially when considering polymer adhesion. The various theories of adhesion will be reviewed and the elastic contact mechanisms, which play an important role in polymer adhesion, will be also discussed.

## **2.2.1 Surface and Interfacial Energy**

### **2.2.1.1 Surface Energy and Surface Tension**

Surface energy is the free energy change  $\gamma$  when the surface area of a medium is increased by unit area [4]. The free energy change per unit area can be expressed in terms of the work,  $W_{11}$ , because the surface area of medium is separated into two half-unit areas from contact, so it becomes:

$$\gamma_1 = \frac{1}{2} W_{11} \quad (2.1)$$

For solids  $\gamma_1$  is usually denoted by  $\gamma_s$  and is given in units of energy per unit area:  $\text{mJ/m}^2$  ( $1\text{mJ/m}^2 = 1\text{erg/cm}^2$ ). For liquids,  $\gamma_1$  is usually denoted by  $\gamma_L$  and is given in units of tension per unit length:  $\text{mN/m}$  which is dimensionally the same as the surface free energy. As shown below in Fig. 2-1, in a system of a liquid in contact with a vapor such as air, the molecules of a liquid attract each other. An equal attractive force in all directions balances the interactions of a molecule in the bulk of a liquid. However, forces acting on molecules on the surface of a liquid are excessive.

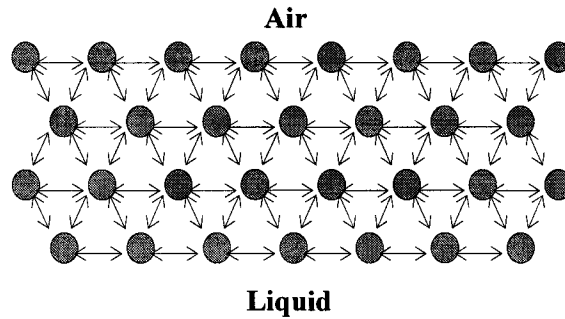


**Fig.2-1.** Intermolecular net forces in the liquid in contact with the air

The net effect of this situation causes free energy at the surface and this excess energy is called as surface free energy. This excess energy exists at the interface of two phases. If one of the phases is the vapor phase of a liquid being tested the measurement is referred to as surface tension. If the surface investigated is the interface of two liquids the measurement is referred to as interfacial tension.

Polar liquids, such as water, have strong intermolecular interactions and thus high surface tensions. Any factor that decreases the strength of this interaction will lower

surface tension. Thus an increase in the temperature of this system will lower surface tension. Any contamination, especially by surfactants, will lower surface tension as well.

### 2.2.1.2 Interfacial Tension: Classical Thermodynamics of Interface

The fundamental equations of interfacial thermodynamics are well explained in many standard texts. According to Wu [3], the interface is a region of finite thickness in which the composition and energy vary continuously from one bulk phase to the other. A net energy is required to create an interface by transporting the matter from the bulk phase to the interfacial zone. The reversible work required to create a unit interfacial or surface area is the interfacial or surface tension and given by:

$$\gamma = \left( \frac{\partial G}{\partial A} \right)_{T,P,n} \quad (2.2)$$

where  $\gamma$  is the interfacial tension,  $G$  is the Gibbs free energy of the total system,  $A$  is the interfacial area,  $T$  is the temperature,  $P$  is the pressure, and  $n$  is the total number moles of material in the system. If there are two homogeneous bulk phases  $\alpha$  and  $\beta$  separated by an interfacial zone  $\sigma$  of thickness  $t$ , the chemical potential of two components (1 and 2) at equilibrium will be:

$$\mu_1^\alpha = \mu_1^\beta = \mu_1^\sigma = \mu_1 \quad (2.3)$$

$$\mu_2^\alpha = \mu_2^\beta = \mu_2^\sigma = \mu_2 \quad (2.4)$$

where  $\mu$  is the chemical potential. The thermodynamic derivations of the Gibbs free energy are then given by:

$$dG^i = -S^i dT + V^i dP + \mu_1 dn_1^i + \mu_2 dn_2^i \quad (2.5)$$

$$dG^\sigma = -S^\sigma dT + V^\sigma dP + \mu_1 dn_1^\sigma + \mu_2 dn_2^\sigma + \gamma dA \quad (2.6)$$

where S is the entropy, V is the volume, n is the number of moles of substances, and i is  $\alpha$  or  $\beta$ . Integrating equation (2.5) and (2.6), we obtain:

$$G^i = n_1^i \mu_1 + n_2^i \mu_2 \quad (2.7)$$

$$G^\sigma = n_1^\sigma \mu_1 + n_2^\sigma \mu_2 + \gamma A \quad (2.8)$$

After dividing equation (2.6) by unit area A, we obtain:

$$f^\sigma = \gamma + \Gamma_1 \mu_1 + \Gamma_2 \mu_2 \quad (2.9)$$

where  $f^\sigma = G^\sigma / A$  is the specific surface free energy and  $\Gamma = n^\sigma / A$  is the surface concentration. Therefore, surface tension  $\gamma$  is the excess specific surface free energy, and it is distinct from the specific surface free energy as we discussed above section. After subtracting equation (2.6) from the total differential of equation (2.8), we obtain the Gibbs-Duhem equation.

$$S^\sigma dT - V^\sigma dP + n_1^\sigma d\mu_1 + n_2^\sigma d\mu_2 + A d\gamma = 0 \quad (2.10)$$

Moreover, dividing equation (2.10) by unit area A gives the well-known Gibbs adsorption equation:

$$\overline{S^\sigma} dT - tdP + \Gamma_1 d\mu_1 + \Gamma_2 d\mu_2 + d\gamma = 0 \quad (2.11)$$

where  $\overline{S^\sigma}$  is the surface entropy per unit surface area and  $t$  is the interface thickness.

### 2.2.2 Work of Adhesion and Wettability

When two phases are brought into contact with one another, in general there is adhesion between their surfaces. Thus Work of adhesion is defined as the free energy change, or reversible work done, to separate unit areas of two media 1 and 2 from contact to infinity  $W_{12}$  and is given by [4]:

$$W_{12} = \gamma_1 + \gamma_2 - \gamma_{12} \quad (2.12)$$

where  $\gamma_1$  and  $\gamma_2$  are the surface free energies of phases 1 and 2, respectively, and  $\gamma_{12}$  is the interfacial free energy between phases 1 and 2. As mentioned before, the work of adhesion is the decrease in Gibbs free energy per unit area when an interface is formed from two individual phases. Thus, the greater the interfacial attraction, the greater the work of adhesion and the smaller the interfacial free energy between phases 1 and 2 will be. Therefore,  $\gamma_{12}$  can be related to the properties of the two individual phases. In the case of identical media ( $1=2$ ), the energy is referred to the work of cohesion  $W_{11}$ . For a solid–liquid interface, phases 1 and 2 are commonly denoted phases S (solid) and L (liquid) so that the interfacial free energy between the liquid and the solid may be written as:

$$\gamma_{SL} = \gamma_S + \gamma_L - W_{SL} \quad (2.13)$$

Wetting may be quantitatively defined by reference to a liquid drop resting in equilibrium on a solid surface as shown Fig. 2-2 [5].

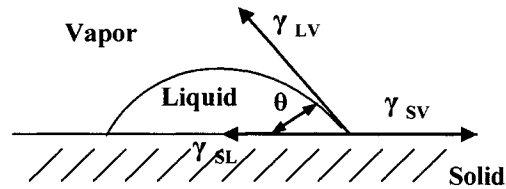


**Fig.2-2.** A liquid drop at equilibrium on a solid surface

The tensions at the three phase contact point are indicated such that LV is the liquid/vapor point, SL is solid/liquid point and SV is the solid/vapor point. Surface energies of phases and equilibrium contact angle  $\theta$  at the three-phase contact point are related by Young's equation:

$$\gamma_{SV} = \gamma_{SL} + \gamma_{LV} \cos \theta \quad (2.14)$$

Banghan and Razouk [6] define the concept of equilibrium spreading pressure,  $\pi_S$ , as:

$$\pi_S = \gamma_S - \gamma_{SV} = RT \int_0^P \Gamma d(\ln P) \quad (2.15)$$

where  $P$  is the vapor pressure,  $P_0$  is the equilibrium vapor pressure,  $R$  is the gas constant,  $T$  is the absolute temperature, and  $\Gamma$  is the surface concentration of the adsorbed vapor.

Equation (2.13) can be rewritten as:

$$\gamma_S = \gamma_{SL} + \gamma_{LV} \cos \theta + \pi_S \quad (2.6)$$

A good wetting occurs when the angle of contact ( $\theta$ ) between the liquid and the solid is less than  $90^\circ$ . Complete wetting occurs when the molecular attraction between the liquid and solid molecules is greater than that between similar liquid molecules. Thus wetting of a liquid on a solid depends on the surface tension of both substances, and spreading over the solid surface is affected by the liquid viscosity and solid surface roughness. For spontaneous wetting to occur:

$$\gamma_{SV} \geq \gamma_{SL} + \gamma_{LV} \quad (2.17)$$

or

$$\gamma_S \geq \gamma_{SL} + \gamma_{LV} + \pi_s \quad (2.18)$$

Neglecting the spreading pressure of the vapor phase of the liquid onto the solid and using the Young-Duprè equation, the solid-liquid work of adhesion becomes:

$$W_{SL} = \gamma_S + \gamma_{LV} - \gamma_{SL} = \gamma_{LV}(1 + \cos\theta) \quad (2.19)$$

To study the nature of interactions at the interface of two materials, Fowkes [7] first proposed that the surface free energy of a component,  $\gamma$ , could be given by the sum of the contributions from different types of force components. In previous studies [7-8], surface free energies and work of adhesion may generally be expressed by the sum of two terms: the first one representative of London's dispersion interactions (superscript D) and the second representative of nondispersion forces (superscript ND), which includes Debye and Keesom dipolar interactions and acid-base interactions. As it has been demonstrated previously, there are three distinct contributions of force for the total long-range interaction between polar molecules, collectively known as the van der Waals force:

these are non-polar dispersion forces (London dispersion forces), dipole-dipole interactions (Keesom interactions), dipole-induced dipole interactions (Debye interactions).

$$\gamma = \gamma^D + \gamma^{ND} \text{ and } W_{12} = W_{12}^D + W_{12}^{ND} \quad (2.20)$$

### 2.2.2.1 Dispersion Interactions (Non-Polar system)

For strictly non-polar system, the interaction between materials 1 and 2 in the medium 3 is mostly given by the following expression [7]:

$$\gamma_{12}^D = (\sqrt{\gamma_1^D} - \sqrt{\gamma_2^D})^2 \quad (2.21)$$

For solids,  $\gamma_S^D$  can be determined by using the contact angle ( $\theta$ ) with a nonpolar liquid of a known  $\gamma_L^D$ , using Young's equation:

$$(1 + \cos \theta) = 2\sqrt{\gamma_L^D / \gamma_S^D} \quad (2.22)$$

For liquids,  $\gamma_L^D$  can be obtained from the contact angle measurement on a known nonpolar solid, e.g., Teflon with  $\gamma_S^D \approx 18 \text{ mJ/m}^2$  according to following:

$$(1 + \cos \theta)\gamma_L = 2\sqrt{\gamma_L^D \gamma_S^D} \quad (2.23)$$

in which  $\gamma_L^D$  is equal to  $\gamma_L$  if the liquid is nonpolar or when there is no polar contribution to the surface free energy of the liquid.



### 2.2.2.2 Non-dispersion Interactions (Polar system)

It is known that interfacial interactions involve van der Waals forces and/or hydrogen bonds. Thus, non-dispersive interactions are of a polar nature. Polar interactions include electron-donor/electron-acceptor interactions (Lewis acid-base interactions). The electron-acceptor parameter of the surface tension of material 1 is expressed as  $\gamma_1^+$ , and the electron-donor parameter of its surface tension as  $\gamma_1^-$ . With these parameters, the surface tension of polar material can be approximately quantified as:

$$\gamma_1^{ND} \approx \gamma_1^{AB} = 2\sqrt{\gamma_1^+ \gamma_1^-} \quad (2.24)$$

with a monopolar material, either  $\gamma_1^-$  or  $\gamma_1^+$  is zero and the term of polar interaction  $\gamma_1^{AB}=0$ . The interfacial tension between phases 1 and 2 can be then obtained:

$$\gamma_{12}^{AB} = 2( \sqrt{\gamma_1^+ \gamma_1^-} + \sqrt{\gamma_2^+ \gamma_2^-} - \sqrt{\gamma_1^+ \gamma_2^-} - \sqrt{\gamma_1^- \gamma_2^+} ) \quad (2.25)$$

Consequently,  $\gamma_{12}^{AB}$  will be negative when  $\gamma_1^+ > \gamma_2^+$  and  $\gamma_1^- < \gamma_2^-$ , or when  $\gamma_1^+ < \gamma_2^+$  and  $\gamma_1^- > \gamma_2^-$ .

From equation (2.20), the total interfacial tension is given by the sum of two distinct contributions; dispersive interactions and non-dispersive interactions. Therefore, the total interfacial tension between phases 1 and 2 can be expressed as:

$$\gamma_{12} = (\sqrt{\gamma_1^D} - \sqrt{\gamma_2^D})^2 + 2( \sqrt{\gamma_1^+ \gamma_1^-} + \sqrt{\gamma_2^+ \gamma_2^-} - \sqrt{\gamma_1^+ \gamma_2^-} - \sqrt{\gamma_1^- \gamma_2^+} ) \quad (2.26)$$

Lastly, the total work of adhesion of polar phases 1 and 2 in polar medium 3 can be then quantified as:

$$W_{132}^{Total} = \gamma_{12}^D - \gamma_{13}^D - \gamma_{23}^D + 2 \left[ \sqrt{\gamma_3^-} \left( \sqrt{\gamma_1^-} + \sqrt{\gamma_2^-} - \sqrt{\gamma_3^-} \right) \right] + \left[ \sqrt{\gamma_3^-} \left( \sqrt{\gamma_1^+} + \sqrt{\gamma_2^+} - \sqrt{\gamma_3^+} \right) - \sqrt{\gamma_1^+ \gamma_2^-} - \sqrt{\gamma_1^- \gamma_2^+} \right] \quad (2.27)$$

and the complete Young equation is modified for polar systems as follows:

$$(1 + \cos \theta) \gamma_L = 2 \left( \sqrt{\gamma_S^D \gamma_S^D} + \sqrt{\gamma_S^+ \gamma_L^-} + \sqrt{\gamma_S^- \gamma_L^+} \right) \quad (2.28)$$

In the special case that only London dispersion forces are important across the interface, the work of adhesion is fully determined because the nondispersive part is equal to zero. Indeed,  $\gamma_1^D$  and  $\gamma_2^D$  can be easily determined by wettability experiments as mentioned earlier. Existence of only London interactions at the interface leads to:

$$G_c \text{ or } F_{ad} \propto W_{12}^D \quad (2.29)$$

where  $G_c$  is the fracture energy of two materials obtained using a mechanical test such as the Double Cantilever Beam test and  $F_{ad}$  is the adhesion force between surfaces in contact, which will be discussed in the pull-off force measurement using Atomic Force Microscopy. We will discuss more details in each subsequent chapter.

### 2.2.3 Mechanism of Adhesion

The mechanism of adhesion is still not completely understood and many studies have been done in order to better understand and analyze it. Among many of the studies, tests have been carried out by measuring strength of adhesive joints, although the methods are

not well suited to theoretical analysis for adhesion mechanism due to indeterminate effects from rheological energy losses in the adhesive and substrate, and other geometrical or loading factors. Therefore, other contributions to the measured values must be subtracted to obtain values of adhesion of adhesive joints.

**Table 2-1.** Comparison between cohesive fracture energy  $G$  and surface tension  $\gamma$  for some materials [3]

Material	$G/2, \text{ erg/cm}^2$	$\gamma, \text{ erg/cm}^2$
Poly (methyl methacrylate)	$2 \times 10^5$	41.1
Polystyrene	$7 \times 10^5$	40.7
Oligomeric polystyrene (MW~3000)	40	40.7
Steel	$1 \times 10^6$	2300

The bonding of an adhesive to a surface is the net effect of mechanical, physical and chemical forces involved. Thus, it is not possible to separate these forces from one another and several theories have been proposed to describe the fundamentals of adhesion. Presently, four main mechanisms are used to describe the involving mechanical, physical and chemical forces involved: (i) mechanical interlocking, caused by the mechanical anchoring of the adhesive in the pores and the uneven parts of the surface; (ii) electrostatic theory developed by Derjaguin on the occurrence of an electrical double layer at the interface between two materials; (iii) other adhesion mechanisms dealing with intermolecular and chemical bonding forces that occur at the interfaces of heterogeneous systems. The chemical adhesion mechanism is explained for the case of the intermolecular forces by the adsorption theory, and in the case of chemical interactions by the chemisorption theory; and (iv) the interdiffusion theory which only

applies to the bonding of polymers. In next sections, the four theories of adhesion are briefly reviewed.

### 2.2.3.1 Mechanical Interlocking

The mechanical interlocking theory of adhesion proposes that good adhesion occurs only when an adhesive penetrates into the pores, holes and other irregularities of the adhered surface of a substrate, and locks mechanically to the substrate. Moreover, the adhesive has to have the right rheological properties to penetrate pore or holes as well as wet on the substrate for better adhesion. In previous work, it was shown that a liquid adhesive placed on a rough substrate spontaneously penetrated into the pores by capillarity. However, it is not the only applicable adhesion mechanism because smooth surface brought into contact can also result in a good adhesion as well.

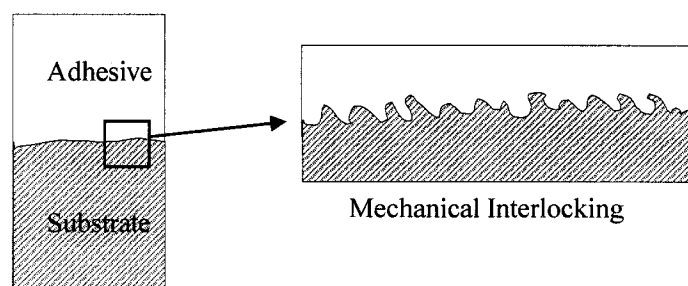


Fig.2-3. A schematic diagram of mechanical interlocking [10]

To find the relation of mechanical interlocking to adhesion, pretreatment methods applied on surfaces were used and it was determined whether or not they enhance adhesion [9]. These pretreatments resulted in microroughness on the surface, and the bond strength and durability are improved through mechanical interlocking provided by the surface roughness. Beyond mechanical interlocking, enhancement of the adhesive joint strength due to the roughness on the surface may also be attributed to other factors

such as formation of a larger surface, improved kinetics of wetting and increased plastic deformation of the adhesive [11].

### **2.2.3.2 Adsorption**

The adsorption theory proposes that adhesion results from intimate intermolecular contact between two materials and involves surface forces that develop between the atoms of the two surfaces.

This theory describes the most important mechanism in achieving adhesion [12]. In this theory, intrinsic adhesion forces are attributed to the surface forces that occur at the adhesive- adherend interface, which result from the variety of forces such as non-polar dispersion forces (London dispersion forces), dipole-dipole interactions (Keesom interactions), and dipole-induced dipole interactions (Debye interactions), which are all generally considered as van der Waals forces. According to Fowkes [5], the calculated attractive forces between two surfaces are significantly higher than the experimentally measured strength of adhesive joints, and this discrepancy between theoretical and experimental strength values is attributed to air voids, defects or other geometric irregularities that may cause stress concentrations during loading of the adhesive joint.

In addition, acid-base interactions and hydrogen bonds, generally considered a type of acid-base interaction, also contribute to intrinsic adhesion forces. A study [13] experimentally demonstrated that, due to acid-base interaction, dipole interactions do not contribute measurably to the enthalpies of molecular interactions, so the intrinsic adhesion forces are now considered to be from two contributions, dispersive and acid-base interactions. To obtain good adsorption, intimate contact is required such that van

der Waals interaction or the acid-base interaction or both occur, hence good wetting is necessary

### **2.2.3.3 Chemical Bonding Theory**

The chemical bonding mechanism proposes that primary chemical bonds may form across the interface. Although chemical bonding at the interface is difficult to detect, because of the thinness of the interface, it is strong and makes a significant contribution to the intrinsic adhesion in some cases. For example, primary chemical bonding has energies ranging between 60-1100 kJ/mol, which are considerably higher than the bond energies from hydrogen bonds of 0.08-5 kJ/mol [14]. In addition, a dramatic increase of the adhesive bond strength can occur due to small amounts (0.001-0.1 mole fraction) of appropriate reactive functional groups incorporated into polymer [3]. At such a low amounts, polymer bulk properties and wettability are generally unchanged and the effectiveness of functional groups in enhancing adhesion is quite specific with respect to surface chemical composition.

### **2.2.3.4 Electrostatic Theory**

The electrostatic attraction theory of adhesion developed by Derjaguin is based on the occurrence of an electrical double layer at the interface between the adherend of two materials. Due to the difference of electronegativities between two materials in contact, there is a transfer of electrons across the interface creating positive and negative charges that attract one another. For example, when an organic polymer is brought into contact with metal, electrons are transferred from metal into the polymer, creating an attracting electrical double layer (EDL).

However, there are three major controversies related to the electrostatic attraction theory [15]:

- (i) The electrostatic double layer can be identified only after separating the adhesive bond.
- (ii) Its effect on the adhesion forces is overconsidered.
- (iii) Overlapping between electrostatic and acceptor-donor interaction.

Since polymers are insulators, it seems difficult to apply electrostatic attraction theory to most adhesive joints involving polymer materials, but it is widely used for charged polymer particles that contact pieces to be coated in coating or painting industry.

#### **2.2.3.5 Diffusion Theory**

The diffusion theory attributes the adhesion of polymeric materials to the interpenetration of chains at the interface. This type of adhesion occurs when both materials are soluble and miscible in each other. Therefore, molecules from one material can cross into the other material at the interface. Solubility matching between two materials in contact is extremely important for good adhesive bonding. As a result, if the solubility parameters between the two materials are close to each other, interdiffusion occurs. To obtain adhesion by interdiffusion, two criteria are required as following [10]:

- (i) The adherend in contact must be mutually soluble and compatible
- (ii) Sufficient temperature is necessary for macromolecules to be mobile

Parameters affecting the diffusion phenomenon are contact time, bonding temperature, molecular weight of the polymers, physical form (liquid, solid), and so on. To describe the interdiffusion phenomenon of polymers, it was shown by Vasinen [16]

that the adhesion of polyisobutylene under a constant welding pressure is a function of temperature and contact time.

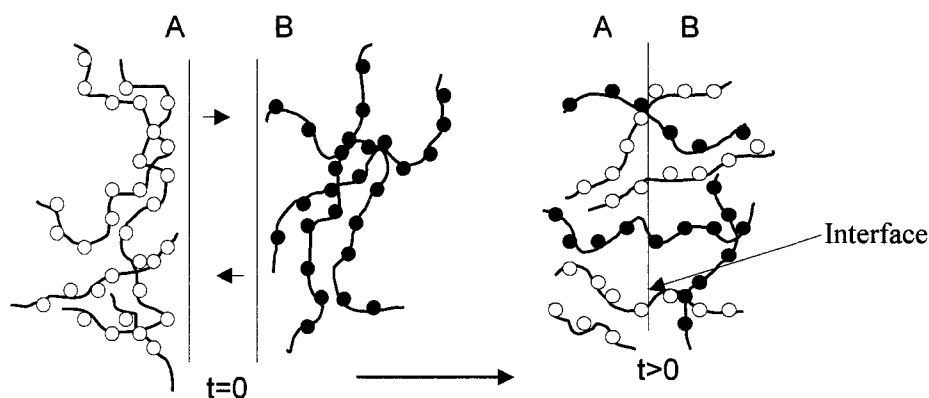


**Fig.2-4.** A schematic diagram of interdiffusion across the interface [10]

The average interpenetration depth,  $\chi$ , of one phase into another is expressed as:

$$\chi \propto \exp\left(\frac{-E}{2RT}\right)t^{1/2} \quad (2.30)$$

where  $E$  is the diffusion activation energy,  $t$  is the contact time,  $R$  is the molar gas constant, and  $T$  is the bonding temperature. In general diffusion theory is applicable when the above criteria are satisfied, so interdiffusion of entire macromolecules across the interface is unlikely to occur between incompatible polymers.

#### 2.2.4 Polymer Particle-Surface Adhesion

As mentioned in previous chapter, AFM has stimulated the study on the adhesion between two solid surfaces. In the pull-off force measurement using AFM, some elastic contact mechanics described the effect of elastic properties in polymeric materials are used to calculate the adhesion energy. The popular elastic contact theory is Johnson-



Kendall-Roberts (JKR) equation [17]. van der Waals forces play very important roles in phenomena involving adhesion forces. In this section, we review the elastic contact theories and van der Waals forces between surfaces.

#### 2.2.4.1 Elastic Contact Mechanics [18]

In order to understand the dependence of the contact radius and the force on the penetration depth, it is required to make some assumptions. In past years, several different theories of such phenomena have been developed to take in account the contact mechanics of a solid particle on surface. These theories are briefly explained below.

##### (i) Hertz Model

Hertz firstly proposed a model for mechanics of contact between a spherical body and a planar surface. [19] Hertz theory dates back to 1881 and it does not take into account either surface forces and adhesion. The geometry of the deformation would resemble that shown in Fig. 2-5a and 2-5b. The tip is considered as a smooth elastic sphere, while the sample is a rigid flat surface. The following equations summarize the relationships from the Hertz model:

$$F_{ad} = 0, \quad (2.31)$$

$$a = \left( \frac{RP}{K} \right)^{1/3}, \quad (2.32)$$

$$a_0 = 0, \quad (2.33)$$

$$\delta = \frac{a^2}{R} = \frac{F}{Ka}, \quad (2.34)$$

and

$$P(x) = \frac{3Ka\sqrt{1-x^2}}{2\pi R} = \frac{3F\sqrt{1-x^2}}{2\pi a^2} \quad (2.35)$$

in which  $F_{ad}$  is the pull-off force,  $P$  is the load applied to a particle normal to the plane of the surface,  $R$  is the radius of the particle,  $a$  is the radius of contact after deformation,  $a_0$  is the contact radius at zero load,  $\delta$  is the deformation of the spherical tip,  $x = y/a$  where  $y$  is distance from the center of the contact circle, and  $K$  is the elastic modulus for the particle-substrate system which is given by:

$$\frac{1}{K} = \frac{3}{4} \left( \frac{1-\nu^2}{E} + \frac{1-\nu_i^2}{E_i} \right) \quad (2.36)$$

In Equation (2.36),  $E, E_i, \nu$  and  $\nu_i$  are the Young modulus and the Poisson ratios of the flat surface sample, and of the tip or the particle on the tip.

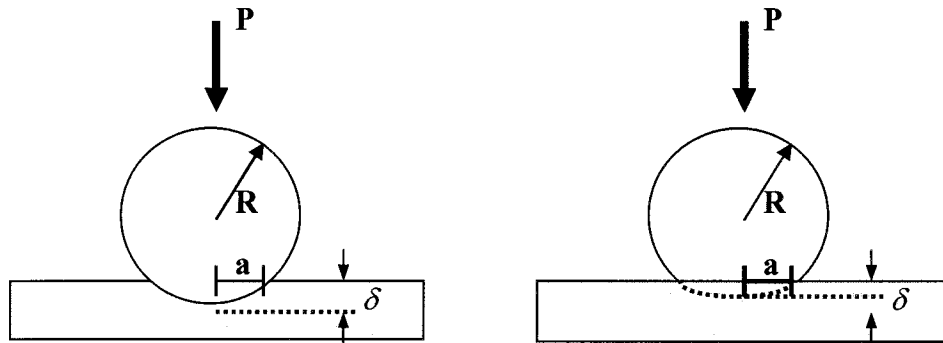


**Fig. 2-5.** Geometry of a contact between a rigid particle and compliant substrate (a) and a compliant particle and a rigid substrate (b) [18]

The Hertz theory is applicable to systems with very low surface forces and where high loads are applied to the particle. Tip and sample deformations can be simply

obtained without consideration of surface forces on the system. However, surface forces must be included in most AFM measurements of particle-surface adhesion. In this environment, one of three following theories has to be used.

(ii) Dejaquin-Müller-Toporov (DMT) Model

In Dejaquin-Müller-Toporov (DMT) theory [20] the elastic sphere is deformed according to Hertz theory, but additionally the theory includes surface forces in both the particle-surface contact area and just outside the contact region, and the external load  $F$  as well. If an external load is applied, the area of contact increases. If a negative load is applied, the contact area diminishes until it becomes zero. The equations describing the DMT model are as following:

$$F_{ad} = 2\pi RW, \quad (2.37)$$

$$a = \left( \frac{R}{K} (P + 2\pi RW) \right)^{1/3}, \quad (2.38)$$

$$a_0 = \left( \frac{R}{K} (2\pi RW) \right)^{1/3}, \quad (2.39)$$

$$\delta = \frac{a^2}{R}, \quad (2.40)$$

and

$$P(x) = \frac{3Ka\sqrt{1-x^2}}{2\pi R} = \frac{3F\sqrt{1-x^2}}{2\pi a^2} \quad (2.41)$$

where  $W$  is the work of adhesion. Other terms are the same as in the Hertz model.

The DMT theory has been well applied for systems with low surface forces and small tip or particle radii. Both the Hertz and DMT theories assume that there is no adhesion hysteresis during loading and unloading processes. This, however, is a physically unrealistic for many elastic systems. Thus other formulations of more complex models have been developed for elastic contact mechanics.

(iii) Johnson-Kendall-Roberts (JKR) Model

Johnson-Kendall-Roberts (JKR) theory [17] has been most widely applied to elastic contact mechanics. In JKR theory, it neglects long-range forces outside the contact area and considers only short-range forces inside the contact region. The equations describing the DMT model are as following:

$$F_{ad} = \frac{3}{2} \pi R W, \quad (2.42)$$

$$a = \left( \frac{R}{K} \left( P + 3\pi R W + \sqrt{6\pi R W P + (3\pi R W)^2} \right) \right)^{1/3}, \quad (2.43)$$

$$a_0 = \left( \frac{R}{K} (6\pi R W) \right)^{1/3}, \quad (2.44)$$

$$\delta = \frac{a^2}{R} - \frac{2}{3} \sqrt{\frac{6\pi W a}{R}}, \quad (2.45)$$

and

$$P(x) = \frac{3Ka\sqrt{1-x^2}}{2\pi R} - \sqrt{\frac{3KW}{2\pi a}} \frac{1}{\sqrt{1-x^2}} \quad (2.46)$$

The JKR model includes the hysteresis in that a neck links the tip and the surface during unloading, as shown in Fig. 2-6. The contact is abruptly ruptured at negative loads, and the contact radius has reduced to  $a_s = 0.63a_0$  when separation takes place;  $a_s$  is the radius of the contact area at separation.

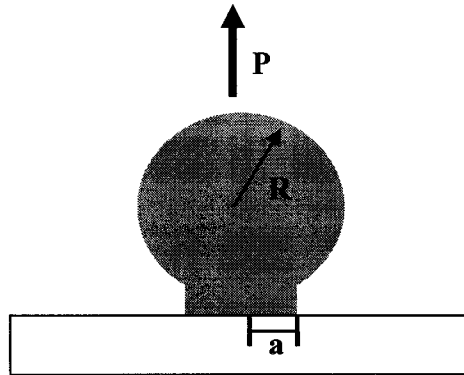


**Fig. 2-6.** Schematic of the formation of a neck between the particle and surface in the JKR theory [18]

The JKR theory is well adapted for systems with high surface energies, large particle radius and low stiffness of materials. One problem in the JKR theory is that it predicts an infinite stress  $x = 1$ , where indicates the distance from the center of the contact is equal to the radius of contact after deformation, at the edge of the contact area. This results from only considering forces inside the contact area, and the assumption in the theory that the attractive forces act over an infinitesimally small range.

#### (iv) Maugis Model

Maugis theory [21] is the most accurate theory in that it applies to all particle-surface systems, from large rigid spheres with high surface energies to small compliant materials

with low surface energies. The full range of material properties is determined by a dimensionless parameter  $\lambda$  in equation (2.47), and it is used to make a decision whether DMT or JKR model is more suitable for a certain system.  $\lambda$  is given by:

$$\lambda = \frac{2.06}{z_0} \left( \frac{RW^2}{\pi K^2} \right)^{1/3} \quad (2.47)$$

in which  $z_0$  is the equilibrium separation. A large value of  $\lambda$  characterizes large particle radii, and compliant materials with high surface free energies. Small values of  $\lambda$  indicate small particle radii and rigid materials with low surface free energies. Thus the adhesion force  $F_{ad}$  becomes  $2\pi RW$  for  $\lambda \rightarrow 0$  (DMT model) and  $\frac{3}{2}\pi RW$  for  $\lambda \rightarrow \infty$  (JKR model).

#### 2.2.4.2 van der Waals Forces between Surfaces

As explained in previous section, van der Waals forces play very important roles in phenomena involving adhesion forces, and it must be taken in account when we consider long-range interactions between two macroscopic bodies since they are always present. Thus, it is necessary to look into the van der Waals forces when considering polymer adhesion.

First, an interatomic van der Waals pair potential in a body is given as  $w = -C/r^6$ , and the interaction energies between two bodies such as particles can be obtained from the integrating the energies of all the atoms in one body with all the atoms in the other. The work done by the attractive forces in bringing the two particles from infinity to a

given separation distance is the Gibbs free energy,  $\Delta G$ , due to van der Waals interaction energies and it is given by [22]

$$\Delta G = - \iint_{V_1 V_2} \frac{C \rho_1 \rho_2}{r^6} dV_1 dV_2 \quad (2.48)$$

where  $dV_1$  and  $dV_2$  are differential volume elements of  $V_1$  and  $V_2$ ;  $\rho_1$  and  $\rho_2$  are the molecular number densities;  $C$  is a coefficient in the atom-atom pair potential. With an assumption of that  $C \rho_1 \rho_2$  is a constant, the Gibbs free energies, for instance, in the case of planar surfaces of thickness  $\delta_1$  and  $\delta_2$  separated by a distance,  $h$ , in vacuum is given by

$$\Delta G = V_A = -\frac{A_{12}}{12\pi} \left[ h^{-2} + (h + \delta_1 + \delta_2)^{-2} - (h + \delta_1)^{-2} - (h + \delta_2)^{-2} \right] \quad (2.49)$$

in which

$$A_{12} = \pi^2 C \rho_1 \rho_2 \quad (2.50)$$

$A_{12}$  is the Hamaker constant for bodies 1 and 2. For  $h \ll \delta_1, \delta_2$ , equation (2.49) can be rewritten as:

$$V_A = -\frac{A_{12}}{12\pi h^2} \quad [J/m^2] \quad (2.51)$$

where  $V_A$  is the attractive potential [22]. In general the Hamaker constants are in the range of  $10^{-21} \sim 10^{-19}$  J.

From equation (2.1) and (2.20), the work of adhesion due to the dispersion force (van der Waals force) for materials 1 and 2 can be expressed as:

$$W_{12}^d = 2\sqrt{\gamma_1^d \gamma_2^d} \quad (2.52)$$

where  $\gamma^d$  is the surface tension of each material due to dispersion interaction energies.

**Table 2-2.** van der Waals interaction free energies between bodies with different geometries [4].  $A$  is the Hamaker constant defined as  $A = \pi^2 C \rho_1 \rho_2$ , where  $\rho_1$  and  $\rho_2$  are the number of atoms per unit volume in the two bodies and  $C$  is the coefficient in the atom-atom pair potential.

Two atoms $w = -C/r^6$	Two spheres $w = \frac{-A}{6D} \frac{R_1 R_2}{(R_1 + R_2)}$
Atom-Surface $w = -\pi C \rho / 6D^3$	Sphere-Surface $w = \frac{-AR}{6D}$
Two cylinders $w = \frac{-AL}{12\sqrt{2}D^{3/2}} \frac{R_1 R_2}{(R_1 + R_2)}$	Two surfaces $w = \frac{-A}{12\pi D^2}$ per unit area

The attraction potential for the given materials is given by:

$$V_A = -\frac{A_{12}}{12\pi d^2} \quad (2.53)$$

where  $A_{12}$  is the Hamaker constant for the two given materials that are being separated to produce two new surfaces from contact, and  $d$  is the intermolecular distance, usually in the range of 0.2~0.3 nanometer. The work of adhesion can be expressed as the change of the Gibbs free energies and then it can be given by the attraction potential energies as well.



$$W_{12}^d = -V_A = \frac{A_{12}}{12\pi d^2} = 2(\gamma_1^d \gamma_2^d)^{1/2} \quad (2.54)$$

In addition, the equation (2.54) can be rewritten to obtain the Hamaker constant for two materials in vacuum using their surface tensions.

$$A_{12} = 24\pi d^2 (\gamma_1^d \gamma_2^d)^{1/2} \quad (2.55)$$

Several van der Waals interaction energies between macroscopic bodies with different geometries are shown in Table 2-2.

## **REFERENCE**

- [1] V. Mangipudi, E. Huang, M. Tirrell, *Macromolecular Symposia*, **102**, pp 131-143 (1996)
- [2] W. A. Zisman, *Ind. Eng. Chem.*, **55**, pp 19-38 (1963)
- [3] S. Wu, *Polymer interface and Adhesion*, Marcel Dekker: New York (1982)
- [4] J. Israelachvili, *Intermolecular and Surface forces (2<sup>nd</sup> ed.)*, Academic Press: London (1992)
- [5] A. J. Kinloch, *J. of Mat. Sci.*, **15**, pp 2141-2166 (1980)
- [6] D. H. Banghan and R. I. Razouk, *Trans. Faraday Soc.*, **33**, pp 1459-1462 (1937)
- [7] F. M. Fowkes, *J. Phys. Chem.*, **67**, pp 2538-2541 (1963)
- [8] J. Schultz, K. Tsutsumi, and J. B. Donne, *J. Colloid Interface Sci.*, **59**, pp 277-282 (1977)
- [9] D. R. Fitchmun, S. Newnan, and R. Wiggie, *J. Appl. Polym. Sci.*, **14**, pp 2411-2457 (1970)
- [10] G. Forches, *Polymer eng. And Sci.*, **35**, pp 957-967 (1995)
- [11] J. R Evans and D. E. Pakcham, *J. Adhesion*, **10**, pp 177-191 (1979)
- [12] L. H. Lee, *Adhesive bonding*, Plenum Press: New York (1991)
- [13] F. M. Fowkes, *J. of Adhesion Sci. and Tech.*, **1**, pp 7-27 (1987)
- [14] A. J. Kinloch, *Adhesion and Adhesive, Science & Technology*, Chapman and Hall: New York (1987)
- [15] B. M. Haines, *In aspects of Adhesion vol.3 (Chap 3)*, Univ. of London Press: London (1967)
- [16] R. M. Vasenin, *In adhesion: Fundamentals and Practice, Part I (Chap 4)*, Ministry of Technology (U.K.), Elsevier: New York (1970)
- [18] E.R. Beach, G.W. Tormoen and J. Drelich, *J. Adhesion Sci. Technol.*, **16**, No. 7, pp 845-868 (2002)

- [19] H. Hertz, *J. Reine Angew. Math.*, **92**, pp 156-171 (1881)
- [20] B.V. Derjaguin, V. M. Muller, and Yu. P. Toporov, *J. Colloid Interface Science*, **53**, pp 314-326 (1975)
- [17] K.L. Johnson, K. Kendall, and A.D. Roberts, *Proc. R. Soc. London*, **A 324**, pp 301-313 (1971)
- [21] D. Maugis, *J. Colloid Interface Science*, **150**, pp 243-269 (1991)
- [22] J. Masliyah, *Electrokinetic Transport Phenomena*, AOSTRA Technical Publication Series **12**, AOSTRA: Edmonton (1994)

# CHAPTER 3

## The Double Cantilever Beam Test

### 3.1 Introduction

Production of improved materials by the blending of polymers is commercially important and combining attractive properties of different polymers has been widely pursued in the industry. However, most polymer blends are thermodynamically incompatible because of the small entropy of mixing in mixtures of long-chain molecules. In addition, the interfaces of incompatible polymers are usually narrow so that there is little chain entanglement, in which is a prerequisite for strength in polymer systems. Many polymer blend applications depend on the adhesion between the component polymers. Although adhesion between different polymers is important in determining the mechanical properties of polymer mixtures, adhesion between polymers is not so obviously and easily measurable, especially on the micron or sub-micron scales seen in polymer blends.

Adhesion refers to the state in which two dissimilar bodies are held together by intimate interfacial contact such that mechanical force or work can be transferred across the interface [1]. The interfacial forces between the two phases may come from van der Waals forces, chemical bonding, or electrostatic forces. The mechanical strength of the system is determined not only by the interfacial forces but also by the mechanical properties of the interfacial zone and the two bulk phases [2]. In studies of bonding strength of bulk materials, it has always been shown that the strain energy released by interfacial failure is greater than the energy required to create two new surfaces.

This discrepancy may be explained by the fact that interfacial fracture occurs under conditions very far from thermodynamic reversibility. The propagation of a pre-existing interfacial crack results in substantial energy dissipation, and leads to large values of the interfacial fracture energy. Therefore, understanding the energy of polymer interfaces relies on identifying the mechanisms of energy dissipation active during crack propagation. In this chapter, the double cantilever beam test (DCB test) has been used to study the adhesion at the interface between polymers due to simply and easily performance of tests. Adhesion of glassy and semi-crystalline polymers to other similar polymers is investigated using the DCB test. The objectives of this study are (i) to investigate the fracture energy between similar and dissimilar polymers and (ii) determine the importance of various affecting factors on the interfacial adhesion.

## **3.2 Fracture Energy**

### **3.2.1 Mechanical Properties of Polymer Interface**

First, it is important to note that there are a number of different modes by which an interface will fail, and the energy dissipation measured in any fracture test will depend on which mode of failure dominates. It is common to focus upon three modes of loading a solid body with a crack. These are illustrated in figure 3-1. The fracture mode I, opening mode, where the crack faces are displaced in a direction normal to the fracture plane. In Mode II, sliding or shearing mode, the motion of the crack faces is that of shear along the fracture plane. In Mode III, tearing mode, the crack surface moves relative to one another, i.e. scissors mode.

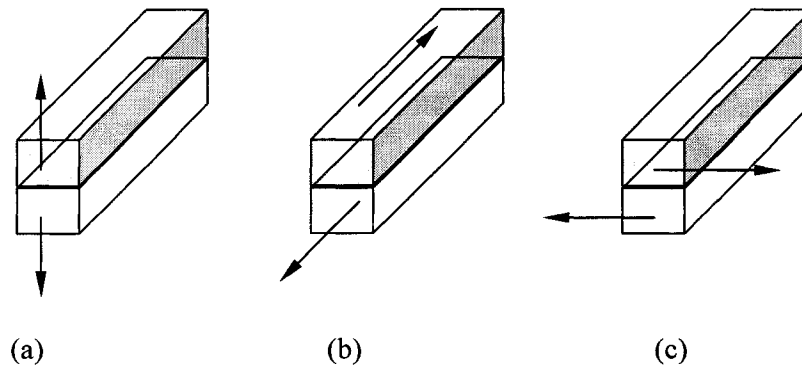


**Fig. 3-1.** Three basic fracture modes; (a) Opening mode, (b) Sliding mode, and (c) Tearing

In general the fracture energy will depend on the ratios of each of these modes in the actual loading situation. Pure mode I fracture is usually the smallest value, as well as the most important both in practical terms and theoretical understanding. The fracture energy for pure mode I fracture is referred to as  $G_{IC}$  and it is a major part of mechanical fracture tests. Stress intensity factors,  $K_I$ ,  $K_{II}$ , or  $K_{III}$  are used to express the criterion for crack propagation for each loading mode respectively and to determine critical lengths given an applied stress or a critical stress values given a crack length. In a mathematical expression, it is expressed as a function of the applied stress and the function depends on specimen configuration and loading mode. In previous work [3], it has been indicated that the interface crack is different from a crack in a bulk material and the direction of crack propagation at interface is determined by a mixture of both mode I and mode II with opening conditions. This is different from a crack in bulk material which normally grows in such a direction that it experiences a pure opening mode, which means that  $K_{II}$  is equal to zero. Therefore, it is necessary with interfacial failure to consider the effects of varying the ratio of mode I to mode II loading on crack propagation.

To understand the fracture behavior of polymers, the Griffith fracture theory has been applied on [4]. In this theory, fracture produces a new surface and the increase in energy required to create the new surface must be balanced by a decrease in elastically stored energy. Also, Griffith suggests that the large discrepancy between the measured strength of materials and the value based on theoretical considerations is attributed to the elastically stored energy concentrated in vicinity of small cracks. Fracture then occurs because of the spreading of cracks that originate in pre-existing flaws.

In general the growth of a crack is associated with an amount of work done,  $dW$ , on the system by external forces and a change  $dU$  in the elastically stored energy  $U$ . The difference between these quantities is then the energy available for the creation of new surfaces. The condition for growth of a crack by a length  $dc$  is given by [5]:

$$\frac{dW}{dc} - \frac{dU}{dc} \geq \gamma \frac{dA}{dc} \quad (3.1)$$

where  $\gamma$  is the surface tension and  $dA$  is the associated increase of surface. If there is no change in the overall extension  $\Delta$  when the crack propagates, then  $dW = 0$  and

$$-\left(\frac{dU}{dc}\right)_{\Delta} \geq \gamma \frac{dA}{dc} \quad (3.2)$$

In above equations, the elastically stored energy decreases and so  $-(dU/dc)_{\Delta}$  is essentially a positive quantity.

The DCB (Double Cantilever Beam) test has been widely used for the measurement of the adhesion at interface between two solid polymers. It is based on a balance between

the stored elastic energy in a beam and the energy necessary to propagate a crack at the interface between the two polymers. In principle, the test consists of creating an initial crack by inserting a razor blade, and then following the propagation of the crack with time. The driving force for the propagation of crack results primarily from the stiffness of the beams separated by the razor blade and this driving force decreases as the crack propagates [6]. As the razor blade is inserted at interface of two jointed beams, the crack propagates to length 'a'. This results in creation of two new surfaces (each of area A), and release of elastic energy stored in the beams. This released elastic energy, G, available for unit increase in crack length, which is called the 'strain energy release rate' (the 'rate' refers to 'release of energy per unit *area*' and not 'release of energy per unit *time*') is given by following equation:

$$G = \frac{dW}{dA} - \frac{dU}{dA} = \frac{1}{B} \left[ \frac{dW}{dc} - \frac{dU}{dc} \right] \quad (3.3)$$

where B is the thickness of the beams. It is assumed that fracture occurs when G reaches a critical value  $G_c$ . The equivalent equation (3.1) is then:

$$G \geq G_c \quad (3.4)$$

and  $G_c$  is equal to  $2\gamma$  in the Griffith equation. The value of G for a homogeneous material, the strain energy release rate, is given by [6]:

$$G = \frac{3}{16} \frac{Eh^3 \Delta^2}{a^4} \quad (3.5)$$



where,  $E$  = Young's modulus of the beam;  $h$  = thickness of the beam;  $\Delta$  = wedge thickness and  $a$  = crack length. An important assumption in this test is that adherends should not deform plastically. This is generally not a problem when using beams that are thick and stiff enough or when the adherends are bonded to a rigid substrate. The decreasing effective cleavage load results in the crack stopping at some equilibrium value, which itself is dependent upon the system conditions. One of the disadvantages of the DCB test is that the cracks may not be easy to view or may propagate unevenly across the specimen width with non-reproducible values of crack length. This test is widely employed to compare different interfacial treatments and, in particular, many studies have been done to show improvement of polymer interfaces reinforced with block copolymers.

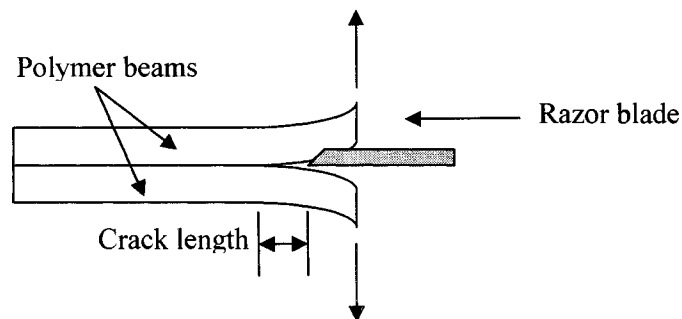


**Fig. 3.2.** Schematic of the DCB fracture test

In general glassy polymers are tough. For example the fracture energy of high molecular weight polystyrene is known as around  $1000 \text{ J/m}^2$ ; four orders of magnitude greater than the value of the surface energy. This significant high energy indicates that mechanisms are available during fracture that can dissipate large amounts of energy as a crack propagates. As the molecular weight of the polystyrene decreases, the fracture energy of the polystyrene also dramatically decreases until a molecular weight that

corresponds quite closely to the critical molecular weight for entanglement. The fracture energy has fallen to around  $1 \text{ J/m}^2$ . The relationship between the fracture energy and entanglement arises because a major mechanism of energy dissipation in the fracture of a glassy polymer such as polystyrene is crazing [7], the microscopic mechanisms of which rely on the polymers being entangled. Thus, the nature of toughness is due to entanglement in bulk glassy polymers. Similarly, the toughness of a polymer interface is determined by the degree of entanglement across the interface.

The study of the fracture energy of the interface between two incompatible polymers using the DCB test was firstly done by Brown [2]. He studied the fracture energy of Polystyrene/Polymethylmethacrylate (PS/PMMA) system and the effect of placing a thin layer of a PS-PMMA diblock copolymer on the interface. He found that the toughness at PS/PMMA interface is surprisingly high with  $G_c$  of about  $200 \text{ J/m}^2$ . This value is substantially greater than the intrinsic work of adhesion in that there are additional loss mechanisms during the fracture of interface. In addition, he observed that the crazes grow down into PS from the interface and the crack tended to follow one such craze and then jump back to the interface.

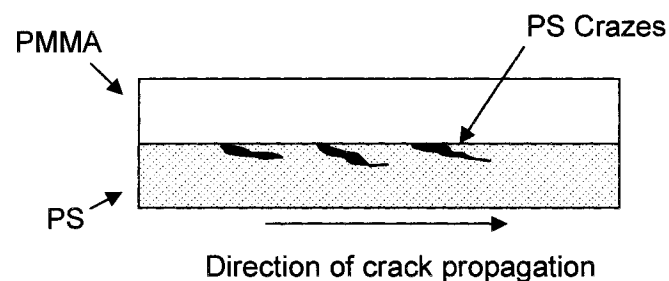


**Fig. 3-3.** Failure of the PS/PMMA interface by the phenomenon of crazing [8]

Both PS and PMMA are glassy polymers that fail by crazing but PS has relatively lower craze stress. High fracture energy results from that crazes grow away from the interface into the PS which has lower crazing resistance. In another work [8], Brown found these crazes could be suppressed by the use of an asymmetric fracture toughness test that tends to push the principal tensile stress into the more craze-resistant material. This was simply done by adhering lower craze stress material to a rigid substrate to prevent. In a system of the PS adhered onto a rigid substrate, he found a  $G_c$  of 5 to 10 J/m<sup>2</sup>. For this reason, the asymmetry caused by bonding the sample to a stiff substrate affects significantly on the fracture toughness at the interface.

According to Brown [7, 8], if the interface has sufficient integrity to induce crazing between glassy polymers, the fracture energy is proportional to the ratio of the square of the areal density of entangled chains ( $\Sigma$ ) to the crazing stress ( $\sigma_{cr}$ ).

$$G_c \propto \frac{\Sigma^2}{\sigma_{cr}} \quad (3.6)$$

This is confirmed by the study of the interface reinforced with block copolymer chains. In his work, the enhancement of adhesion depends on the density of the copolymers at the interface and on the length of each copolymer block. With these two variables, interfacial failure can occur by one of three modes:

- (i) Chain pullout, in which the entangled chain is pulled out from the bulk
- (ii) Chain scission, in which a C-C bond breaks in the entangled chain instead of being pulled out from the bulk

- (iii) Crazeing, in which it begins with the formation of microvoids and fibrils with plastic deformation at the interface before complete interfacial failure.

Above equation is valid only if all interfaces between glassy polymers that have sufficient integrity to induce crazeing. Otherwise, mostly likely the interfaces fail through a scission mechanism.

Helfand et al. [9] have theoretically explained the incompatible interface between two immiscible polymers of infinite molecular weight and described the diffusion of one polymer into another by solving the diffusion equation of a random walk in a potential field due to the presence of an incompatible monomer. In their study, the interfacial profile is characterized by an interfacial width  $w_I$  given by:

$$w_I = \left[ \frac{2(b_1^2 + b_2^2)}{12\chi} \right]^{1/2} \quad (3.7)$$

Where  $b$  is the statistical segment length of a polymer and  $\chi$  is the Flory-Huggins interaction parameter. In addition, they yield a complex, but tractable expression for the interfacial tension of polymer pair:

$$\frac{\gamma}{kT} = \left[ \chi(\rho_A \rho_B)^{1/2} \right]^{1/2} \left( \frac{\beta_A + \beta_B}{2} + \frac{1}{6} \frac{(\beta_A - \beta_B)^2}{\beta_A + \beta_B} \right) \quad (3.8)$$

where  $\rho_i$  is the density of the polymer  $i$  and the parameter  $\beta_i$  is obtained from the statistical segment length of polymer  $b_i$  by:

$$\beta_i = \left( \frac{1}{6} \rho_i b_i^2 \right)^{1/2} \quad (3.9)$$

### 3.3 Experimental Procedure

#### 3.3.1 DCB test

Fracture energy of Polystyrene/Polymethylmethacrylate (PS/PMMA) system and Polystyrene/Polypropylene (PS/PP) system was investigated with different thickness of specimens and different jointing temperature using the DCB test. The fracture energy of the PS/PMMA interface was investigated by using the DCB test. Fracture energy release rate,  $G_i$ , was measured using the DCB test applying the following equation. [6]

$$G_i = \frac{3\Delta^2 E_1 h_1^3 E_2 h_2^3}{8a^4} \times \frac{E_1 h_1^3 C_2^2 + E_2 h_2^3 C_1^2}{(E_1 h_1^3 C_2^3 + E_2 h_2^3 C_1^3)^2} \quad (3.10)$$

where  $C_i = 1 + 0.64h/a$ ,  $h_1$  and  $h_2$  are the thickness,  $E_1$  and  $E_2$  are the elastic moduli of two polymers,  $\Delta$  is the thickness of the razor blade and  $a$  is the crack length. This equation is used for PS/PMMA system that is freestanding. In the system where one of the beams is adhered onto a rigid substrate, the  $G_c$  is given by the following equation [3]

$$G_c = \frac{3\Delta^2 h^3 E}{16a^4 (1 + 0.64h/a)^4} \quad (3.11)$$

where  $h$  and  $E$  are the thickness and elastic modulus of the unadhered beam respectively. This equation is employed to obtain the  $G_c$  of PP/PS system where PP was bonded to rigid aluminum substrates. The crack length was measured 24hrs after the razor blade was inserted. Once a crack is observed to advance, the loading on the specimens was stopped and the crack was allowed to advance at constant displacement until the stress at the crack tip is reduced enough to prevent further cracking. In practice, most of the growth process was completed after 15 min. Although the crack will continue growing

slowly even after several hours probably due to a polymer chain creep relaxation phenomena. For the precise measurement of crack length, the optical microscope (model: zeiss microscope) was used. The  $G_c$  values obtained from each of the 10-15 crack length measurements with different thickness of polymer beams were calculated by using equations (3.10) and (3.11). In order to relate the interface structure to mechanical strength, we have worked for fracture energy release rates of PS/PMMA and PS/PP interface as a function of jointing temperature and the contact time between the polymers using the DCB test, respectively.

### **3.3.2 Sample Preparation**

Polystyrene/Polymethylmethacrylate (PS/PMMA) and Polystyrene/Polypropylene (PS/PP) systems were studied where both polymers in each system are incompatible. Pellets of the polystyrene (PS) and Polymethylmethacrylate (PMMA) were stored in a vacuum oven at 80°C overnight to remove volatiles inside the pellets. After that, the PS and PMMA pellets were hot-pressed into 6.5 cm × 6.5 cm plate using a Carver Model C laboratory press under a pressure of 0.5 ton using aluminum molds with covered Teflon sheets. The molding temperature was used for PS was 200°C and that for PMMA was 210°C. For different thicknesses of polymers beams, various thickness molds were used. After molding, the sheets of PS and PMMA were cut into beams 6.5cm × 1.5 cm using an electric saw and then the edges of beams were smoothed using sand paper. For PS/PMMA system, the prepared beams of PS and PMMA were put in an oven at 80°C until they were heated up to the same temperature. Therefore, moisture on the surface of the beams was removed. The PS beams were placed onto beams of PMMA when they were still hot and then two polymer beams were assembled under very slight pressure in

the laboratory press with a prescribed annealing temperature and annealing time. For temperature dependence of  $G_c$ , four different temperatures between 100°C and 130°C were used to anneal and bond PS/PMMA samples. Annealing temperature of 100°C was used to see whether some motion of the molecule at the interface could be observed at temperature just below glass transition temperature of PS and PMMA,  $T_g$ . The effect of annealing time was also observed because it could affect the stability of fracture energy. After the two polymer beams were bonded to each other; the specimens were cooled in air at room temperature.

For PS/PP system, the procedure of specimen preparation was the same as that for the PS/PMMA system. However, PP pellets were pressed at 160°C. PP pellets were preheated to soften for 3min, and pressed under 0.5 ton for 7min to fill the aluminum molds. After molding, the PP beams were placed in a vacuum oven at 150°C for 1hr. PS beams were also heated up to 110°C and then the PP layer was placed onto PS to be bonded. The sample was annealed for a predetermined amount of time at a prescribed temperature and it was cooled down to room temperature. For PS/PP system, one side of PP beam was glued to a tape-covered aluminum plate to make PP layers stiff. A razor blade was perpendicularly inserted at the interface and driven forward to propagate a crack. With both PS/PMMA and PS/PP systems, crack propagation tests were performed to obtain fracture energy.

To see the effect of block copolymer on the fracture energy at the PS/PMMA interface, PS-b-PMMA diblock copolymer was used. Solutions of diblock copolymer/ $\text{CH}_2\text{Cl}_2$  (Methyl chloride) were used with different weight concentration (5 wt. %, 8 wt. %, and 10 wt. %) to prepare the copolymer layers with different thicknesses. Solutions

were spin-coated on the surface of both the PMMA and the PS beams by using the spin caster WS-200-4T2 (Laurel Tech. Corp.) at 2000 RPM for 2 minutes. Both PS and PMMA beams covered by diblock copolymer layer were then dried in oven at 80°C to evaporate the solvent. After that, two polymer beams were bonded as described in preparation of PS/PMMA samples.

**Table 3.1.** Polymers used in the DCB test

Polymer (Abbreviation)	Supplier (Product No.)	Glass transition temp. $T_g$	Molecular weight ( $M_w$ , g/mol)	Density ( $\text{kg/m}^3$ )	Melt Flow Index (MFI, g/10min)
Polypropylene (PP)	Exxon (PP1042)	-23°C	-	900	1.9
Polystyrene (PS)	Dow (Styron 666D)	105°C	160,000	1050	8.0
Poly- methylmethacralate (PMMA)	Atoglas (Plexiglas V826)	108°C	-	1192	1.6

### 3.4 Results and Discussions

#### 3.4.1 Fracture Energy of PS/PS and PS/PMMA

For the PS/PP system, crack propagation occurred quickly immediately after the razor blade was inserted at the interface and the fracture toughness energy was shown to be zero most times. It is taken account that the crystallinity in polypropylene, which characterizes its ductility and toughness, makes it difficult for these semicrystalline polymers to adhere with other polymers. Moreover, this is emphasized when the second component in contact is a glassy polymer such as polystyrene, which will have a drastically different thermal expansion. Therefore, large differences in thermal expansion and the creation of residual stresses result in the weak interface between semicrystalline



PP and amorphous PS. To promote the interfacial adhesion of semicrystalline PP/amorphous PS, both diblock copolymers and graft copolymers formed through *in situ* reaction can significantly enhance the interlayer adhesion.

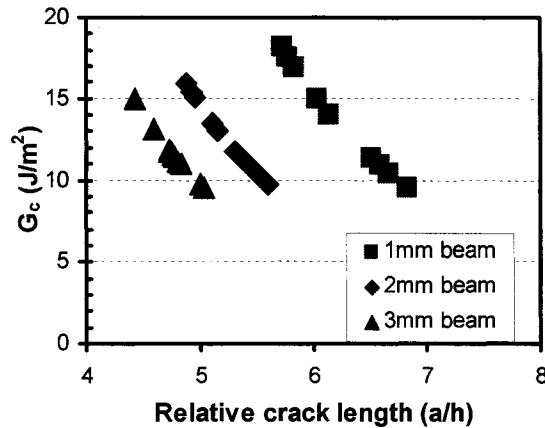


**Fig. 3-4.**  $G_c$  of PS/PMMA samples with different beam thicknesses at 120 °C for 1hr

For the PS/PMMA system, this test was carried out manually. Usually, the crack obtained looks semicircular. In a case where the shape of crack was not uniform; an average crack length was calculated. It was hard to make the insertion of the razor blade into the interface with a very slow constant speed when the test is performed manually. Although some errors of derivation were quantified in the manual test, the repeatable fracture energies of PS/PMMA system were able to obtain with same procedure. We found the average of strength of  $12.8 \pm 2.6 \text{ J/m}^2$  with varying thickness of polymer beams, which is significantly lower than the fracture strength of pure polystyrene or polymethylmethacralate and higher than the surface energy of the polymers. In comparison to a freestanding result of 60~100  $\text{J/m}^2$  by Brown [8] and a difference by a factor of 5~8 was observed. However, there are several differences in the preparation of

samples and in polymers used with different molecular weight that may explain this difference in comparison to previous work. On the other hand, the value of strength obtained from above experiment is similar to the experimental fracture energy of  $18 \text{ J/m}^2$  by Brown et al. [10]

### 3.4.2 Temperature Dependence of $G_c$ of PS-PMMA Interface

The  $G_c$  of PS-PMMA samples were measured at four different temperatures between  $100^\circ\text{C}$  and  $130^\circ\text{C}$ . Each specimen was annealed at four different temperatures for 1hr and it was shown that interfacial fracture energy is independent of temperature with an average  $12.8 \pm 2.6 \text{ J/m}^2$  except for the case of  $100^\circ\text{C}$  annealing temperature. For the case of  $100^\circ\text{C}$  annealing temperature the values of interfacial fracture energy shows  $0.69 \pm 0.37 \text{ J/m}^2$  and the scatter of crack lengths was observed. This indicates that the samples had insufficient adhesion at the interface, meaning that interfacial entanglement is not sufficient. Therefore, the interfacial region is narrow so that it is easy to pull out an unentangled polymer layer from another. As shown previously, interaction parameter determines interfacial thickness and  $G_c$  is related to the square of interfacial thickness. In fact, the temperature dependence on  $\chi$  can be given by [11]:

$$\chi(T) = \frac{A}{T} + B \quad (3.12)$$

where A and B are experimentally determined constants. From equation (3.7), the interfacial width is inversely proportional to the root of the Flory-Huggins interaction parameter. Further, the critical fracture energy can have the relationship with the interfacial width as following [12]:

$$G_c \propto w_i^2 \quad (3.13)$$

Therefore, we can write the relation between  $G_c$  and temperature as following:

$$G_c(T) \sim \frac{1}{(A/T + B)} \quad (3.14)$$

As result, in the case where  $A/T \gg B$ ,  $G_c$  varies linearly with temperature whereas, in case where  $A/T \ll B$ ,  $G_c$  is independent of temperature. From the above results we would then predict little or no change in  $\chi$ , i.e., it is independent in the range of temperature between 110°C and 130°C. In previous work  $\chi$  has been recently measured for a PS-PMMA diblock system as a function of temperature within this temperature range by Russel et al. [13] as:

$$\chi(T) = \frac{3.902}{T} + 0.0284 \quad (3.15)$$

where T is the temperature in degrees Kelvin.

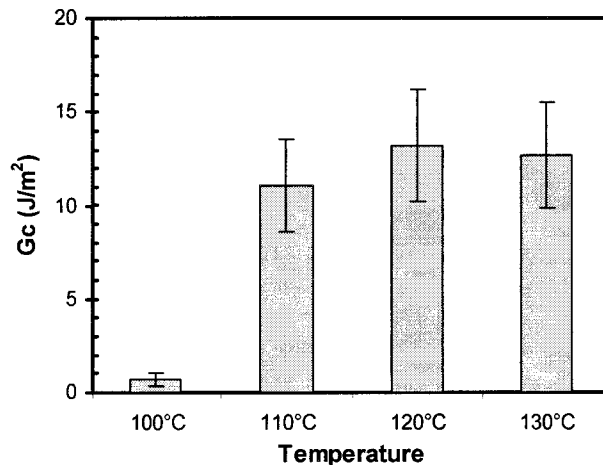


**Fig. 3-5.**  $G_c$  of PS/PMMA samples annealed at four different temperatures between 100 and 130 °C for 1hr

The interaction parameter,  $\chi$ , only changes by 0.1% for the temperature range of 110~130°C. This change can be acceptable within the experimental value of  $12.8 \pm 2.6$  J/m<sup>2</sup>.

### 3.4.3 Effect of Annealing Time on PS/PMMA Interface

The interfacial fracture energy continues to increase with annealing time. The continued increase of the interfacial strength is caused by the interdiffusion of molecular segments. To study the effect of annealing time on PS/PMMA interface, samples with different annealing times (2min, 5min, 10min, 30 min, and 60 min) were prepared at a fixed temperature 120°C. Each sample, we measured the crack length up to 10 times and the crack length was averaged, and the fracture energy was calculated from equation (3.10). A correlation between the annealing time and the interface depth for PMMA was observed by Vasenin [14] and an interfacial width is predicted to grow with a  $t^{1/2}$  dependence:

$$w_i \propto t^{1/2} \quad (3.16)$$

Fig. 3-6. shows that the fracture energy increased with increasing annealing time from 2 to up to 30 minutes. However, it was observed that fracture energy did not significantly increase on annealing samples more than 30 minutes, and it was even found to be slightly less at 60 minutes than at 30 minutes.

If the interface of PS/PMMA system is assumed to fail by the scission mechanism, the fracture energy has a relationship with the characteristic number of entanglements,  $N_{ent}$ . The characteristic number of entanglements that provide physical links between

polymers in contact is inversely proportional to their spacing, and the entanglements are limited by the interfacial width,  $w_I$ , such that:

$$N_{ent} = \frac{w_I}{L_e} \quad (3.17)$$

where  $\overline{L_e}$  is the mean entanglement length scale for the polymer pair [12].

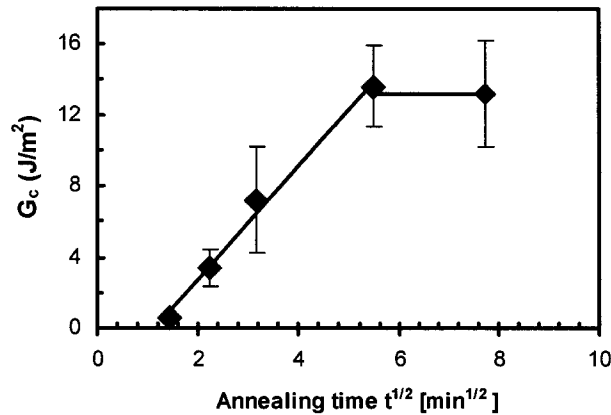


**Fig. 3-6.**  $G_c$  of PS/PMMA samples annealed for different times at the fixed temperature 120°C

As a result, we assume that the fracture energy proportionally increases to the square root of the annealing time. From above results, it seems to be approximately adapted in an initial stage within standard deviation ranges. The bond strength continuously rises with annealing time after the interfacial contact is completed. However, the fracture energy does not continue to significantly increase with contact time after 30 minutes, and it may explain why the interfacial adhesion of PS/PMMA reaches critical fracture energy after an annealing time of 30 minutes. For more accurate result for effect of annealing time on interfacial strength, the more experiments with other factors are required.

### 3.4.4 Effect of Surface Roughness on PS/PMMA Interface

As explained in previous chapter (2.2.3), adhesion increases generally with increasing surface roughness, especially for the bond strength of adhesive to a substrate. Roughness tends to lower the contact angle when the intrinsic angle  $\theta_0$  is less than  $90^\circ$ , or increase it when the intrinsic angle is greater than  $90^\circ$  [1].

To prepare a rougher surface, the surface on the side of polymer beam was pretreated by using the grinder with a sand paper (Grit 240) at 200 RPM for 30 seconds. On the other hand, the polymer samples were prepared by using a silicon wafer during hot-pressing for a smoother surface. For the more precise comparison of different pretreatment on the surface of specimen in contact, the surface topography was investigated by using the Atomic Force Microscopy (AFM). To determine roughness of polymer surface, three images of each beam were scanned in a scan size of  $25 \times 25 \mu\text{m}$ . The roughness of surface was calculated by using the root mean square (RMS) roughness [15], and the smoother surface has an around 9-12 nm roughness and the rougher surface has over  $2 \mu\text{m}$ .

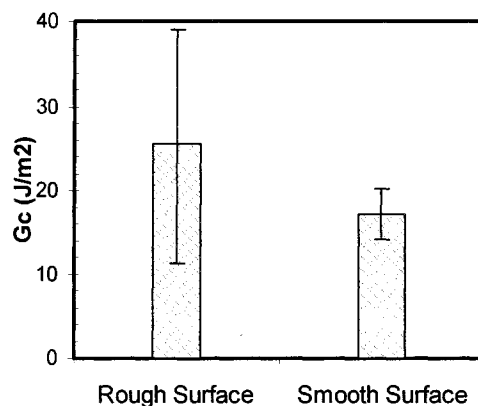


**Fig. 3-7.** Comparison Gc of PS/PMMA samples annealed at temperature  $120^\circ\text{C}$  between pre-treated surfaces using sand paper and silicon wafer

As shown above Figure 3.7, the fracture energy increases from higher surface roughness due to pre-treatment on the surface of polymer beams using the sand paper. However, the mechanical interlocking mechanism only increases the bond strength, and rougher surface may also cause the increase of viscoelastic and plastic dissipation of energy. Although the surface roughness increases the fracture energy of PS/PMMA system, it also affects large data scatter due to inconstant contact area between polymer beams.

### **3.4.5 Contributions of Diblock Copolymer on Adhesion of PS/PMMA**

A-B block copolymers are known to act as interfacial agents between incompatible polymers A and B [16-19]. They reinforce the interface with each block dissolved in the relevant homopolymers [20-23]. Thus, it has indicated that a thin layer of block copolymer considerably improve the adhesion between incompatible polymers.

The interface between 2mm beams of PS and PMMA was modified by a spin coated layer of the PS-b-PMMA copolymer with two different molecular weights (25K and 50K g/mol). This PS/PMMA beam with a diblock copolymer layer at the interface was annealed at 120°C for 1hr under a slight pressure in order to maintain the beams in contact. Fig. 3-8 shows the fracture energy ratio of the modified PS/PMMA interface over the unmodified interface, which was measured by the DCB test. The fracture energies for the interface modified by the diblock copolymer were found over 4 times higher than those for the unmodified interface. In addition, it was found that the diblock copolymer molecular weight influences on the interfacial fracture energy. Brown [10] has shown that the maximum interfacial fracture energy depends on the diblock molecular weight as long as the molecular weight is less than 80K. Brown has also revealed that the

toughness of PS/PMMA interface is increased by up to a factor of 50 when high molecular weight of diblock copolymer (over 80K) was used to enhance the interfacial strength [19]. The fracture energy value for reinforced interface was close to the cohesive fracture energies of PS and PMMA. However, the fracture energies were not tremendously increased compared to the values obtained by Brown due to the use of lower diblock molecular weight (25K and 50K). When 25 K molecular weight diblock copolymer was used to modify the interface between PS and PMMA, fracture energy increased with increasing the concentration of copolymer in CH<sub>2</sub>Cl<sub>2</sub> solution. In other words, the toughness is improved as the thickness of copolymer layer is increased. This suggests that block copolymer can be used for a simple method to reinforce and saturate the interface between incompatible polymers.

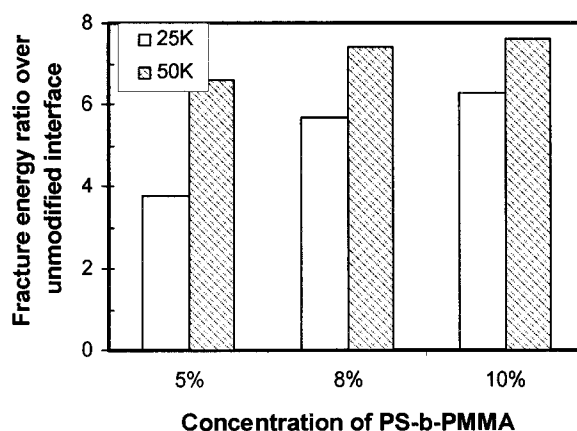


**Fig. 3-8.** Fracture energy ratio of the modified PS/PMMA interface over the unmodified interface at the fixed temperature 120°C for 1hr.

On the other hand, the fracture energy was not significantly increased with the concentration of copolymer solution when 50 K molecular weight diblock copolymer was used. The only small difference of fracture energies was found within standard deviation ranges between 8 wt.% and 10 wt.%. This implies the fracture energy reaches to a



maximum value at a certain value of thickness. The effect of diblock copolymer on the interfacial fracture energy was briefly investigated in this section. To better understand the effect of thickness of copolymer layer, it is required to measure a precise thickness of copolymer using an adequate apparatus such as the ellipsometry.

### 3.5 Conclusions

In attempting to understand adhesion of amorphous and semicrystalline polymers, several contributions should be taken into account. Difference in thermal properties between amorphous and semicrystalline polymers results in residual stresses at the interface, and leads to poor interfacial adhesion. PS/PP system was used to study the adhesion of amorphous-semicrystalline polymers using the double cantilever beam (DCB) test. Most times, the interfacial fracture energy of PS/PP system was zero due to a large difference in thermal property. To enhance the adhesion of glassy polymer to semicrystalline polymer, addition of a diblock copolymer or the formation of a copolymer through *in situ* reaction at the interface will be applied.

Adhesion of another polymer system, PS/PMMA, was measured using DCB test as well. In the test, a thumbnail shaped crack was created at the interface, and the crack generally propagated as the razor blade was inserted at the interface and it mostly stopped growing about 15 minutes after the razor blade was wedged between the bonding polymer beams. To consider various factors affecting the adhesion of PS/PMMA system, different bonding conditions such as the thickness of specimen, annealing temperature, annealing time, and surface roughness of the specimen were used.

First, different samples do not significantly change the bond strength and the relative crack length ( $a/h$ ) in which  $a$  is the crack length and  $h$  is the thickness of bonding polymer beams. The value  $a/h$  was mostly found to be in the range between 4.5~6. In addition, fracture energy has shown to about 12-13 J/m<sup>2</sup> with different thickness of samples. Secondly, fracture energy does not have significant temperature dependence when the bonding polymers are above their glass transition temperatures. Between the range of temperature 110°C and 130°C, the Flory-Huggins interaction parameter,  $\chi$ , has almost no change so that the critical fracture energy is independent of the range of temperature. The change seen with different annealing temperature is acceptable within the experimental standard deviations. The interfacial fracture energy tends to proportionally increase with the square root of the annealing time at lower time after polymer beams are bonded. Up to 30 minutes annealing time after polymer beams were bonded, the fracture energy significantly increases, but it reached at a maximum after 30 minutes. From previous work, interfacial width is predicted to grow with  $t^{1/2}$  dependence and this may be adapted in the PS/PMMA system up to 30 minutes. Meanwhile, the adhesion of PS/PMMA increases with increasing surface roughness. However, the mechanical interlocking mechanism is not only a reason for the increase of bond strength. In fact, mechanical interlocking is not an adhesion mechanism at the molecular level; it is merely a means of affecting the contact area on surfaces. To find the effect of diblock copolymer on the interfacial fracture energy was investigated using different molecular weights and different concentrations (thickness) of copolymer. The fracture energy for the interface modified by the diblock copolymer was increased over 4 times higher than those for the unmodified interface. This suggests that the block copolymer can be used

for a simple method to reinforce and saturate the interface between incompatible polymers. In this DCB test, the fracture energy was not found in PS/PP system. When a flaw was once initiated, a crack was propagated quickly under a small driving force. Thus, we did not determine interfacial fracture energy under this low strength by using the DCB test. In addition, sensitivity in bonding conditions, pre-existing flaws and invisible defects in samples led to significant errors in values determined using the DCB test. For these reasons, a new adhesion measurement using Atomic Force Microscopy (AFM) will be studied in the next chapter.

## **REFERENCE**

- [1] S. Wu, *Polymer Interface and Adhesion*, Marcel Dekker: New York, Chap. 11 (1982)
- [2] K. Cho and H. R. Brown, *J. Polym. Sci. Polym. Phys.*, **28**, pp 1699-1718 (1990)
- [3] M. F. Kanninen, G. T. Hahn, and M. Sarrate, *Int. J. Frac.*, **9**, pp 83-92 (1973)
- [4] A. A. Griffith, *Phil. Trans. Roy. Soc.*, **221**, pp 163 (1921)
- [6] J. G. Williams, *Polym. Eng. Sci.*, **17**, pp 144-149 (1977)
- [7] H. R. Brown, *Macromolecules*, **24**, pp 2752-2756 (1991)
- [8] H. R. Brown, *J. Mater. Sci.*, **25**, pp 2791-2794 (1990)
- [9] E. Helfand, and A. M. Sapse, *J. of Chemical Physics*, **62**, pp 1327-1331 (1975)
- [10] H.R. Brown, K. Char, and V. R. Deline, *Macromolecules*, **26**, pp 4155-4163 (1993)
- [11] R. J. Young, and P. A. Lovell, *Introduction to Polymers (2<sup>nd</sup>)*, Stanley Thorne Ltd.: Cheltenham, Chap. 3 (1991)
- [12] P. J. Cole, R. F. Cook, and C. W. Macosko, *Macromolecules*, **36**, pp 2808-2815 (2003)
- [13] T. P. Russel, R. Hjelm, and P. Seeger, *Macromolecules*, **23**, pp 890-893 (1990)
- [14] R. M. Vasenin, *In adhesion: Fundamentals and Practice*, Elsevier: New York, Chap. 4 (1970)
- [15] E. R. Beach, G.W. Tormoen and J. Drelich, *J. Adhesion Sci. Technol.*, **16**, pp 845-868 (2002)
- [16] R. Fayt, R. Jerome, and Ph. Teyssie, *Polym. Eng. Sci.*, **27**, pp 328-334 (1987)
- [17] R. E. Cohen and A. R. Ramos, *Macromolecules*, **12**, pp 131-134 (1979)

- [18] T. Inoue, T. Soen, T. Hashimoto, and H. Kawai, *Macromolecules*, **3**, pp 87-92 (1969)
- [19] H. R. Brown, *Macromolecules*, **22**, pp 2859-2860 (1989)
- [20] J. Noolandi, and K. M. Hong, *Macromolecules*, **15**, pp 482-492 (1982)
- [21] J. Noolandi, and K. M. Hong, *Macromolecules*, **17**, pp 1531-1537 (1984)
- [22] L. Leibler, *Makromol. Chem., Macromol. Symp.*, **16**, pp 1-17 (1988)
- [23] J. J. Benkoski, P. Flores, and E. J. Kramer, *Macromolecules*, **36**, pp 3289-3302 (2003)

# CHAPTER 4

## Study of Polymer Adhesion Using Atomic Force Microscopy

### 4.1 Introduction

Polymers are being used in an increasingly wider range of applications in industry. A good understanding of the surface characteristics of polymers is required because many critical interactions between a polymer and its environment occur at the surface. For instance, an important aspect of a polymer used in a medical device is often at the interface between the body and the device. The interaction between the polymer and its environment depends in large part on surface composition and structure. Since surface composition and topography play an important role in ultimate polymer properties, precise surface characterization can be a key part in developing new materials and in understanding problems and behavior in existing materials. However, most of the studies characterizing surface properties of polymers, such as surface tension and adhesion force, over the last few decades have been performed by conventional macroscopic mechanical tests. As discussed in the previous chapters, these conventional techniques are usually applicable only to macroscopic bodies, and unfortunately are not suitable for micro or nanoscale characterization. Thus, the experimental values from the conventional tests do not necessarily represent intrinsic surface properties. Recently, Atomic Force Microscopy (AFM) has been used to characterize polymer surfaces with its high-resolution surface mapping capabilities. In addition, AFM can be employed to directly measure adhesion force between individual polymer particle and other particles and between individual polymer particles and polymer surfaces, so that mechanics of polymer surfaces can be

investigated [1]. Therefore, understanding the fundamentals of polymer particle-surface interactions using AFM is becoming increasingly important.

In this chapter, we will briefly introduce the basics of AFM technique and review the polymer particle-surface adhesion. The pull-off force using AFM will be measured to determine polymer-polymer adhesion. In addition, the investigation of the surface properties of polymer using AFM will be discussed.

## **4.2 Background**

### **4.2.1 Atomic Force Microscopy**

Atomic Force Microscopy (AFM) has been applied to the investigation of surface phenomena at the micron or nanometer scale. It can be used to image surfaces and to study the interaction and adhesion of particles. The widespread utilization of AFM is due to its ease of use, the molecular-level information that it provides, and the variety of surfaces that can be studied in various environments. In an AFM, a very fine tip (radius $\approx$ 30nm) positioned on the end of a flexible cantilever moves over the surface of the sample in a direction perpendicular to the longest axis of the cantilever. The tip and cantilever are displaced vertically upon encountering a surface morphology. A laser beam, which is bounced off the rear of the cantilever, detects this displacement. The sample, which is supported on a piezoelectric displacement system, is moved up and down to maintain the deflection of the cantilever at a constant value. The z-displacement of the sample can thus be displayed as a function of x- and y- positions to provide a morphological image of the sample. At the same time, the laser beam can be used to detect lateral (torsional) movements of the tip and cantilever, as the sample is rastered.

These movements are a convolution of morphological effects and tip-sample friction. Therefore, by monitoring both vertical and lateral tip movements, the surface morphology and friction coefficient can be simultaneously mapped across a sample surface.

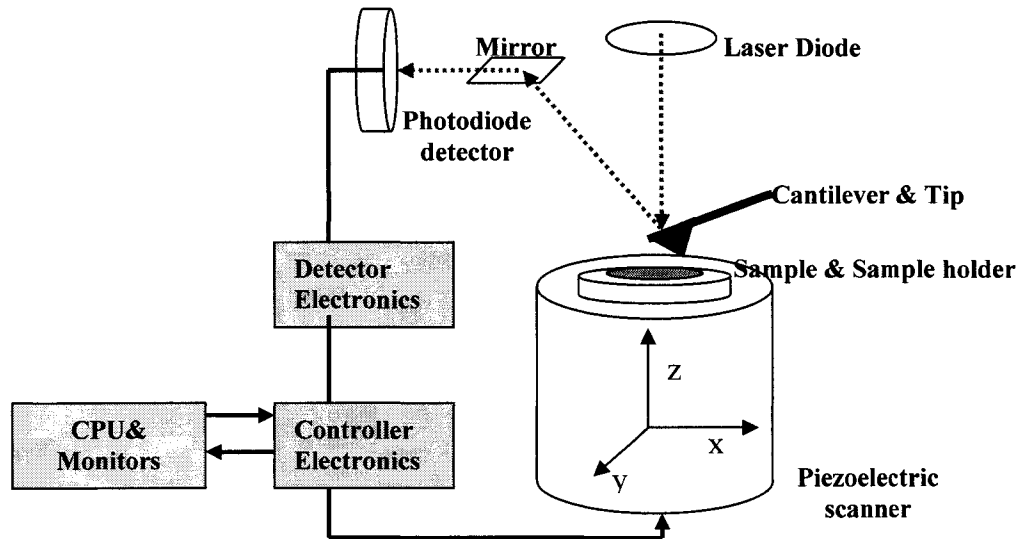


**Fig. 4-1.** A basic schematic of AFM; Feedback loop maintains a constant deflection between the cantilever and the sample or a constant oscillation amplitude of the cantilever

Another important type of measurement is the “*Force Curve*”. In this measurement, the tip moves up and down over a single location, i.e. moving in and out of contact with the sample. During these cycles the deflection of the cantilever is monitored, providing an indication of the tip-sample interaction forces as a function of separation. As the tip is withdrawn from the surface, tip-sample adhesion leads to a minimum in the force curve before the tip jumps back away from the surface. A particular strength of AFM is its ability to operate in liquid environments. In this case, the effects of a liquid medium on the interaction between two surfaces of samples can be observed.



#### 4.2.1.1 Contact Mode

A common operation mode in AFM is the contact mode where the tip scans the sample in close contact with the surface. The force on the tip is repulsive with a mean value of  $10^{-9}$  N [2]. This force is set by pushing the cantilever against the sample surface with a piezoelectric actuator. In contact mode, the deflection of the cantilever is sensed and compared to a constant value of deflection in a DC feedback amplifier. If the measured deflection is different from the desired constant value, the feedback amplifier applies a voltage to the piezoelectric actuator to move up or down the sample. As a result, the cantilever restores itself to the desired value of deflection. The voltage that the feedback amplifier applies to the piezoelectric actuator is a measure of the height of the sample surface. It is displayed as a function of the in-plane position of the sample. Under ambient conditions, sample surfaces are covered by a layer of adsorbed gases consisting primarily of water vapor and nitrogen. When the probe touches this contaminant layer, the formation of a neck that links the probe and the surface occurs and the cantilever is pulled by surface tension toward the sample surface. The magnitude of the force depends on the probe geometry, but is typically on the order of 100 nN. Due to this capillary force, operating AFM is often carried out in a liquid. There are many advantages to operate AFM with the sample and cantilever immersed in a liquid. These advantages include the elimination of capillary force, the reduction of Van der Waals force, the effect of vibration and the ability to study important processes at liquid solid interfaces. Interfacial forces and morphology variation at the liquid/solid interface can also be investigated as a function of the solvent quality, the ionic strength, and pH [2]. However there are also some disadvantages to working in a liquid. For instance, leaks can be a

problem. More fundamental problems such as sample damage on hydrated and vulnerable biological samples can also happen.

#### **4.2.1.2 Tapping Mode**

Tapping mode allows high-resolution topographic imaging of sample surfaces that are easily damaged, or difficult to image by other AFM techniques. Tapping mode overcomes problems associated with friction, adhesion, electrostatic forces, and other difficulties experienced in conventional AFM scanning modes by alternately placing the tip in contact with the surface and then lifting the tip off the surface to avoid dragging the tip across the surface. Tapping mode imaging is performed by oscillating the cantilever tip at or near the cantilever's resonant frequency using a piezoelectric actuator. The piezoelectric actuator makes the cantilever oscillate with a high amplitude (typically greater than 20nm) when the tip is not in contact with the surface. The oscillating tip is then moved toward the surface until it begins to lightly touch, or tap the surface. During scanning, the vertically oscillating tip alternately contacts the surface and lifts off, generally at a frequency of 50,000 to 500,000 cycles per second [3]. As the oscillating cantilever begins to intermittently contact the surface, the cantilever oscillation is necessarily reduced due to energy loss caused by the tip contacting the surface. The reduction in oscillation amplitude is used to identify and measure surface features. During tapping mode operation, the cantilever oscillation amplitude is maintained constant by a feedback loop. When the tip passes over a bump in the surface, the cantilever has less room to oscillate and the amplitude of oscillation decreases. The oscillation amplitude of the tip is measured by the detector and input to the feedback electronics. The feedback loop then controls the tip-sample separation to maintain a

constant amplitude and force between the tip and the sample. When the tip contacts the surface, the high frequency (50k - 500k Hz) makes the surfaces stiff (viscoelastic), and the tip-sample adhesion force is greatly reduced [3]. Tapping mode prevents the tip from sticking to the surface and causing damage during scanning. Unlike contact mode, when the tip contacts the surface, it has sufficient oscillation amplitude to overcome the tip-sample adhesion force. Another advantage of the Tapping mode imaging is its large and linear operating range. This makes the vertical feedback system highly stable and ensures reproducible sample measurements.

#### 4.2.1.3 Force-Distance Curve

AFM can also be used to measure the vertical force that the tip applies to the surface. With this technique, the long-range attractive or repulsive forces between the probe tip and the sample surface can be determined, explaining chemical and mechanical properties like adhesion and elasticity. Force-curves (Force vs. Distance curve) typically show the deflection of the AFM cantilever as the fixed end of the cantilever is brought vertically towards and then away from the sample surface.

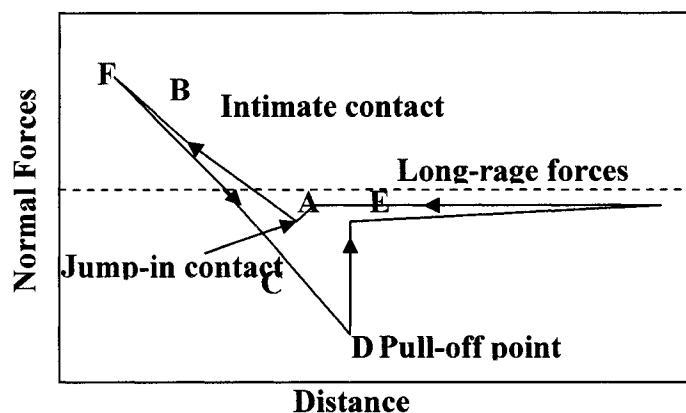


**Fig. 4-2.** The force-distance curve and different regimes of the tip-surface contact: A: Jump-in contact (contact repulsive mode), B: Loading part (force modulation mode), C: Attrition (contact attraction mode). D: Pull-off point (adhesion), E: Dynamic, non-contact mode; F: Maximum loading, the indentation point [4]

The deflection of the cantilever is measured and plotted at many points as the z-axis scanner extends the cantilever towards and then retracts it away from the surface. Similar measurements can be made with oscillating probe systems like tapping mode and non-contact AFM. This type of work for oscillation probe system is just beginning. Measurements of cantilever amplitude and cantilever phase versus separation can provide more information about the details of magnetic and electric fields over surfaces and also about viscoelastic properties of sample surfaces [4].

#### 4.2.2 Colloid Probe AFM

Colloid probe is a probe with a colloid particle in the place of a conventional tip. A colloid can be placed at the apex of a cantilever. A most important advantage of using colloid probe in AFM is that it can directly measure the interactions (the adhesion force) between a sample surface and the colloidal particle. In general deflection of the cantilever and distance between the sample and the probe are measured. The results are then converted an interaction force. In previous sections, we looked upon the elastic contact mechanics and long-range interactions by van der Waals forces between two bodies. We now apply these theories to colloid probe in AFM.

Previous work [2] showed that the net force, which is the sum of interactions between the tip and the surface is divided to three contributions: (1) surface force,  $F_s$ , (2) force due to the sample deformations,  $F_d$ , and (3) the deflection force of cantilever,  $F_c$  as shown in Figure 4-3. Interaction force,  $F_i$ , is the sum of surface forces,  $F_s$  and the sample deformation force,  $F_d$ . The surface and deformation forces are of the same order of magnitude. The interaction forces are balanced by the cantilever bending force,  $F_c$ . For

the interactions of a spherical particle in contact with a solid surface, both of the long-range interactions and the adhesion force from solid-body contact must be considered.

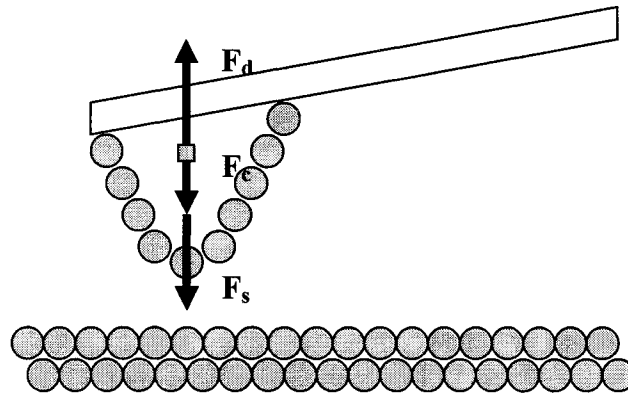


**Fig.4-3.** The interaction force  $F_i = F_s + F_d$  is a sum of many interactions, where  $F_s$  is the surface force and  $F_d$  is the sample deformation. The interaction force is balanced by force  $F_c$  [2].

As we already discussed in chapter 2, the long-range interactions can be described by DLVO theory, while JKR (Johnson-Kendall-Roberts) theory is applied to take into account the elastic contact mechanics. DLVO and JKR are regarded as different and separate theories. However, it can be assumed that the shortest distance, which is commonly an intermolecular distance at equilibrium, is obtained from the distance where the DLVO interaction is equal to the JKR adhesion work [5]. To express interaction forces in terms of van der Waals interaction energies, a useful approximation, the Derjaguin approximation is usually applied. Based on the Derjaguin approximation, the interaction force  $F(h)$  between two spheres at a short distance  $h$  is given by [6]:

$$F(h)_{sphere} = 2\pi \frac{r_1 r_2}{r_1 + r_2} W(h)_{plane} \quad (4.1)$$

where  $W(h)_{plane}$  is the interaction energy per unit area of two planes at a surface separation distance  $h$  when two radii  $r_1$  and  $r_2$  are much larger than surface distance  $h$ . If

it is assumed that  $r_1$  is much larger, i.e.  $r_1 \gg r_2$ , which can occur in the case of a sphere near a plane surface, the interaction force can be expressed as:

$$F(h)_{sphere} = 2\pi R W(h)_{plane} \quad (4.2)$$

The attractive potential energies can be regarded as the work of adhesion where a particle is in contact with a plane surface as mentioned earlier. As a result, a simple thermodynamic model can be used to predict the ratio of the adhesion forces for different functional groups. The adhesion force can be written as:

$$F \sim R W_{132} \quad (4.3)$$

where  $R$  is the radius of a spherical particle on a AFM cantilever and  $W_{132}$  is the free energy change on separating unit area of two materials 1 and 2 in medium 3 as shown in chapter 2.

$$W_{132} = \gamma_{13} + \gamma_{23} - \gamma_{12} \quad (4.4)$$

where  $\gamma_{12}$  is the interfacial energy between materials 1 and 2. Here, in this experiment, material 1 is a plane polymer surface (sample); material 2 is a polymer particle (tip); and medium 3 is the air. We can estimate  $\gamma_{13} = \gamma_1$ ;  $\gamma_{23} = \gamma_2$ ; and  $\gamma_{12} = \gamma_1 + \gamma_2 - 2(\gamma_1 \gamma_2)^{1/2}$  using the combination relation [7]. Therefore, equation (4.4) can be written as:

$$F = 4\pi R (\gamma_1 \gamma_2)^{1/2} \quad (4.5)$$

Since many of polymers are compressible in nature, and they deform elastically at contact, Johnson-Kendall-Roberts (JKR) theory has been well applied to describe the

adhesion energy for polymer contacts. From section (2.2.4), we know that the radius of contact area decreases from  $a$  to  $0.63 a$  at which point the spheres spontaneously separate from contact, and the adhesion force is approximately 75% of the adhesion force in DeJaquin-Müller-Toporov (DMT) model in which two particles in contact are completely rigid. Thus, the force required to separate a sphere and flat surface of polymer is given by:

$$F_{ad}^{JKR} = 3\pi R(\gamma_1\gamma_2)^{1/2} \quad (4.6)$$

This force can be calculated from the force required to pull the particle on the cantilever off the surface in the force measurement by AFM. This force is referred to as *pull-off force* and is calculated from Hooke's law,

$$F = k\Delta z \quad (4.7)$$

where  $k$  is the spring constant of the AFM cantilever and  $\Delta z$  is the maximum deflection of cantilever that occurs when lifting the particle off from the surface. Thus, the surface energy of material can be estimated using AFM by measuring its adhesion force with another material of a known surface energy by means of equation (4.6).

## 4.3 Experimental Procedure

### 4.3.1 Materials and Sample Preparation

To study the polymer particle-surface adhesion using AFM, two different polymer-polymer systems were used. First, the system of a Polypropylene (PP) particle on the Polystyrene (PS) surface was used and then a Polystyrene particle on Polymethylmethacrylate (PMMA) surface was investigated.

To prepare thin PS and PMMA films, solutions of PS/ CH<sub>2</sub>Cl<sub>2</sub> (Methylene chloride) and PMMA/ CH<sub>2</sub>Cl<sub>2</sub> with different weight concentration (0.2 wt. %, 0.5 wt. %, 0.8 wt. %, 1 wt. %, and 2 wt. %) were used. The solutions were spin-coated using the spin caster WS-200-4T2 (Laurel Tech. Corp.) at 2000 RPM onto silicon wafers cleaned with ethanol and chloroform. After spin casting for 1 minute, films were dried overnight in a vacuum oven at 90 °C to evaporate the remaining solvent.

To make PP particles in a diameter of about 10 μm, two immiscible polymers (PP and PS) were mixed to create a blend. Pure PS and PP pellets were obtained from industry (see Table 4-1). Prior to their use, the PS and PP pellets were placed in the vacuum oven at 80 °C overnight to remove volatiles inside the pellets. The blend of PS/PP with a weight ratio of 80/20 wt. %, and total sample mass of 1.5g, was mixed in the Alberta Polymer Asymmetric Minimixer (APAM, see Fig. 4-4.) at 200 °C and 10RPM for 10 minutes.

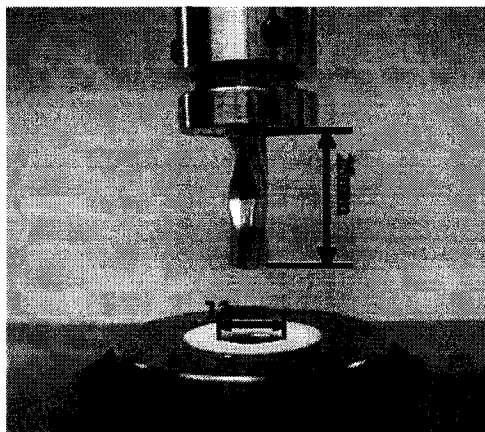


**Fig. 4-4.** Alberta Polymer Asymmetric Minimixer (APAM)

Due to interfacial tension between two immiscible polymers, some spherical PP particles with a diameter around 10 μm were obtained as shown in Fig. 4-5. After mixing of PS/PP



pellets, the blend of PS/PP was cooled down at ambient condition for 3 min. A sample of the blend was then diluted in  $\text{CH}_2\text{Cl}_2$  (methyl chloride) solvent in order to dissolve the PS phase to isolate PP particles. To isolate PP particles from PS matrix, a syringe driven filter unit (Pore size:  $0.22\mu\text{m}$ ; Millipore) was used. As seen in the SEM micrograph of PP particles in the filter (see Fig. 4-5), they were most likely to be embedded in pores of the filter. This made it difficult to find particles using an optical microscope (the Zeiss microscope) for attaching the particles to AFM cantilevers.

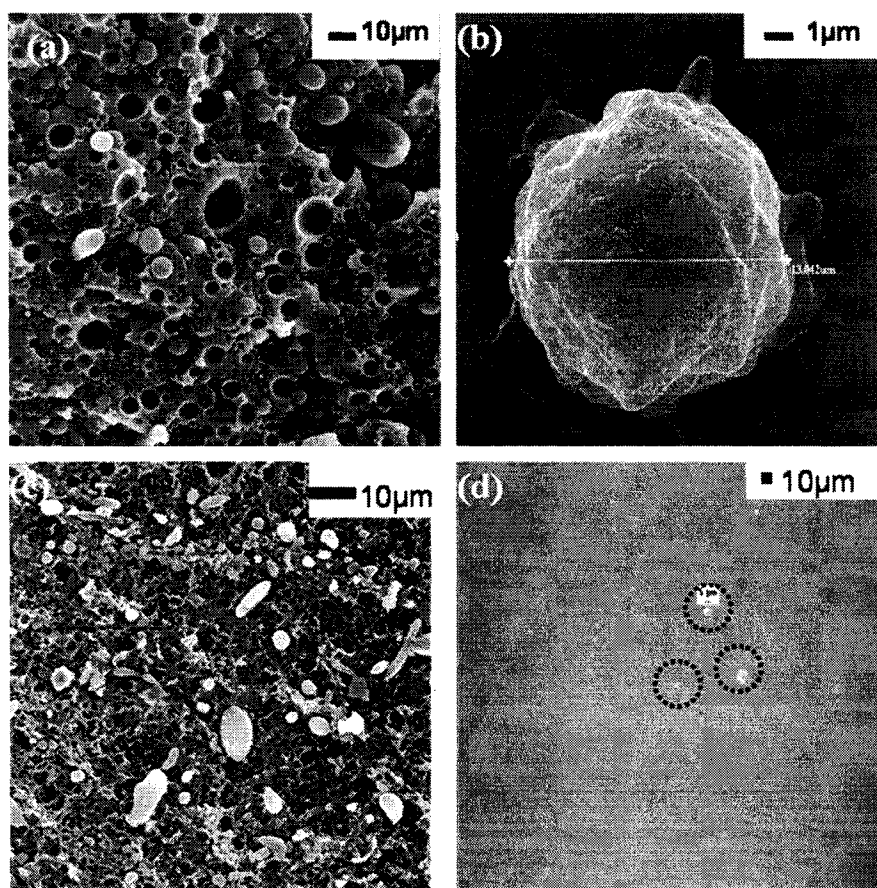


**Fig. 4-5.** (a) SEM micrographs of morphology of PP/PS (20/80 wt. %) blend, (b) PP particle obtained from the solution of PP/  $\text{C}_6\text{H}_4(\text{CH}_3)_2$ , (c) SEM micrograph of isolated PP particles using the syringe driven filter & (d) A picture of the filter surface using the Zeiss optical microscope

Another method was attempted to make spherical PP particles by means of dissolving PP pellets in  $C_6H_4(CH_3)_2$  (Xylene) and then evaporating the solvent. In this case, 0.2 wt. % PP was dissolved in Xylene at 145 °C for 2~3 hours. After evaporating the Xylene solvent at room temperature, beads of PP were left on the substrate. However, it was found that the surface of PP particles was too rough to regard them as perfectly spherical particles. For this reason, we used spherical PP particles from Equistar Chemicals, LP. (Houston, TX) and spherical PS particles from Bangs Laboratory, Inc. (Fishers, IN) in this study.

**Table 4-1.** Properties of used polymers in this study

Polymer (Abbreviation)	Supplier (Product No.)	Molecular Weight ( $M_w$ , g/mol)	Glass Transition Temp. ( $T_g$ , °C)	Density ( $g/cm^3$ )	Elastic Modulus (MPa)	Mean Diameter ( $\mu m$ )
Polypropylene (PP)	Equistar Chemicals, LP. (FP800-00)	-	-	0.909	-	10-12
Polystyrene (PS)	Bangs Lab. Inc. (PS06N)	-	-	1.062	-	5.5
Polystyrene (PS)	Dow (Styron 666D)	160,000	100°C	1.050	2916	-
Polymethyl Methacrylate (PMMA)	Atoglas (Plexiglas V826)	-	114°C	1.19	3086	-

#### 4.3.2 Surface Imaging and Pull-off Force Measurements

The topography and the roughness of polymer film were investigated directly by Nanoscope III Multimode AFM (Digital Instruments) in the tapping mode. Scan size of PS and PMMA films was  $10 \times 10 \mu m$  and  $5 \times 5 \mu m$  respectively. The scan rates were in the range of 0.8~1.5 Hz. A single crystal silicon probe, which has a spring constant and a

drive frequency of 40 N/m and 458 KHz, respectively, was used to scan polymer surfaces.

For pull-off force measurements, a silicon nitride probe with triangular cantilevers (Digital Instruments) was employed. A polymer particle was glued using the epoxy glue on a cantilever with spring constant of 0.58 N/m. In the above polymer particle-surface systems, pull-off force measurements were performed using Nanoscope III Multimode AFM under ambient conditions. To determine the pull-off forces of polymer particle-polymer surface for the system of a PP particle on the PS surface and the system of a PS particle on the PMMA surface, up to 100 force measurements were carried out for each system. Basically the contact point was adjusted after every five times of force measurement. It is evident that multiple contact points were used for pull-off force measurements.

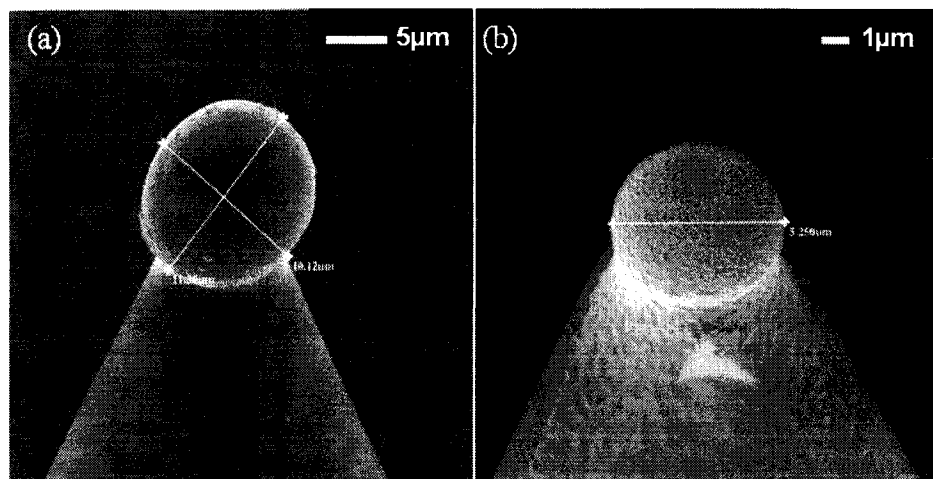


**Fig. 4-6.** SEM images of polymer particles on the AFM cantilever glued by epoxy glue a) PP particle ( $R=5\mu\text{m}$ ) & b) PS particle ( $R=2.75\mu\text{m}$ )

The ramp sizes (distance of piezoelectric movement in the direction normal to the surface) and the loading range were slightly varied during the measurements. Thus, the

measured pull-off forces were investigated as a function of the applied load. Since cast polymer solutions of different concentrations were used to make thin film, film of different thickness was obtained. The thickness of each film was measured by scratching method using AFM, and the effect of polymer film thickness on the measured pull-off forces was investigated. Since the roughness of surfaces in contact plays an important role in determining the adhesion force, the effect of roughness dependency was examined to better understand the influence of nanoscale roughness on adhesion between polymer surfaces

#### **4.4 Results and Discussions**

##### **4.4.1 Determination of Polymer Film Thickness**

Accurate determination of cast film thickness plays an important role in many areas of surface science. The thickness of cast film was measured to establish a relationship with the pull-off forces. For thin films which are relatively soft compared to the substrate, for instance, polymer films on silicon wafer, thickness was determined by scratching the films and performing AFM imaging of the scratch. Each film made by spin casting was scratched by a sharp blade with circumspection so that there was no damage to the silicon wafer substrates. The scratch depths were then measured at different sections of the film.

Films, when cast from the same conditions, produce comparable film thicknesses. The variation of thickness of PS and PMMA film cast with solutions of different concentration is shown in Figure 4-8. Film thickness increases linearly from 15 to 240 nm as concentration increases from 0.2 wt.% to 2 wt.%.

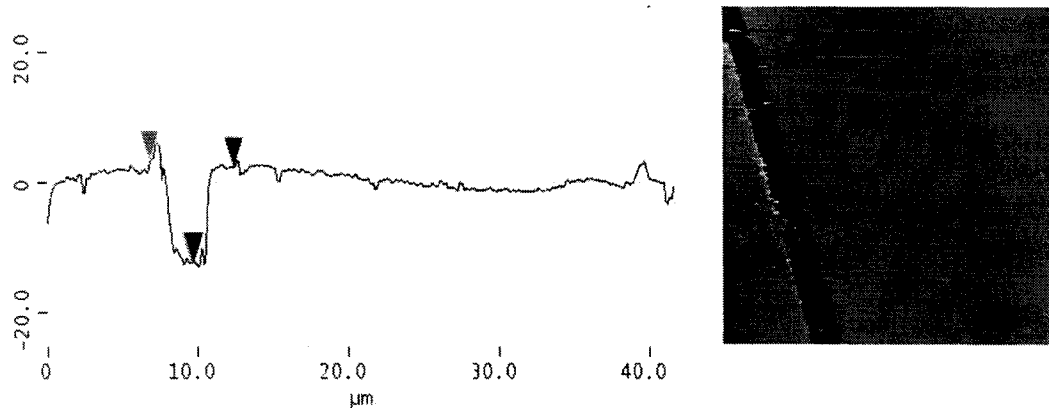


**Fig. 4-7.** Image of the scratch and its cross-section of PS film from 0.2 wt.-% solution. The average film thickness is 14.1nm.

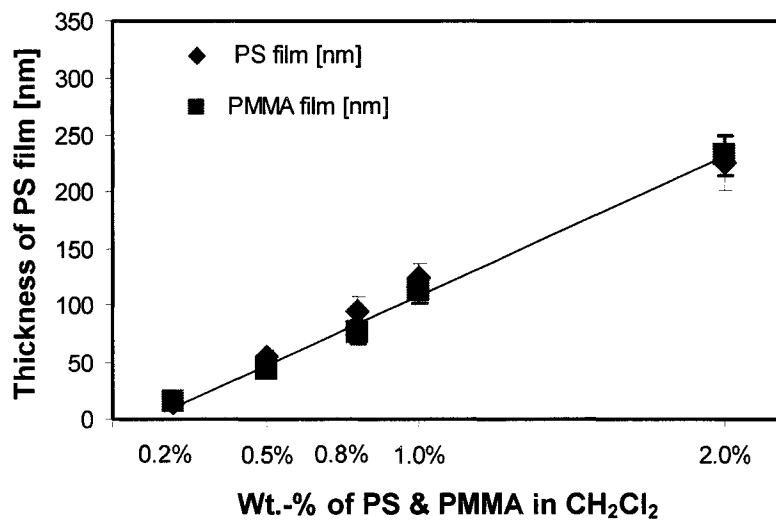


**Fig. 4-8.** Variation of thickness of the PS and PMMA films with concentration of cast solution. The film thickness increases with concentration.

We also see that there is a greater variation of the film thickness within the film as the concentration of cast solution increases. This may result from the higher viscosity with increasing concentration of cast solutions so that a decrease in film thickness is seen as we move radially outward from the center of the samples. Since the scratches were performed manually. Some experimental errors were expected in measurement. The thickness of all sample films was also measured using Tencor Alpha-step 200 Stylus Profiler in the Nanofab laboratory. These results were comparable with those obtained from AFM imaging.

**Table 4-2.** Thicknesses of polymer film measured by; first row: scratching method using AFM; second row: Alpha-step 200 Profiler.

	0.2 wt.-%	0.5 wt.-%	0.8 wt.-%	1 wt.-%	2 wt.-%
PS [nm]	14.4±1	54.4±6.5	94.1±13.2	124.3±11.9	226.2±24.2
	17.0±2.3	59.0±3.7	92.0±5.8	114.0±5.8	232.5±10.5
PMMA [nm]	15.2±2.4	44.3±7.1	76.9±9.6	113.5±11.7	232.5±12.5
	17.0±2.4	37.5±2.5	68.8±2.2	110.0±3.5	228.8±4.1

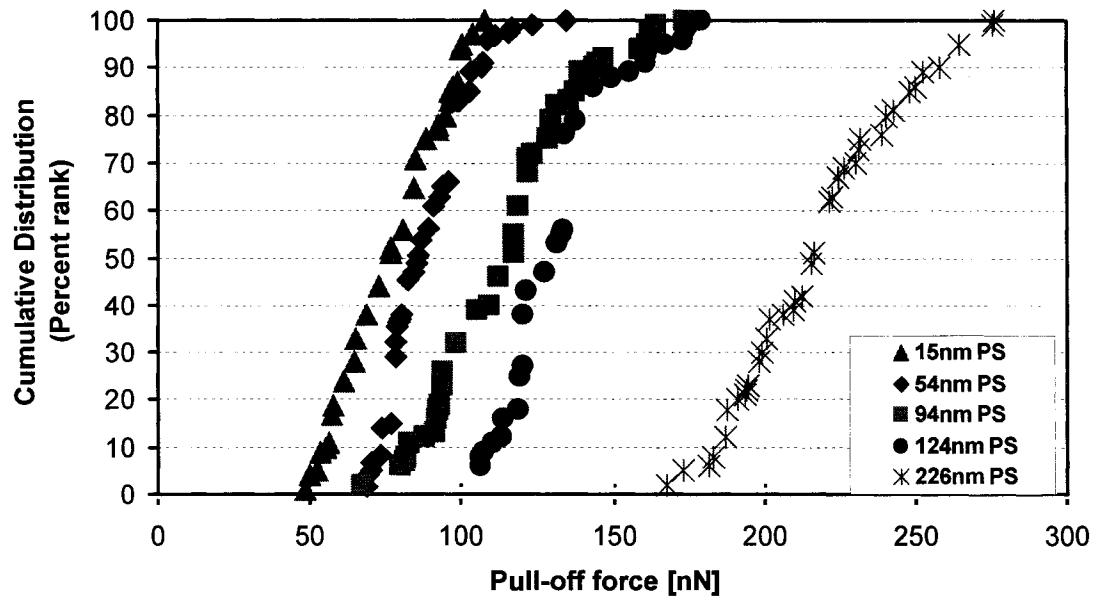
#### 4.4.2 Distribution of Measured Pull-off Force

To study polymer particle-surface adhesion, two systems of a polymer particle on a polymer surface were investigated using AFM in the force mode. Scan rates for force measurement were varied over a small range from 1.1-1.9 Hz to reduce loading/unloading hysteresis. The ramp size was in the range of 1250-2500 nm. The pull-off forces were measured with various maximum applied loading. In the PP/PS system, a small increase in pull-off force was found with increasing the load over the investigated load range of 10-400 nN as seen in Fig. 4-10. In case of the PS/PMMA system, the pull-off force did not change significantly with the load in the range of 10-350 nN. With the PP

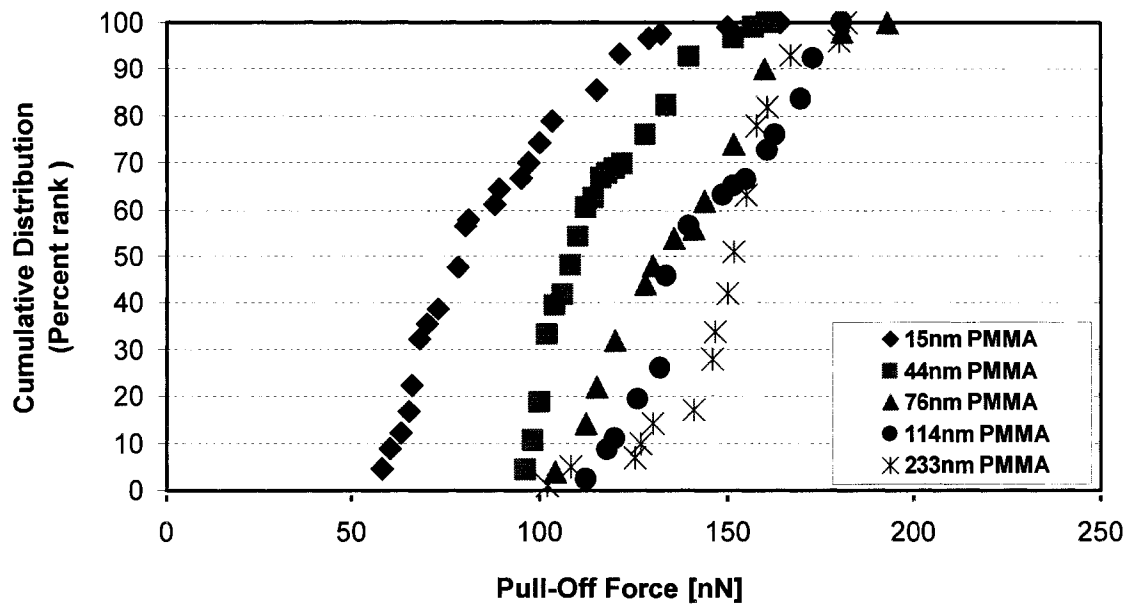
particle, it can be demonstrated that the lighter loading leads to an incomplete contact although there is no clear reason for this. As a result, it could cause inconsistent contact area between the particle and the surface and hence errors in the force measurement. On the other hand, the contact area is not expected to increase substantially with increasing the loading force between the PS particle and the PMMA surface due to the rigidity of both materials.

The measured pull-off forces for a PP particle on the PS surface and a PS particle on the PMMA surface are shown in Fig. 4-9. The measured pull-off forces for two systems are found to be in the range of 70-280 nN and 60-180 nN, respectively. The measured pull-off forces for the PP particle-PS surface system increased with concentration of PS solutions used for film preparation (i.e. greater film thickness). In particular, the pull-off force increased up to 280 nN in the range of 124 nm and 226 nm thickness of PS film. A similar trend was found in the system of PS particle on PMMA surface. However, the measured pull-off forces for a PS particle on PMMA surface did not increase significantly over PMMA film thickness range of 15nm and 233 nm. Nevertheless it was observed that the pull-off force increased with the thickness of the cast film. It is evident that the thickness of substrate film influences the adhesion force between polymer particle and polymer surface. In order to see the effect of film thickness on the adhesion forces, T-tests were carried out. The results will be presented in the next section.

A challenge in interpreting the results of adhesion force measurement is that the adhesion values obtained are scattered over a range with a deviation of about 10 % up to 15 %. Although the measurements were done with identical experimental conditions, sometimes different pull-off force values were obtained.



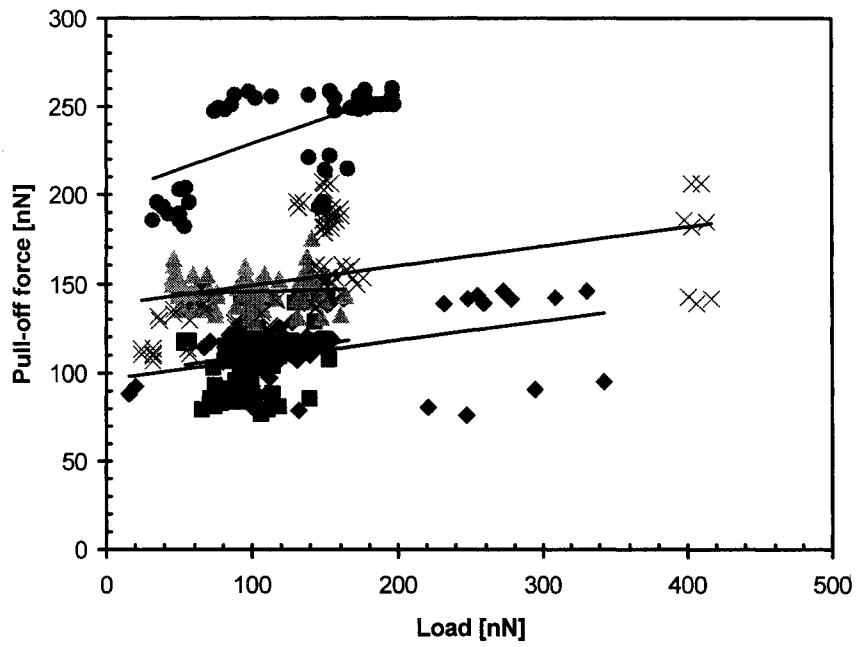
(a)



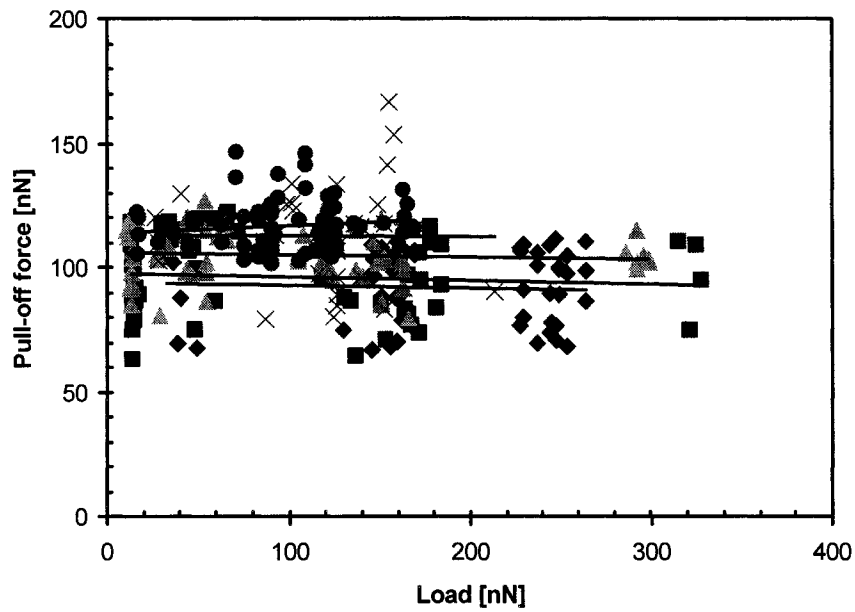
(b)

**Fig. 4-9.** Cumulative distribution versus pull-off force of Polymer particle-surface (a) a PP particle on the PS surface (b) a PS particle on the PMMA surface





(a)



(b)

**Fig. 4-10.** Pull-off force vs. applied loading force during contact between a PP particle and the PS surface (b) a PS particle and the PMMA surface ( $\blacklozenge$  PS: 14.4 nm & PMMA: 15.1 nm;  $\blacksquare$  PS: 54.4 nm & PMMA: 44.3 nm;  $\blacktriangle$  PS: 94.1 nm & PMMA: 76 nm;  $\times$  PS: 124.3 nm & PMMA: 113.5 nm;  $\bullet$  PS: 226.2 nm & PMMA: 232.5 nm)

This poses challenge to obtain quantitative adhesion data via AFM force measurement. Many factors must be considered, and one factor is asperities on the PP or PS particles and the roughness of polymer films. The surface roughness is at least partially responsible for the significant disparities in measured adhesion forces of polymer particle-polymer surface. In a previous study [8], Biggs et al. showed that the measured adhesion force of a PS particle on a PS surface is approximately 100 times smaller than the predicted values. The Rabinovich model shows that the size, shape, distribution and mechanical properties of asperities on surfaces affect the actual contact area, which is directly correlated to adhesion forces. More details about the effect of nanoroughness on the pull-off forces will be discussed in the next section

#### **4.4.3 Determination of Surface Energy of Polymer Using AFM**

As we discussed in JKR model, the pull-off force can be expressed as surface energies by means of equation (4.6). We determined surface energies of polymers used in this study, The surface energy of polystyrene was obtained from the pull-off force measurements between the PS particle ( $R=2.75\mu\text{m}$ ) and a PS thin film made from the solution of 2 wt.-% PS in  $\text{CH}_2\text{Cl}_2$ . The normalized pull-off forces for PS-PS system were measured to be  $50\pm 7$  mN/m. The surface energy of PS was then calculated to be  $5.3\pm 0.8$  mJ/m<sup>2</sup>. These normalized pull-off forces are similar to the values from previous work ( $35.9\pm 2$  mN/m), also determined using AFM [9]. With this surface energy for the polystyrene, surface energies for each polymer were estimated by equation (4.6). Calculated surface energies from pull-off force data for polymer samples are shown in Table 4-3.

**Table 4-3.** Surface energies of polymers determined by pull-off force measurements and Literature values

Material	Surface energy by current work [mJ/m <sup>2</sup> ]	Literature values [19] [mJ/m <sup>2</sup> ]
Polystyrene	5.3± 0.8	40.7
Polypropylene	2.0±0.3	29.3
Poly (methyl methacrylate)	3.2± 0.5	41.1

#### 4.4.3.1 Discrepancies in Adhesion Measurement

As shown in Table 4-3, a difference of almost one order of magnitude between calculated values from the measured pull-off forces in this study and literature values from traditional methods (i.e. contact angle measurement) was observed. This deviation may possibly be attributed to using larger probes for pull-off force measurements. In general, using a larger spherical probe particle attached to the cantilever is likely to have a rougher surface. This will reduce actual particle-surface contact area, and therefore, significantly influence the measured pull-off forces. From previous work [10], surface energies of polymers determined by the pull-off force measurements using a unmodified sharp tip (R=70 nm) have been compared with those derived from contact angle measurements. The two methods yielded close values. On the other hand, the pull-off force for PS-PS system using a PS bead is shown to be approximately 100 times smaller than the literature value [8]. This finding indicates that the surface asperities have greater effect in the system of larger particles in contact with a nanoscale rough surface. In addition, multiple contacts during measurements may induce plastic deformation of surface asperities.

Contamination of the polymer particle and surface by adsorbates or dust is a problem in the pull-off force measurements [22]. All force measurements should be carried out with a cleaned probe and surface. However, probe and surface samples are usually contaminated during measurements. Moreover, as shown by the SEM micrograph of a PP particle on the AFM cantilever (Fig. 4-6), the particle was already partially contaminated by dust particles during sample preparation. Surface contamination of a particle and surfaces occurs during the probe preparation, sample storage and experiment. As a result, the pull-off forces were initially high due to necking between dusts on the particle and the surface, whereas the forces were usually lower after samples were cleaned via UV-radiation exposure. This demonstrates that the contamination on surfaces has an effect on the adhesion forces and should be minimized.

#### **4.4.4 The Effect of Film Thickness on Pull-off Force of Polymers**

As mentioned previously, the measured pull-off force increases with increasing the thickness of film. However, the results do not agree with an analytical approach by the JKR theory. For a spherical particle-flat surface interaction, the pull-off force is proportional to the radius of the particle and independent of the film thickness in the JKR theory. Although the JKR theory has been mostly used to calculate the adhesion energy from the pull-off force in a polymeric particle-surface system in previous studies, there are some issues in using the JKR equation. It is assumed in the theory that the adhesion energy is a constant over the contact area and does not change with either the time of contact or the load applied between the contact surfaces. This assumption is controversial and sometimes not true. When the adhesion energy changes with both the

load and the loading time, the JKR curves between load and contact area do not coincide for loading and unloading [11,12,13].

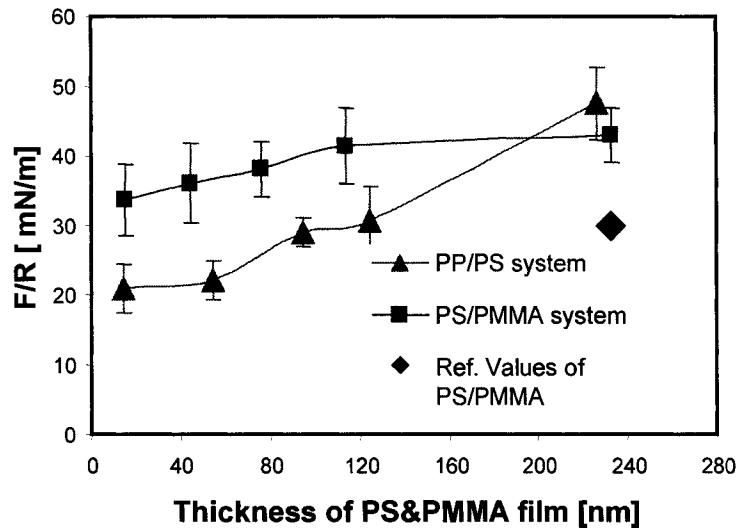


**Fig. 4-11.** Graph of the normalized pull-off force (by the radius of the polymer particle) versus film thickness (♦ value is the normalized pull-off force for PS/PMMA system from a previous study [9])

Recently, Yang [14] has analytically shown that the pull-off force is independent of the film thickness for the system of rigid sphere-thin film under assumption of the contact radius much larger than the film thickness. The contact radius is proportional to  $1/3$  power of the sphere radius and the square root of the film thickness when the sphere is detached from the film. In a conical indenter system, however, the pull-off force depends on the film thickness. For a friction condition between a film and a substrate, the pull-off force is proportional to the square root of the film thickness, while it is proportional to  $3/4$  power of the thickness for the fully contact condition between them. Unfortunately, we have not investigated the contact area when the polymer particle was loaded on the surface. Consequently, the ratio of the contact radius to the film thickness was not precisely determined in this study. Thus, it is not apparent whether this analytical

approach can be applied to the polymeric systems since the polymer particles used might also deform. The contact interface between the rigid indenter and the thin film is assumed to be frictionless in the Yang's analysis. The dependence of the film thickness on the pull-off force is not clearly understood. A better approach should consider the effect of sticky contact between a polymer particle-polymer surface system.

#### **4.4.4.1 T-test of Pull-off Force Results**

In order to ensure the effect of film thickness on pull-off force, an attempt was made to compare statistically pull-off force results between different film thicknesses. An independent two-sample t-test was performed using statistical software, MINITAB (Minitab Inc.) From t-tests in PS/PMMA system (see Appendix I for t-test results), we found there is no data difference of pull-off force results ( $p$ -value  $> 0.05$ ) between cases for 95 % confidence when 114 nm and 233 nm thickness PMMA film were used. As a result, the pull-off force in PS/PMMA system is slightly increased and then reaches a critical value in the range of 114 nm and 233 nm thickness of PMMA film. In the case of the PP/PS system, it is evident that pull-off force increases in the range of 14 nm and 226 nm of PS film with 95 % confidence.

#### **4.4.5 The Effect of Surface Roughness on Pull-off Force of Polymers**

Nanoscale surface roughness significantly affects the adhesion forces between surfaces. Since the size, shape, distribution and mechanical properties of asperities on surfaces affect the actual contact area, the adhesion forces are directly affected. Rumpf [15] proposed the effect of nanoscale surface roughness on the adhesion forces. However, the radius of the asperity,  $r$ , is not easily measured in practice. Rabinovich et al. [16] modified the Rumpf model to determine the adhesion forces with root-mean-square

roughness (rms) instead, which can be easily measured. The modified Rumpf model is then expressed as:

$$F_{ad} = \frac{AR}{6H_0^2} \left[ \frac{1}{1 + R/(1.48rms)} + \frac{1}{(1 + 1.48rms/H_0)^2} \right] \quad (4.8)$$

where A is the Hamaker constant, R is the radius of the contacting particle and r is the radius of the asperity, and  $H_0$  is the distance of closest approach between surfaces in contact, approximately 0.3 nm. In this model, the first term in the bracket represents the interaction of the particle in contact with the asperities on the surface whereas the second term in the bracket expresses the “non-contact” force between the adhering particle and flat surface that are separated by a distance equal to the radius of the asperity. However, the roughness of the experimental surfaces is not adequately described by the geometry proposed in the Rumpf model. For this reason, Rabinovich et al. have proposed a new model that more accurately describes the geometry of roughness on the surface. The proposed model is expressed as:

$$F_{ad} = \frac{AR}{6H_0^2} \left[ \frac{1}{1 + \frac{58R(rms_2)}{\lambda_2^2}} + \frac{1}{\left(1 + \frac{58R(rms_1)}{\lambda_1^2}\right) \left(1 + \frac{1.82rms_2}{H_0}\right)^2} \right] \quad (4.9)$$

The first roughness to be defined,  $rms_1$ , is associated with the longer peak-to-peak distance,  $\lambda_1$ , which is the width of the asperities. The second,  $rms_2$ , occurs on all samples and has a peak-to-peak distance,  $\lambda_2$ , of approximately 250 nm. This equation is based on

the van der Waals interactions and the modified Rumpf model with the improved geometrical consideration.

As we discussed in the previous section, a difference of one order of magnitude between the calculated surface energies (or the work of adhesion) from measured pull-off forces and literature values was observed. This could be due to the nanoscale roughness of the surface on the adhesion force. In other studies, it has been demonstrated that the asperities on a substrate comparable in size to a particle in contact can increase or reduce the actual contact area. [15,16,17,18,23,24,25] In this section, we compare the measured pull-off forces to that predicted by Rabinovich model in order to investigate the effect of the nanoscale roughness of the sample surfaces on the adhesion forces.

#### 4.4.5.1 Surface Roughness Analysis for Polymer Surfaces

To determine the surface roughness of polymer films, three images of PS and PMMA films were scanned by AFM at a scan size of 10×10 μm and 5×5 μm, respectively. The roughness of surface was calculated using the root mean square (RMS) roughness given by:

$$RMS(R_q) = \sqrt{\frac{\sum (Z_i - Z_{ave})^2}{N}} \quad (4.10)$$

where  $Z_i$  is the current  $Z$  value,  $Z_{ave}$  is the average of the  $Z$  values ( $Z$ -axis representing topographical feature height), and  $N$  is the number of points within the given area [17]. Since each film was prepared by spin-casting, the surface roughness was less than 1 nm



in all polymer films. From surface roughness profiles obtained using AFM, the parameters of  $rms_1$  and  $\lambda_1$  were zero in all polymer surfaces.

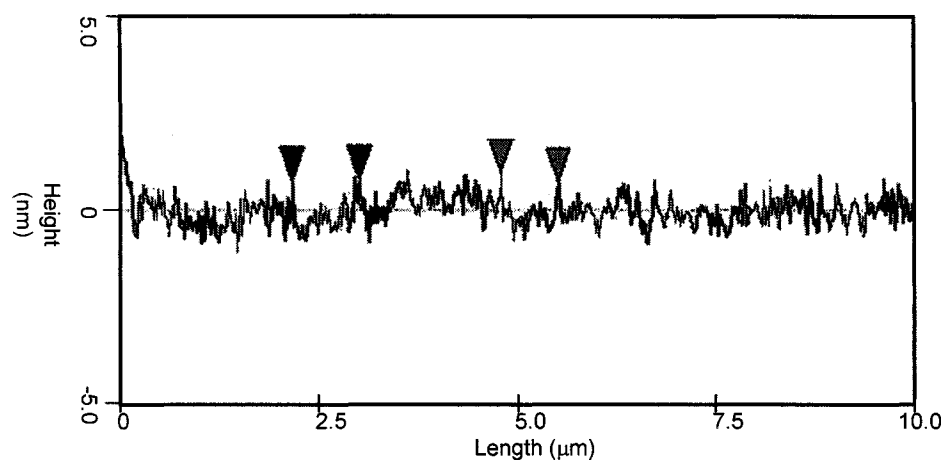


**Fig. 4-12.** A surface roughness profile of PS film with about 230 nm thickness; in all polymer films used in this study, the parameters of  $rms_1$  and  $\lambda_1$  can be regarded as zero. (Height data scale: 10 nm)

The second root mean square roughness,  $rms_2$ , was obtained from the analysis of all images of each film. It varied from 0.3 to 0.6 nm, which is very close to that of silicon wafer, 0.17nm [18]. It was expected that the roughness of the surface should be proportional to the thickness of the deposited film. However, the RMS did not increase with thickness of the film. Since PS and PMMA are amorphous polymers, the roughness of the polymer film prepared by spin-casting did not depend on the thickness of polymer film. The RMS was inconsistent due to partial contamination on the surface. The second peak-to-peak distance,  $\lambda_2$ , is taken as approximately 250nm according to Rabinovich's work.

#### 4.4.5.2 Comparison of Measured Pull-off Forces to Rabinovich Model

Comparison of measured pull-off forces to the modified Rumpf model and Rabinovich model is shown in Fig. 4-13. To calculate the adhesion forces by two models,

Hamaker constants for the polymers used were found from literature [19]. From the graph, we see that the modified Rumpf model underestimates the pull-off forces in the systems investigated in this study. It should be noted that the Rumpf model predicts a decrease of more than two orders of magnitude in spite of only 1 nm increase of RMS in the current systems. This is because the first term, the contact term, in equation (4.8) dominates. On the other hand, the experimental values are found to be close to the values calculated by Rabinovich model except for the cases of a PP particle on the PS film made from 0.2 and 0.5 wt.% solutions. While the contact term proportionally dominates the adhesion force calculation with increasing RMS roughness in the Rumpf model, Rabinovich defines two scales of RMS roughness in geometry of the surface and thus, does not have the same limitation. As a result, Rabinovich's prediction provides closer values to our measured values than those calculated by the Rumpf model.

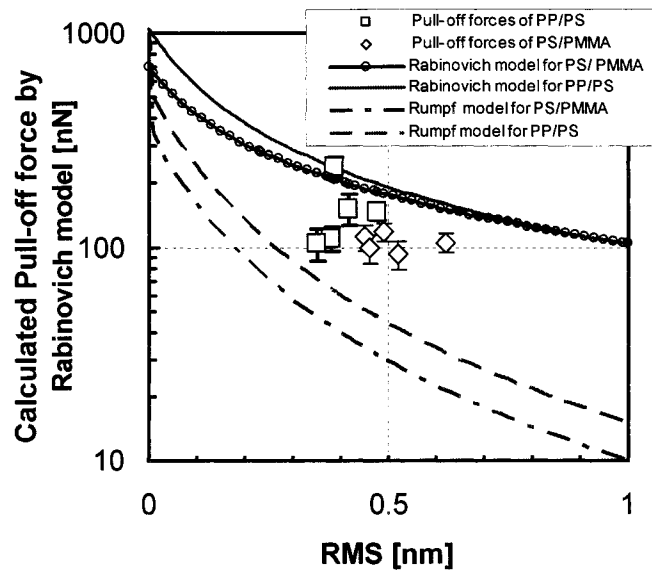


**Fig. 4-13.** Comparison of measured pull-off forces with values predicted by the modified Rumpf model and the Rabinovich model. The surface roughness affects the dramatic decrease.

This result proves that the secondary roughness plays a significant role in controlling the adhesion force, especially where the radius of a particle in contact is much larger than the surface roughness. In this investigation, we assume that the van der Waals forces nearly dominate the polymer particle-surface interactions because all the samples are nonpolar polymers. Therefore, Rabinovich model is used to predict the adhesion force. However, we still note a discrepancy between the theoretical and measured values. A reason for the discrepancy is that the local deformation of the particle or the surfaces of polymer is ignored. A precise Hamaker constant is also required to determine adhesion forces in Rabinovich model. Frank et al. [20] have revealed that the physical properties of spin-cast polymer films can differ substantially from those of corresponding bulk materials and the Hamaker constant derived from the refractive index value of thin polymer films is lower than that of bulk materials from the literature. In addition, the roughness of the particle surface was not investigated. Several studies have reported that asperities on a compliant particle will flatten out during the force measurement with high loads [21]. It is not clear that this would happen in our systems since plastic deformation was not confirmed. However, we suspect that plastic deformation at nanoscale does occur. To better analyze the adhesion forces, plastic deformation should be also considered since it causes an inconsistent contact area between a particle and surface.

In spite of some defects, the Rabinovich model gives a more accurate value compared to the nearly 5-10 times overestimation of adhering by other models such as the JKR model. It will be demonstrated that a significant decrease of the adhesion force over a factor of five was experimentally observed due to surface roughness as small as 1nm.

## 4.5 Conclusions

Polymers are widely used in many applications in industry. Atomic force microscopy has been recently developed for the technology of surface analysis and has provided abilities for the study of surfaces and their interactions at the nanometer level. Recently many experimental techniques to characterize properties of polymer have been improved by using AFM, since surface composition and topography play an important role in properties of the polymer. The contact mode in AFM where the tip scans the sample in close contact with the surface is the common mode used in AFM while the tapping mode has been developed for high-resolution topographic imaging of sample surfaces that are easily damaged, such as polymer thin films. AFM force-distance curve analysis can help characterize the properties of polymer surfaces.

AFM can also be used to determine adhesion forces between polymer surfaces. The measured pull-off force can be used to provide a local estimate of surface energy of materials. Two systems of polymer particle-polymer surface have been investigated to determine the adhesion force by means of the pull-off force measurement using AFM. The results show a range of adhesion forces between 70-280 nN for the PP/PS system and 60-180 nN for the PS/PMMA system. However the results are scattered over a range of values in both systems. This could occur due to various factors such as maximum applied load, loading/unloading cycle, sample contamination, and asperities on the sample surfaces. Thus, more systematic work is needed to fully reproduce the results. It is also found that the measured pull-off force increases with increasing polymer concentration of the cast solution (i.e. film thickness). Therefore, the thickness of the polymer film may affect polymer particle-polymer surface interactions. At present, we

can not clearly explain the dependence. We found a difference of almost one order of magnitude for the values of the measurement pull-off force when compared with the calculated values by JKR model. Once again, this discrepancy depends on surface roughness (relative to the curvature of the tip), tip shape uniformity, and other factors. For this reason, the effect of roughness of the sample surfaces on the adhesion force has been considered using the Rabinovich model. Unlike the JKR model, the Rabinovich model matches closely with the measured pull-off forces. It is evident that the surface roughness influences the adhesion force due to the reduction of actual contact area. Therefore, surface roughness should be taken into account when interpreting the adhesion force.

Compared the work of adhesion measured from the pull-off force with the fracture energy in PS/PMMA system,  $10^3\sim 10^4$  orders of magnitude were observed. A dependency is mainly attributed to the mechanism of entanglement at the interface when the DCB test was used to determine the intrinsic adhesion. This indicates that a direct measurement using AFM is a very attractive technique for determination of the intrinsic adhesion, especially at microscopic or sub-microscopic levels. AFM technique provides a promising approach for studying polymer surfaces and adhesion.

## REFERENCE

- [1] Martin Götzinger and Wolfgang Peukert, *Powder Tech.* **130**, pp 102-109 (2003)
- [2] Sergei S. Sheiko, *Advances in Polymer Science* **151**, pp 61-174 (2000)
- [3] MultiMode™ SPM Instruction Manual, Digital Instruments
- [4] B.D. Patner and V.V. Tsukruk, *Scanning Probe Microscopy of Polymers*, ACS Symposium Series **649**, pp 5-11 (1996)
- [5] G.A. Willing, T.H. Ibrahim, F.M. Etzler, and R.D. Neuman, *J. Colloid and Interface Science*, **226**, pp185-188 (2000)
- [6] B.V. Derjaguin, *Kolloid Zeits*, **69**, pp 154-164(1934)
- [7] J. Israelachvili, *Intermolecular and Surface Forces (2<sup>nd</sup> ed.)*, Academic Press: London (1992)
- [8] M. Reitsma, V. Craig, and S. Biggs, Conference paper of the 27th Australasian Chemical Engineering Conference (CHEMECA 99) (1999)
- [9] K. Feldman, T. Tervoort, P. Smith, and N.D. Spencer, *Langmuir*, **14**, pp 372-378 (1998)
- [10] A. El Ghzaoui, *J. Appl. Phys.*, **85**, pp 1231-1233 (1999)
- [11] P. Silberzan, S. Perutz, E. J. Kramer, and M. K. Chaudhury, *Langmuir*, **10**, pp 2466-2470 (1994)
- [12] D. Ahn, and K. Shull, *Macromolecules*, **29**, pp 4381-4390 (1996)
- [13] S. Pertuz, E. J. Kramer, J. Baney, C. Y. Hui, and C. Chen, *J. Polym. Sci. Part B: Polym. Phys.*, **36**, pp 2129-2139 (1998)
- [14] F. Yang, *J. Phys. D: Appl. Phys.*, **35**, pp 2614-2620 (2002)
- [15] H. Rumpf, *Particle Technology*, Chapman & Hall: London/New York (1990)
- [16] Y. I. Rabinovich et al., *J. of Colloid and Interface Science*, **232**, pp 10-16 (2000)
- [17] E.R. Beach, G.W. Tormoen and J. Drelich, *J. Adhesion Sci. Technol.*, **16**, pp 845-868 (2002)

- [18] Y. I. Rabinovich et al., *J. of Colloid and Interface Science*, **232**, pp 17-24 (2000)
- [19] S. Wu, *Polymer Interface and Adhesion*, Marcel Dekker: New York (1982)
- [20] C. W. Frank et al., *Science*, **273**, pp 912-915 (1996)
- [21] M. Reitsma, V. Craig, and S. Biggs, *International J. of Adhesion & Adhesives*, **20**, pp 445-448 (2000)
- [22] G. F. Meyers, B. M. Dekoven, and M. T. Dineen et Al., *Microstructure and Microtribology of Polymer Surfaces*, ACS Symposium Series **741**, pp 190-211 (1999)
- [23] G. Toikka, RA Hayes, and J. Ralston, *J. of Colloid Interface Sci.*, **180**, pp 329-338 (1996)
- [24] DM Schaefer, M. Carpenter, B. Gady, R. Reifenberger, LP DEmejo, and DS Rimai, *Fundametnals of adhesion and interfaces*, VSP: Utrecht (1995)
- [25] H. Mizes, *J. of Adhesion*, **51**, pp 155-165 (1995)

# CHAPTER 5

## Influence of Interfacial Adhesion on Impact Properties of Polymers

### 5.1 Introduction

Blending two or more polymers or copolymers is a widely accepted method for producing new materials in industry. Such a process often provides a new material having better properties than its constituents due to desirable combination of characteristics, e.g., impact strength. Impact strength is one of the most important mechanical properties of polymer blends since it determines to a large extent, the utility of these materials in consumer applications. In general, the interfacial adhesion between the dispersed particles and the matrix plays an important role in the toughening of polymers. The effect of interfacial adhesion on the impact strength has been of great interest because low adhesion at the interface due to high interfacial tension may lead to poor mechanical properties. For a constant interfacial adhesion, it has been shown that the impact strength is influenced by morphological parameters. It has been found that several characteristics of a polymer blend such as the size of dispersed particles, the size distribution and volume fraction of dispersed particles influence the impact properties of a blend [1].

In this chapter, we will investigate the morphology of a polystyrene/polypropylene blend with different weight ratio compositions and the influence of interfacial adhesion between the dispersed phase particles and the matrix phase on the mechanical properties of the blends, especially impact strength, and the change of the properties experienced upon the addition of a compatibilizer into the polymer blend. In addition, the effect of



particle size and the interparticle distance of the minor phase blended with the compatibilizer in the matrix phase will also be presented.

## 5.2 Toughened Polymers

Glassy polymers, such as polystyrene have properties which are suitable for many applications but they mostly tend to be brittle particularly when notched or subjected to high strain-rate impact loading. For this reason, toughened polymers have been developed in which a glassy polymer matrix is toughened by means of blending with a second rubbery phase which is dispersed as particles in the glassy matrix. The particles are usually spherical and the second phase is above its glass transition polymer,  $T_g$  (i.e., rubbery polymer). This can lead to a significant enhancement in the mechanical behavior of the polymer.

A well-known example is high impact polystyrene (HIPS), in which the addition of a small amount of co-polymerized polybutadiene provides a considerable improvement in elongation to failure. In general, the failure mechanism for such polystyrene is crazing. This crazing involves the absorption of energy, and most methods of toughening brittle polymers involve modifying the polymers to obtain high levels of crazing or shear yielding. This is done by addition of spherical rubber particles that have a Young's modulus about 3 orders of magnitude lower than that of the matrix glassy polymer [2]. This causes a stress concentration near the equators of the particles while mechanical deformation occurs. This stress concentration leads to crazing around every particle and consequently stress distributes over a large volume of material rather than just at the crack tip. Thus, the polymer can absorb a large amount of energy during deformation.

It has been reported that there are many factors that influence the molecular and morphological structures of the rubber-toughened polystyrene. The most important characteristics of these two phase blends are molecular weight of the matrix, phase volume ratio, particle size, size distribution, interfacial bonding, and rubber crosslinking density. In general, the impact strength of the rubber/PS blend increases with increasing rubber phase volume, but good adhesion between the rubber particles and the PS matrix is critical. If the interfacial adhesion between the rubber particles and the PS is weak, it leads to formation of voids at the interface and to initiation of cracks [3,4]. In studies on toughening PS, it has been reported that rubber particles of 1 to 3  $\mu\text{m}$  in diameter and strong interfacial adhesion are required for effective toughening [5,6]. More recently, many studies have shown that toughening of PS is effective with bimodal rubber particle size population if most particles are below 1 $\mu\text{m}$  [7,8]. Moore studied rubber-reinforced polystyrenes prepared by graft copolymerization using various butadiene polymers and copolymers, and concluded that a particle size of over 2  $\mu\text{m}$  with a polybutadiene molecular weight of over 110,000 was required to obtain significant reinforcement [9]. In the other work, it was found that the optimum rubber particle size for toughening PS was influenced by the interfacial adhesion, with the best results obtained for 0.2  $\mu\text{m}$  particles of acrylonitrile– butadiene rubber [10]. As a result, it shows there are conflicting results in the literature with respect to particle sizes, particle distribution, and the importance of interfacial adhesion. Nevertheless, though the previous experimental results in the literature seem to be inconsistent due to various factors, three conditions are agreed upon to be essential to produce a toughened polymer [11]:

- (i) The glass transition temperature of the elastomeric component should be well below the test temperature. To have good impact strength at room temperature, the rubber should have a  $T_g$  at least 20-40°C lower, to compensate for the high rate of deformation in an impact test.
- (ii) The elastomeric material must form a dispersed phase in the brittle polymer.
- (iii) There must be good adhesion between the two phases.

As mentioned earlier, combination of different polymers into multiphase systems has been performed to produce new attractive materials. Despite enhanced performance of blends of different polymers in industry, the advantage is not evident if there is weak interfacial adhesion and poor stability of the dispersed phase. The incompatibility between two components in blends leads to a sharp and weak interface giving poor mechanical properties. In addition, high interface tension and low adhesion between two phases give poor stress transfer across the interface in that a fracture path may preferentially follow the weak interface between the polymer phases. This poor interfacial adhesion can be modified by the addition of compatibilizers which can significantly improve the mechanical properties of the blends. Adhesion can be improved by increasing the similarity in solubility behaviour of the two components by using a copolymer for one or both of the polymers. For the blends of PS/PP, polystyrene-block-poly(ethylene-butylene)-block-polystyrene (SEBS) or ethylene vinyl acetate (EVA) can be used as the compatibilizers to enhance phase adhesion. As seen in Fig. 5-1, SEBS is a thermoplastic triblock copolymer composed of a rigid segment, polystyrene, and a compliant rubbery segment, poly(ethylene-butylene) (PEB) in chemical structure. Thus, SEBS adheres to both PS and PP components of the blend due to the affinity of the end

blocks with PS component and the expected affinity of the EB (ethylene-butylene) midblock with PP [12].

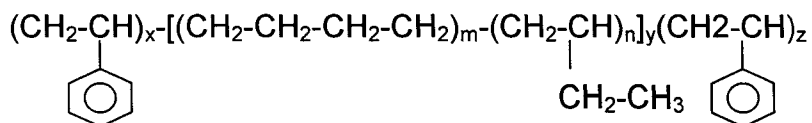


**Fig. 5-1.** Structure of poly(styrene)-*block*-poly(ethylene-butylene)-*block*-poly(styrene) (SEBS). The polymer used in this work contains 30% of PS and 70 % of PEB copolymer

In the case of using EVA as a compatibilizer, both affinity and polarity concepts are important. In general, free radicals have a tendency to gain or loss electrons, and hence they have the character of being electrophilic or nucleophilic. A free radical electrophilic reaction is caused by electron withdrawal, whereas a free radical nucleophilic reaction is caused by electron release. An electrophilic radical will then add to a monomer containing an electron releasing group, while a nucleophilic radical acts reversely. In EVA copolymer, the vinyl acetate group tends to withdraw electrons, while in polystyrene the phenyl group tends to release electrons. The transition states for addition to the opposite monomers are thus stabilized [13].

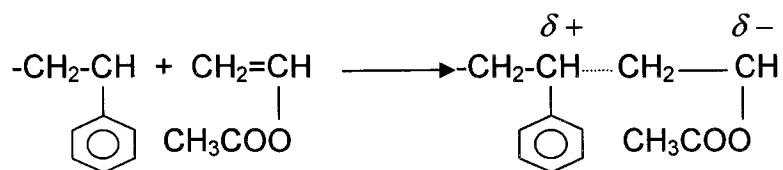


**Fig. 5-2.** Free radical reaction in polystyrene and vinyl acetate group. The phenyl group releases the electrons and the vinyl acetate group withdraws the electrons.

Impact strength is one of the most important mechanical properties of polymer blends and it has generated great interest since it determines the utility of these materials.

Impact testing is generally performed with a swinging or a dropping weight. The objective of these tests is to measure the amount of energy transferred or lost from the striking body. For bodies without flaws or notches, the transferred energy consists of energy to initiate a crack and energy to propagate a crack. The two common swinging weight impact test methods are the Charpy and Izod methods which have been widely used to measure in past. In these methods, a notched bar or an unnotched is impacted by a striker-pendulum released from a standard height. The difference between the starting height of the weight and the height that the pendulum swings past the impact is a measure of the amount of energy absorbed by the impact. The shorter the after-swing, the greater the energy absorbed by the specimen and hence the greater impact resistance or toughness. The absorbed energy is expressed per unit cross section area of specimen. Recently the drop-weight method has been preferred for impact testing of materials because a greater range of testing parameters is possible and the results are more readily analyzed. A typical drop-weight testing apparatus is shown in Fig. 5-3.

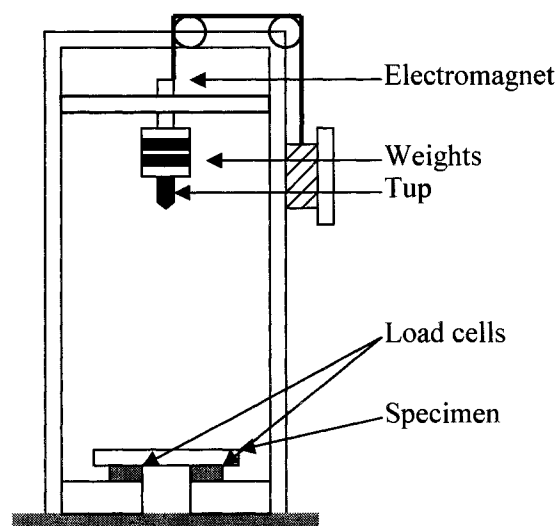


**Fig. 5-3.** Drop weight impact tester

Drop-weight testing has important advantages compared to other impact tests. [14]

- (i) It is applicable for molded samples, molded parts, etc.
- (ii) It is unidirectional with no preferential direction of failure. Failures originate at the weakest point in the sample and propagate from there.
- (iii) Samples do not have to shatter to be considered failures. Failure can be defined by deformation, crack initiation, or complete fracture, depending on the requirements.

In this drop-weight impact test, impact energy depends on the mass and the drop height, and impact velocity. The mass may remain consistent while the drop tower heights are changed slightly to obtain different impact energies and different impact velocity values. On the other hand, the mass may be changed and the drop tower height kept constant to obtain different impact energy values at a constant impact speed. Thus, drop-weight impact test is carried out either under conditions where the impact energy is far in excess of that required to penetrate the specimen or at low levels of impact energy so that damage resistance and the possible initiation of a crack can be observed.

## **5.3 Experiments**

### **5.3.1 Materials and Blends Preparation**

The polymers used in this study were a matrix of polystyrene (MFI 8.0 g/10min) provided by Dow Chemical Co. (styron 666D) and a minor phase of polypropylene (MFI 1.6 g/10min) supplied by ATOFINA Petrochemicals, Inc. (ATOFINA polypropylene)

The blends of PS and PP were prepared by melt extrusion in a 25mm-diameter Mega twin-screw extruder (Coperion Corp., Model: ZSK-25) at 100 rpm with different weight compositions. The total feed rate of materials was 3.0kg/h and each feed rate of PS and

PP were changed to obtain the required blend composition. Mixing speed was also investigated in the range of 100-250 rpm with a fixed weight ratio (80/20) of PS/PP blend in order to vary the PP particle size. The temperatures of barrels 1~9 in the extruder were room temperature for barrel 1, 180°C for barrel 2, and 200°C for barrel 3~9, respectively and the die pressure for all runs was between 120~160 psi. The blends were then immediately quenched in a water bath and subsequently pelletized. The pelletized blends were dried in a vacuum oven overnight at 80 °C to remove remaining volatiles inside the pellets. To investigate the effect of compatibilizer, polystyrene-block-poly(ethylene-butylene)-block-polystyrene (SEBS), triblock copolymer containing 30 % styrene content was used in this study. The SEBS supplied by Shell Chemical Company (CAP-75G) was mixed into PS/PP (80/20) blend with different compositions (6.7 % wt.%, 12.5% wt.%, and 17.6 % wt.%) in the twin extruder at the same processing conditions as when prepared for binary blends of PS/PP. For impact testing, 6.7 % wt.%, 12.5% wt.%, and 17.6 % wt.% SEBS were used to prepare the compatibilized PS/PP blend specimens.

**Table 5-1. Properties of used polymers in this study**

Polymer (Abbreviation)	Supplier (Product No.)	Molecular weight (M <sub>w</sub> , g/mol)	Density (kg/m <sup>3</sup> )	Glass Temp. (T <sub>g</sub> , °C)	Melt Flow Index (MFI, g/10min)
Polypropylene (PP)	Atofina (Atofina PP)	60,000	942 (25°C) <sup>a</sup> 817 (200°C) <sup>b</sup>	-23	1.6
Polystyrene (PS)	Dow (Styron 666D)	160,000	1050 (25°C) <sup>a</sup> 1022 (200C) <sup>b</sup>	105	8.0
Styrene-ethylene/ butylenes-styrene (SEBS)	Shell (CAP-75G)	75,000	920(200C) <sup>b</sup> -	-	

a. Provided by supplier

b. Calculated according to Van Krevelen [38]

After preparing binary PS/PP blends and ternary PS/PP/SEBS blends, the pelletized blends were moulded with Teflon sheets using a Carver Model C laboratory press under 2 tons of loading pressure using an aluminum mold into 10cm × 10cm plate with a thickness of 3 mm. This plate was trimmed to prepare specimens for impact testing. The molding temperature was 200°C and the preheated time of 7 min and the annealing time of 5 minutes were applied.

### 5.3.2 Impact Test

Impact strength of unnotched samples was measured using a drop weight impact tester, model Instron Dynatup-8250. The samples were impacted at 3.0 m/s at room temperature. The hammer mass of 1.813 kg was used to generate the maximum load up to 1.557kN, respectively. The time of range of 15 msec was recorded the load history. Five samples were tested in each case at identical experimental conditions and their average impact energies were calculated.

In this drop weight impact test, load-time or load-displacement curves are used to investigate the impact properties. The initial peak in load-time curves corresponds to the crack initiation. The trace beyond the maximum load corresponds to crack propagation. The area under the load-time curve,  $\int P dt$ , is called the impulse, where  $P$  is the load. Displacement using the load measurement can be obtained based on Newton's 2<sup>nd</sup> Law:

$$mg - P(t) = ma(t) \quad (5.1)$$

where  $g$  is the acceleration due to gravity,  $m$  is the mass of falling weight, and  $a$  is the acceleration of falling weight. Using equation (5.1), we can have



$$a(t) = g - \frac{1}{m} P(t) \quad (5.2)$$

$$v(t) = \int_0^t a(t) dt \quad (5.3)$$

$$x(t) = \int_0^t v(t) dt \quad (5.4)$$

Thus, total absorbed impact energy is calculated by the integration of the product of load and velocity with respect to time. The total energy absorbed during impact is given by then [22]:

$$E = \int_{t_0}^{t_f} P v dt \quad (5.5)$$

where  $t_0$  is the time of initial impact, usually considered as 0, and  $t_f$  is the time for completion of penetration. The impact energy consists of the initiation energy,  $E_i$  and the propagation energy,  $E_p$ . In this study, this total absorbed energy during impact is employed to compare to the impact property of each polymer blend.

### 5.3.3 Analysis of Interfacial Adhesion

Unfortunately, there is no satisfactory method to measure the interfacial adhesion between the matrix phase and the dispersed phase particles. Thus, the relative measurement of PS surface/PP particle interfacial adhesion was carried out using Atomic Force Microscopy in a previous chapter. The varying degree of interfacial adhesion between two phases in the blend can be obtained by changing the level of compatibilizer

due to the modification of the interface. To investigate the influence of compatibilizer for the interfacial adhesion in PS/PP blend, the PS surface was modified by spin-coating a layer of copolymer with thickness approximately the radius of gyration,  $R_g$ . A dilute copolymer solution was employed to make a thin film on the PS surface. The work of adhesion calculated by the pull-off force measurement using AFM was then compared to that of uncompatibilized PS/PP system. This data was used to investigate the effect of interfacial adhesion on the increase in impact properties in compatibilized PS/PP blends.

#### 5.3.4 Scanning Electron Microscopy (SEM) and Images Analysis

To analyze the morphology of blends, particle sizes and interparticle distances, the specimens were cryogenically fractured and attached to an SEM sample holder using carbon tape. They were then carbon coated with a sputtering machine and imaged in a scanning electron microscope (SEM, Hitachi S2700). Images with 300 up to 400 PP particles were taken for each system and investigated by using SigmaScan Pro5, an image analysis program (SPSS Inc.), to obtain average particle sizes. To measure the diameters of the dispersed phase, this study was followed by a method in previous works [16,17]. The particle size of the dispersed phase was measured with SigmaScan Pro5 software. The area of each particle was determined and the equivalent diameter was obtained by assuming that the particle cross-section was circular in shape, i.e.:

$$D_{eq} = \sqrt{\frac{4A}{\pi}} \quad (5.6)$$

This equivalent diameter ( $D_{eq}$ ) was used to obtain the number average diameter ( $D_n$ ) and volume average diameter ( $D_v$ ):

$$D_n = \frac{\sum_{i=1}^n D_{eq,i}}{n} \quad (5.7)$$

$$D_v = \frac{\sum_{i=1}^n D_{eq,i}^4}{\sum_{i=1}^n D_{eq,i}^3} \quad (5.8)$$

where  $n$  is the number of particles. More than 300 particles were used to determine the average diameter of each blend. The polydispersity of particle was determined as  $D_v/D_n$ . The shape factor of the particles was also calculated. It was determined from  $4\pi \times A / P^2$ , where  $A$  is drop area and  $P$  is drop perimeter. A perfect circle has a shape factor of 1.00 and a line has a shape factor of 0.00. The shape factor for dispersed particles obtained from the SEM micrographs was close to 0.86, suggesting that the particles were regarded as spherical shape. The uncertainty on the average diameter measurements by this method is  $\pm 10\%$  [16]. These number average diameter ( $D_n$ ) and volume average diameter ( $D_v$ ) are used as average particle size throughout this study.

### 5.3.5 Transmission Electron Microscopy

Samples for PS/PP (80/20) blend with different concentrations of the compatibilizer were cut by an ultramicrotome at room temperature, and the surfaces obtained were investigated using transmission electron microscopy (TEM) and atomic force microscopy (AFM). The cross section of the blends with a thickness 60~80 nm was imaged using a Hitachi H-7000 TEM.

## **5.4 Results and Discussions**

### **5.4.1 Morphology study of Polymer Blends**

When two incompatible polymers are blended during melt extrusion, one phase is mechanically dispersed inside the other. In other words, one component forms the discrete phase in the other component forming the continuous phase. Therefore, the two incompatible polymers remain separated and form a two-phase system. The discrete phase size is influenced by composition, viscosity ratio and elasticity ratio of the individual components, shear stress, and the interfacial tension between the components [15,16,18]. A characteristic of most immiscible polymer blends is that they spontaneously separate into phases of different compositions. The morphology and the adhesion between components significantly affect the useful physical and mechanical properties of the blends. For uncompatibilized blends such as PS/PP blends, the final particle size increases with the dispersed phase content due to increased coalescence. The particle size distribution also becomes wider at high concentrations of the dispersed phase [19].

In first, SEM analysis was carried out with cryogenically fractured specimens. The micrographs of each sample are shown in Fig. 5-4. All micrographs show a high incompatibility between two polymer phases. As shown, a sharp interfacial boundary still exists even in all cases. In addition, the discrete particle sizes tend to increase with increasing dispersed phase content due to coalescence and eventually a co-continuous phase is detected for PS/PP (50/50) blend. More irregularly shaped holes and a particle size distribution are also shown as the dispersed phase increases. It is obvious that the domain size of particles (PP) is smallest when the dispersed phase content is least. Coalescence occurs during processing at higher contents of the dispersed phase, resulting

in the larger particle size [18]. Void holes in the matrix are found in all of PS/PP blends indicating a poor adhesion between two phases.

On the other hand, Fig. 5-5 shows a reduction in the size of PP particles and a better distribution of the particles in PS matrix by adding a 6.7% wt.% of SEBS to the PS/PP blends, when compared to uncompatibilized blends. In incompatible PS/PP blends, a two-phase morphology with dispersed PP particles in the PS matrix is detected due to high interfacial tension and coalescence. However, rough fracture surfaces deformation, and much finer dispersion are observed in the micrograph of compatibilized PS/PP blends. The analysis of particle size and particles distribution will be present in the next section.

For the PS/PP (50/50) blend, the co-continuous morphology of the PS/PP/SEBS blends is quite different from that of the uncompatibilized PP/PS blend. A new irregular phase forms, which tends to envelop small PP particles, and areas of co-continuity are also found but on a much finer scale when compared to uncompatibilized PS/PP blend. Not only the reduction of interfacial tension but also the distribution of SEBS in PS and PP phases changes the viscosity ratio and influences the morphology development. The fracture surface exhibits a level of plastic deformation, the presence of stretched and broken fibrils of material, which suggests the blend should have a higher strain and toughness. In micrographs of fracture surfaces of compatibilized PS/PP (70/30), we see very small irregular particles embedded strongly in the matrix. Unlike the fracture path in uncompatibilized PS/PP blends follows the phase boundary, in the compatibilized blends perspicuous fractures are mostly observed in PS matrix.

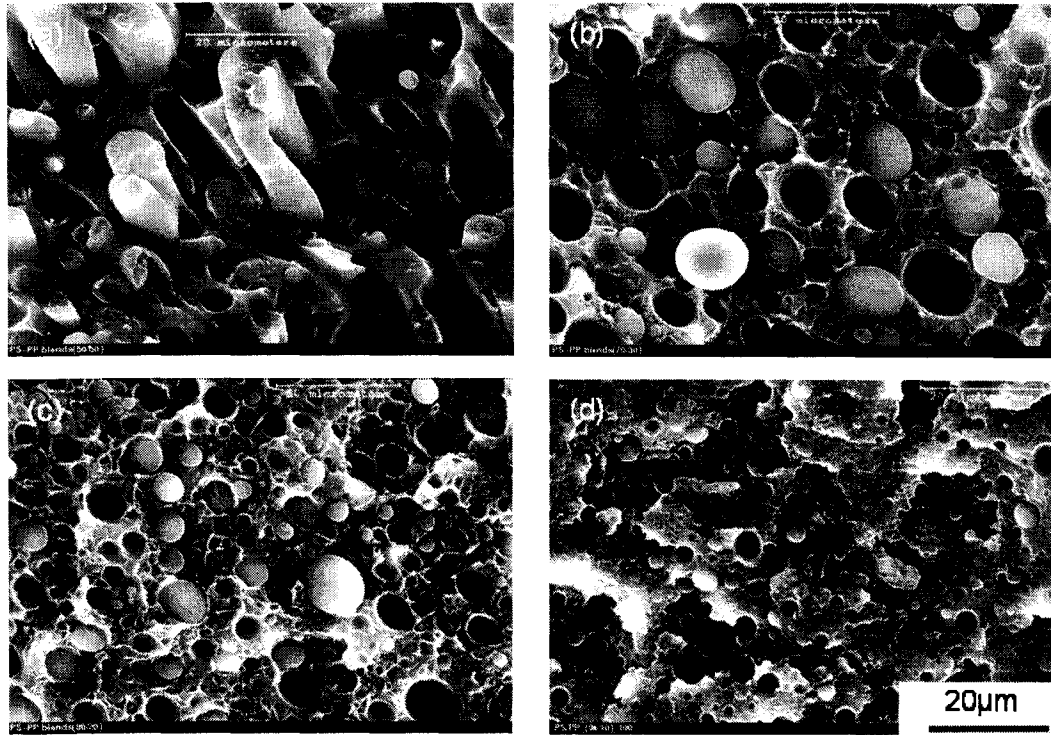


**Fig. 5-4.** Morphology of PS/PP blends with different weight ratios. (a) 50/50, (b) 70/30, (c) 80/20, (d) 90/10 PS/PP blends

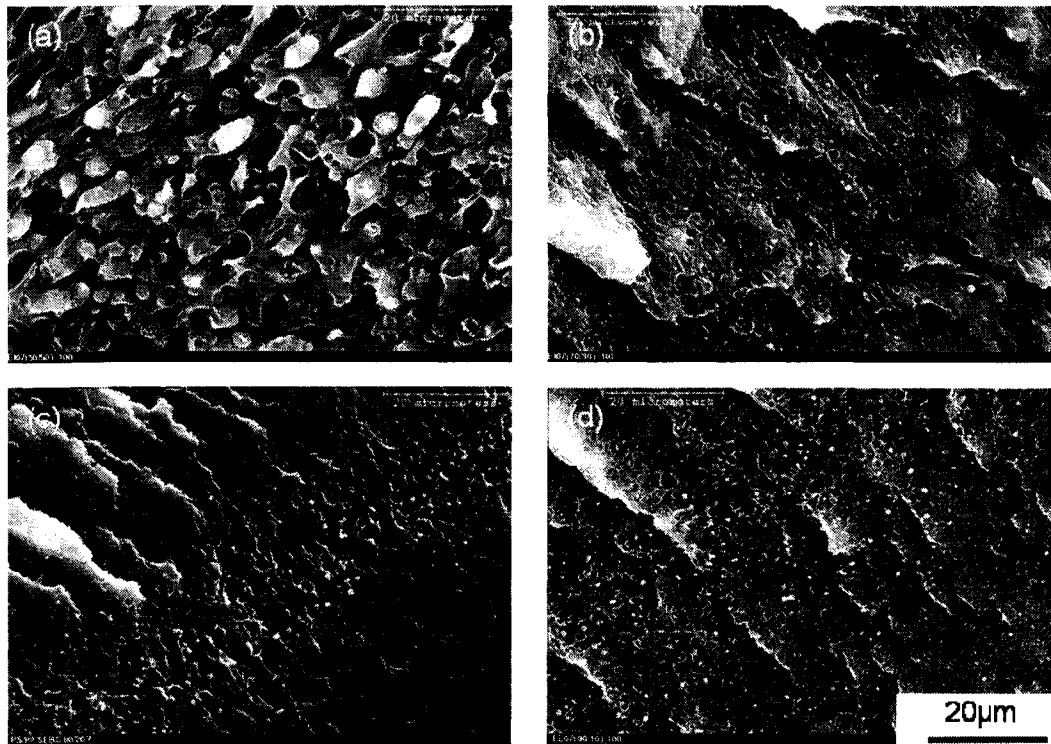
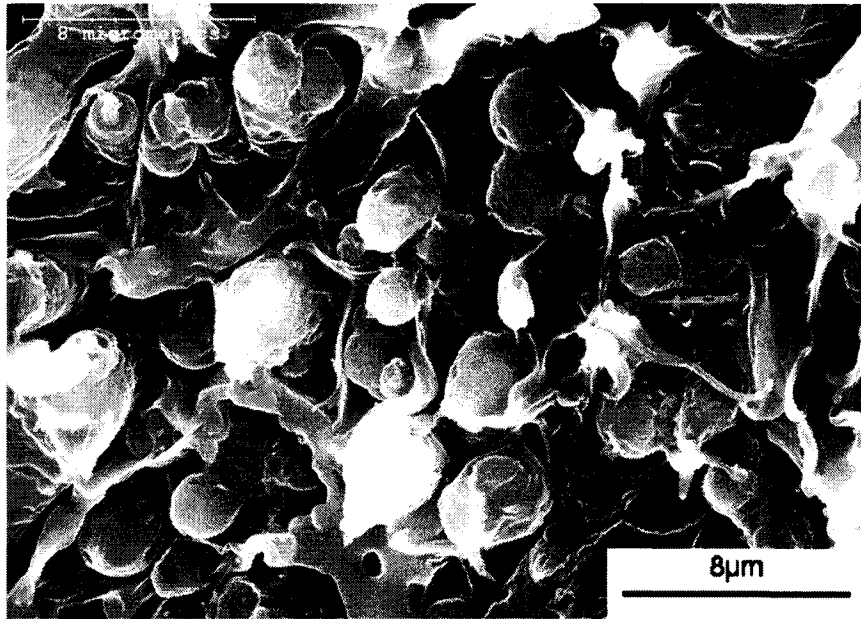
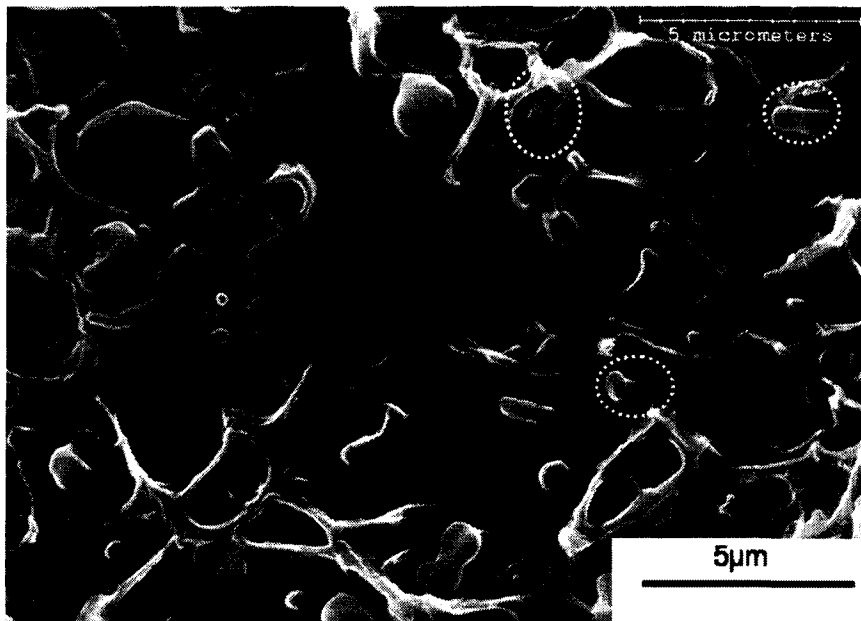


**Fig. 5-5.** Morphology of PS/PP blends with addition of 6.7% wt.% SEBS as a compatibilizer (a) 50/50, (b) 70/30, (c) 80/20, (d) 90/10 PS/PP blends

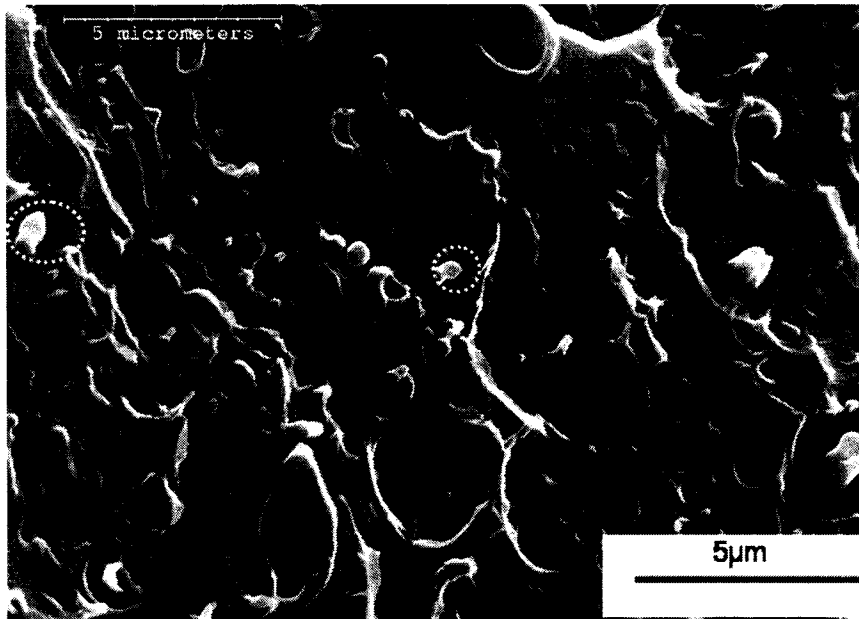


(a)

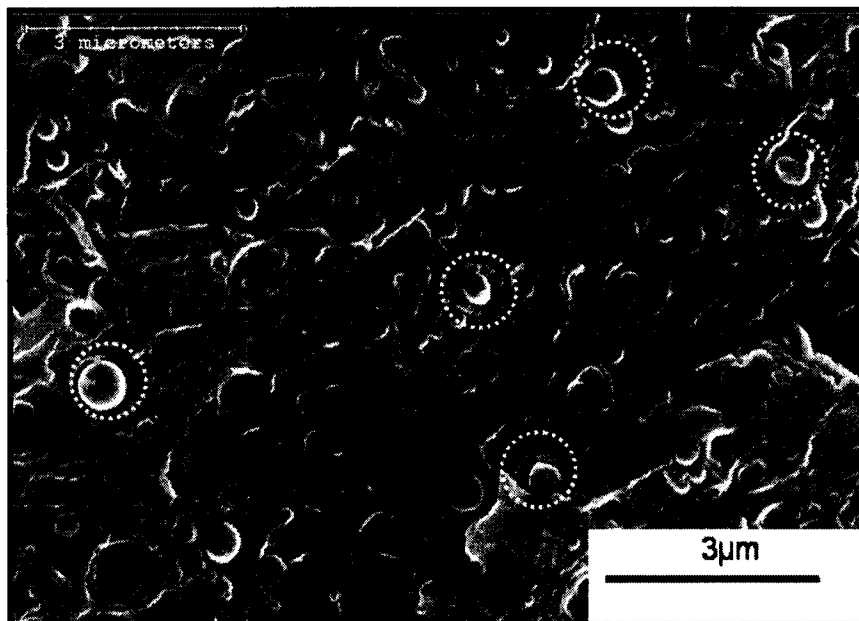


(b)

**Fig. 5-6.** The enlarged micrographs of PS/PP blends with addition of 6.7% wt.% SEBS (a) 50/50, (b) 70/30, (c) 80/20, (d) 90/10 PS/PP blends. The dispersed PP particles connected to the matrix PS are observed in circles.



(c)



(d)

**Fig. 5-6 (cont'd).** The enlarged micrographs of PS/PP blends with addition of 6.7% wt.% SEBS (a) 50/50, (b) 70/30, (c) 80/20, (d) 90/10 PS/PP blends. The dispersed PP particles connected to the matrix PS are observed in circles. .



Furthermore, the phase structure of uncompatibilized blends is coarser compared with compatibilized blends. This means the presence of a compatibilizer led to a finer structure. The fracture surface also shows a pattern that infers different fracture propagation due to the incorporated copolymer. Reduction of particle size and better dispersion of particles were found in the compatibilized PS/PP (90/10) blend. The fibrils connecting the matrix and the dispersed particles, were not clearly observed by the compatibilizer in all PS/PP blends containing SEBS. In some cases, the fibrils connecting the matrix and the dispersed particles were found in the high magnification SEM micrographs of 90/10 PS/PP blend. Noolandi [20] has theoretically revealed that this copolymer is placed at the interfacial area between phases in a polymer blend, increasing the adhesive strengths. On the other hand, micelles were also observed in all blends with the addition of SEBS. This indicates that the rest of the copolymers tend to form micelles in the matrix phase PS.

To investigate the effect of SEBS content on morphology modification of PS/PP blends, different concentrations (1 wt.%, 2wt.%, 5wt.%, 6.7 wt.%, 12.5 wt.%, and 17.6 wt.%) of SEBS were used in PS/PP blends with the fixed weight ratio 80/20. Micrographs of compatibilized blends are shown in Fig. 5-7. As the content of SEBS increases in the blend, the dispersion of particles increases and their size is decreased. This finding demonstrates a better interfacial adhesion and emulsification is obtained by increasing SEBS content. The decrease in size of the dispersed PP particles as well as a new irregular reticulate morphology was observed in compatibilized blends. This behavior was evident as the content of compatibilizer increased in the blends. This suggests that critical amount of a compatibilizer is located at the PS/PP interface, and after saturation of the interface, the rest of the compatibilizer, SEBS in this study, is

distributed in homopolymers, mainly in PS. Such modified morphology also has been found by Sciamanna et al. [25]. They have studied the effect of addition of different compositions of several types of styrene-butadiene-styrene (SBS) triblock copolymers, with different content of styrene, to a fixed weight ratio of PS/PP blend. They have stated that styrene content in the SBS and hydrogenation are important factors to improve the interfacial adhesion of PS/PP blends. The SBS envelops PP particles and connects them into complex PP/SEBS aggregates with a reticulate morphology.

Similar to the SBS copolymer, SEBS consists of the two rigid PS blocks attached by the flexible PEB block. Thus, the styrene block is compatible with PS and the EB block is compatible with PP by an interface layer that enhances the compatibility between PS and PP components. In other words, SEBS can reduce the interfacial tension and improve interfacial adhesion between PS and PP phases. In some cases, SEBS fibrils connecting PP and PS phases were found in high magnification SEM micrographs; however, they cannot clearly distinguish the SEBS phase in the blend. The formation of micelles in the matrix phase PS was also observed. In fact, SEBS is more likely to form micelles or mesophases in the blend as the content increases.

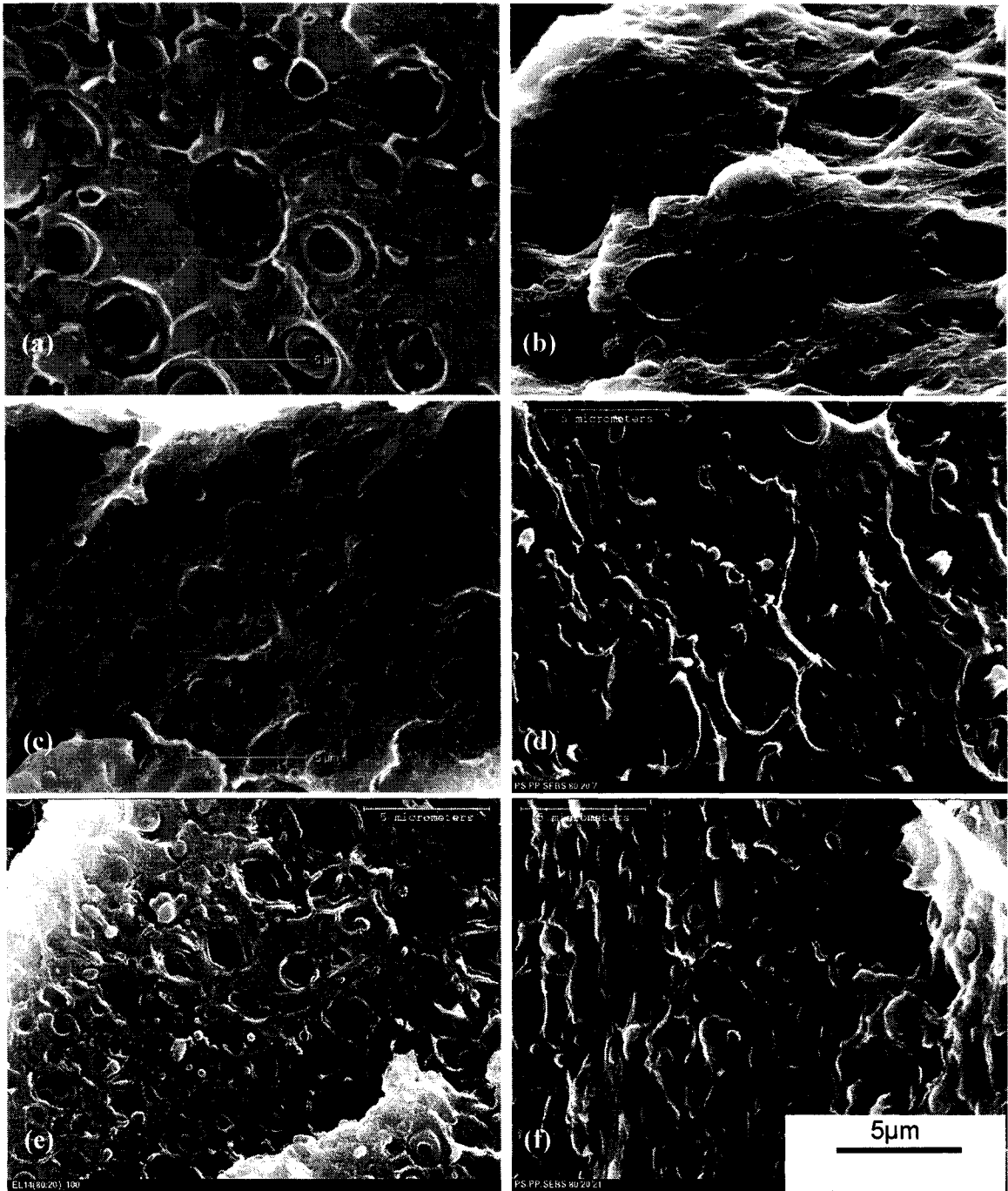


**Fig. 5-7.** Morphology of PS/PP (80/20) blend containing (a) 1 wt.% (b) 2 wt.% (c) 5 wt.% (d) 6.7 wt.% (e) 12.5 wt.% and (f) 17.6 wt.% of SEBS. The fibrils connecting the matrix and the dispersed particles, was observed in PS/PP blend with addition of 1 wt.% and 2 wt.% SEBS.

#### 5.4.2 Mechanical Compatibilization of Polymer Blends

In general, blending of a brittle high-modulus polymer with a ductile polymer with proper interfacial adhesion leads to improvements in mechanical properties (i.e. tensile and impact behavior). However, blending of PS/PP leads to brittle blends since they are thermodynamically immiscible [4, 21]. For this reason, although PS and PP are two important commercial polymers, only a few studies have been done to achieve the most advantageous combination of their properties [21].

In this study, unnotched impact strength of binary PS/PP blends was investigated using a drop weight impact tester, Dynatup-8250. The load-time curves recorded for each composition blend were shown in Fig. 5-8, Fig. 5-9, and Fig. 5-10. As seen in Fig. 5-8, load-time curves for homopolymer PS and PS/PP blend are nearly triangular shaped with no propagation. This indicates pure PS and PS/PP blend are brittle because the applied impact energy is quickly transferred over the specimens, and not absorbed to resist crack propagation. Therefore, all of the specimens were easily broken. As the PP content increased, the maximum load which can be regarded as an indication of a material stiffness slightly decreased, whereas time to the maximum load increased. This indicates that stiffness reduction in conjunction with a small increase of ductility in PS/PP blends with increasing PP content. However, due to a poor interfacial adhesion the impact absorption was not enhanced significantly in the range of 100/0 and 70/30 PS/PP composition. On the other hand, for PS/PP (50/50) blend, the impact energy absorption is larger by about 150 % than that of homopolymer PS due to the co-continuous morphology. A reason for this result is that the ductile PP phase forms cylinder shaped rods instead of spherical particles in the blend and resists breaking.

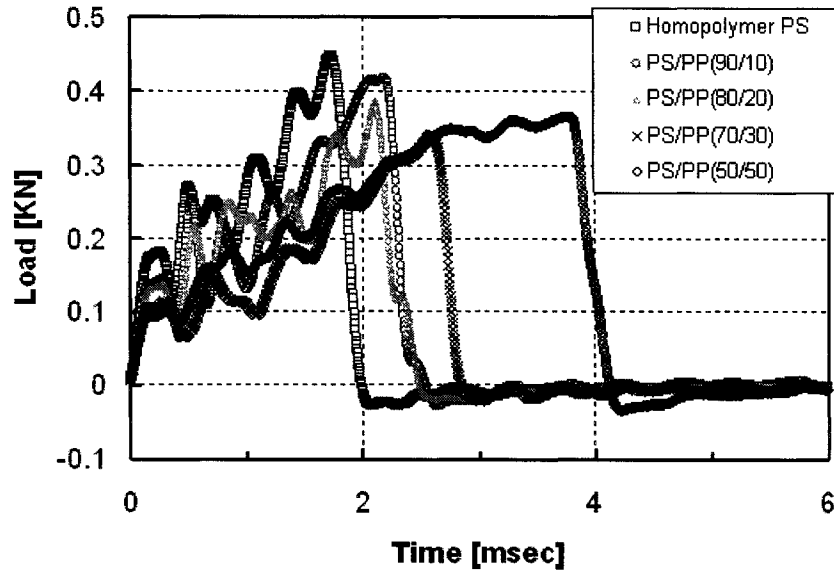


Fig. 5-8. Load-time trace for uncompatibilized PS/PP blends

Table 5-2. The average values of impact test results for uncompatibilized PS/PP blends

	The weight ratio of PS/PP				
	100/0	90/10	80/20	70/30	50/50
Impact energy [J]	8.267	8.266	8.267	8.268	8.285
Energy to max load [J]	1.273	1.374	1.329	1.300	1.995
Total absorbed energy [J]	1.377	1.479	1.436	1.515	2.077
Maximum load [KN]	0.453	0.436	0.359	0.326	0.352
Time to max load [msec]	1.716	2.039	2.324	2.534	3.166
Total time [msec]	1.950	2.405	2.669	3.225	3.932
Deflection at max load [mm]	5.040	5.984	6.823	7.457	9.133
Total deflection [mm]	5.689	6.995	7.783	9.331	11.157

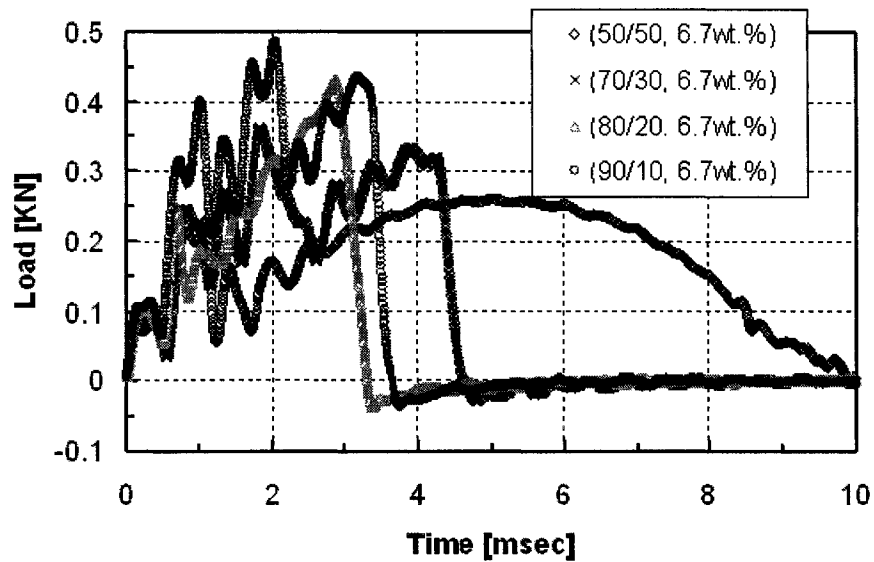
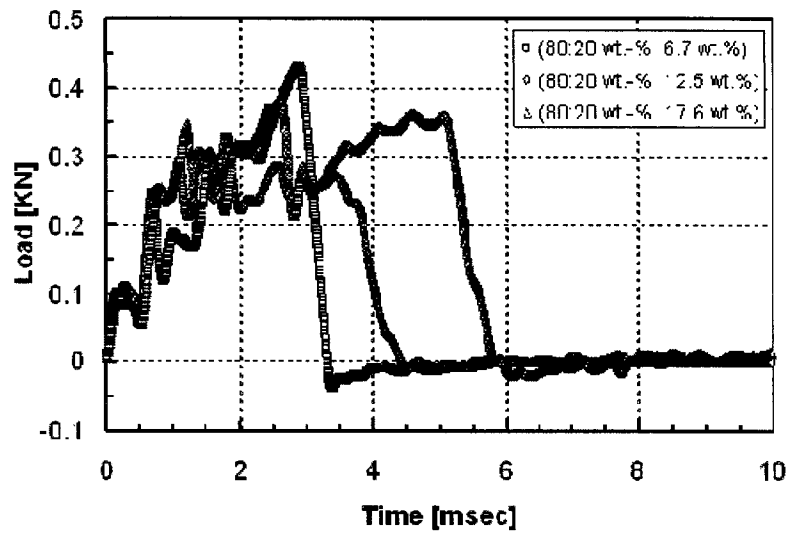


Fig. 5-9. Load-time trace for compatibilized PS/PP blends

Table 5-3. The average values of impact test results for compatibilized PS/PP blends

	The weight ratio of PS/PP			
	90/10	80/20	70/30	50/50
Impact energy [J]	8.280	8.275	8.275	8.264
Energy to max load [J]	1.797	1.643	1.229	2.623
Total absorbed energy [J]	2.826	1.962	1.967	3.780
Maximum load [KN]	0.473	0.366	0.312	0.267
Time to max load [msec]	2.339	2.584	2.702	5.069
Total time [msec]	3.876	3.283	3.917	9.094
Deflection at max load [mm]	6.756	7.508	7.924	14.360
Total deflection [mm]	10.708	9.405	11.168	23.644



**Fig. 5-10.** Load-time trace for PS/PP blends with addition of different concentrations of SEBS

**Table 5-4.** The average values of impact test results for compatibilized PS/PP blends

	Concentration of SEBS in PS/PP(80/20) blend			
	0 wt.%	6.7 wt.%	12.5 wt.%	17.6 wt.%
Impact energy [J]	8.267	8.275	8.278	8.272
Energy to max load [J]	1.329	1.643	1.253	1.684
Total absorbed energy [J]	1.436	1.962	2.072	3.332
Maximum load [KN]	0.359	0.366	0.325	0.417
Time to max load [msec]	2.324	2.584	2.193	2.447
Total time [msec]	2.669	3.283	4.040	5.711
Deflection at max load [mm]	6.823	7.508	6.388	7.101
Total deflection [mm]	7.783	9.405	11.419	15.141

This cylinder shaped phase acts like fibers in the PS matrix and makes it tougher and resistant to an impact in the direction of the cylinder shaped phase.

As explained above, PS/PP blends are brittle and the adhesion between the phases is very weak due to their immiscibility. As a result, stress applied to the blend will not be transferred to the dispersed phase and, therefore, mechanical properties are lower than those predicted by the weighted average of the properties of the individual components [23]. To make these brittle blends into useful polymeric materials with a combination of desirable properties of each component, we need an appropriate modification of the interfacial adhesion. For this reason, block copolymers with blocks having the same or similar chemical compositions to the blend components as the compatibilizer are used to enhance the interfacial adhesion.

In Fig. 5-11, the absorbed impact energy between compatibilized and uncompatibilized PS/PP blends is compared with PP content. As seen in Fig. 5-11, SEBS acting as a compatibilizer obviously improved the impact property in all PS/PP blends. The impact energy increase was about 30 % up to 90 % depending on blend composition. This can be explained using a direct evidence of ligaments of the SEBS triblock copolymer connecting both phases in Fig. 5-6. This improved interfacial adhesion enables the applied stress to be transferred over the dispersed phase. Such stress transfer made it possible for dispersed PP particles to absorb additional energy and dissipate it contributing to better impact properties. The time to maximum load and deflection at maximum load were increased by addition of compatibilizer whereas maximum load was slightly reduced. The enhanced ductility can be also attributed to the butadiene in the SEBS and the size reduction of the PP particles in the blends. Such an improvement of



impact properties by addition of block copolymer for PS/PP blends agrees to the previous studies where styrene-butadiene-styrene triblock (SBS) copolymer was used in PS/PP blends [24,25,26].

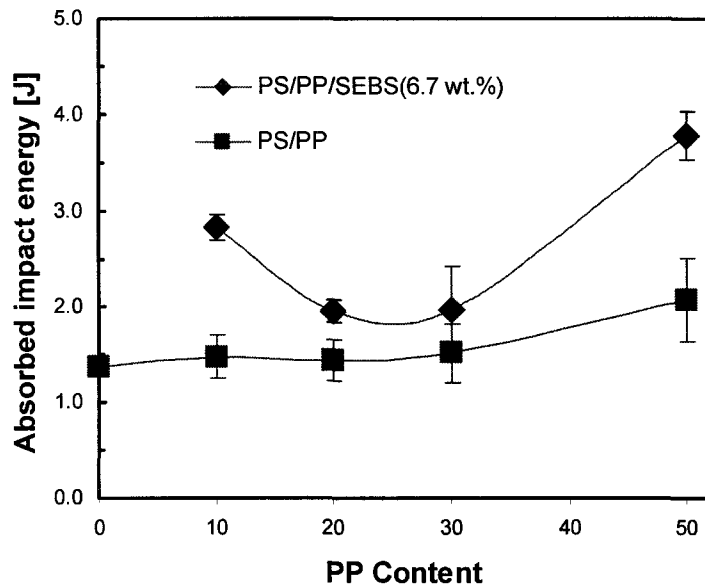


**Fig. 5-11.** Comparison of the absorbed impact energy between compatibilized and uncompatibilized PS/PP blends. The impact property is improved by the reduction of particle size and the interface modification.

Compatibilized PS/PP (50/50) blend exhibited significantly increased absorbed impact energy due to high PP of dispersed phase concentration, since PP has mechanically a ductile behavior. Unlike uncompatibilized blends, reduction of loading stress can be attributed to PP particles because the modification of interface between two phases enhances the efficiency of stress transfer from the PS matrix to the PP dispersed phase. However, a larger impact absorption was obtained in PS/PP (90/10) blend than in PS/PP (70/30) and (80/20) blends. A main reason for the improved impact behavior in compatibilized PS/PP (90/10) blend is the reduction of particle size and the very good dispersion of particles. Baker et al. [9] have demonstrated the improvement of impact

properties is not only a result of interfacial adhesion itself but also a result of particle size reduction. The influence of the size of the dispersed phase on the mechanical properties of polystyrene blends has been studied by van der Sanden [28]. He stated that the interparticle distance between the dispersed phase particles plays a significant role in determining whether a blend of PS with another polymer will have a brittle fracture or ductile fracture. If the value of interpartile distance is larger than the critical interparticle distance, brittle fracture of the ligament will occur. If brittle fracture cannot occur, complete deformation of the ligament will take place, eventually leading to fully ductile macroscopic fracture behaviour. The influence of particle size and interparticle distance in compatibilized blends will be more discussed in more detail in next section.

To see the effect of SEBS content on mechanical compatibilization, various concentrations (6.7 wt.%, 12.5 wt.%, and 17.6 wt.%) were used on the PS/PP blend with the fixed weight ratio 80/20. As seen previously in Fig. 5-7, the fracture surface was reticulated, and in consequence a new phase formed when SEBS was in excess of the interfacial saturation concentration. Fig. 5-12 is verifies the assumed compatibilization effect on the impact property of PS/PP blend. A linear improvement in impact property was expected with increasing compatibilizer content and the measured absorbed impact energy was expected to approach a certain value at a critical concentration. However, there was not a great difference between the absorbed impact energy of blends containing 6.7 wt.% and 12.5 wt.% of SEBS; In different way, it still increased even after exceeding 12.5 wt.% of SEBS. Although the values of the impact absorption are not greatly different between 6.7 wt.% and 12.5 wt.% of SEBS , the load-time (or the load-deflection) showed a slightly different trend. There was an increase of total deflection

and a reduction of deflection at maximum load for PS/PP (80/20) blend containing 12.5 wt.% SEBS compared to the blend with 6.7 wt.% SEBS. This indicates that the PS/PP blend changes to have more ductile behaviors at higher concentration. It is found that total deflection increase is in accordance with increasing SEBS content meaning the blend becomes tougher through addition of compatibilizer. On the other hand, large deviation values were found in the blend with 12.5 wt.% SEBS. This results from micelles formed in the matrix PS decreasing mechanical properties of the blend. At 17.6 wt.% of SEBS, the deflection at maximum load is slightly higher than at 12.5 wt.% since the styrene content in copolymer increases the overall styrene content in the blend and results in the blend rigidity.

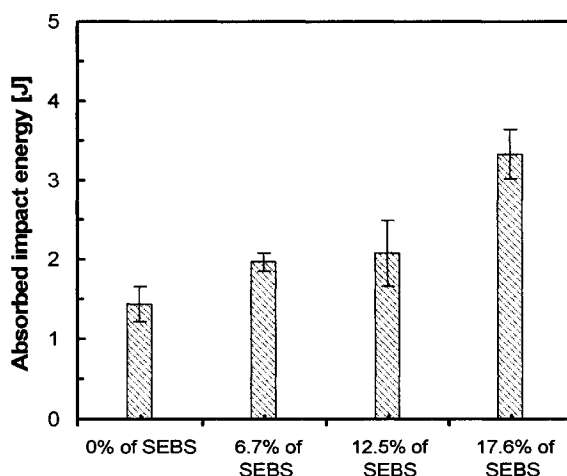


**Fig. 5-12.** Comparison of the absorbed impact energy as a function of SEBS content. The impact property is improved by the increase of interfacial adhesion and the dispersion of excessive compatibilizer in the bulk polymer.

### 5.4.3. Analysis of Particle Size and Interfacial Adhesion

#### 5.4.3.1 Interfacial Adhesion

To investigate the influence of compatibilizer for the interfacial adhesion in PS/PP blend, two PS surfaces with thickness of about 124 nm and 226 nm, respectively, were

modified by spin-coating a layer of SEBS using a dilute solution (0.2 wt.% in  $\text{CH}_2\text{Cl}_2$ ). The work of adhesion calculated by the pull-off force measurement using AFM was then compared to that of PS/PP system. In compatibilized blends, only a critical amount of SEBS is located at the interface between PS and PP phases; we assume that copolymer with thickness approximately the radius of gyration,  $R_g$  ( $\approx 16\text{nm}$ ) [29] will be located at the interface.

In the pull-off force measurements, it was found that the pull-off forces were 392.6 nN and 369.4 nN for a PP particle on the SEBS/PS double layer film. A dependency was found in about 20 nN between when using a PS film with 124nm thickness and the other film with 226nm thickness. These values are significantly higher than values determined from the PS/PP system. Although other factors affecting for the increase of the pull-off force still remain, this test suggests the copolymer, SEBS improves the interfacial adhesion in the PS/PP system.

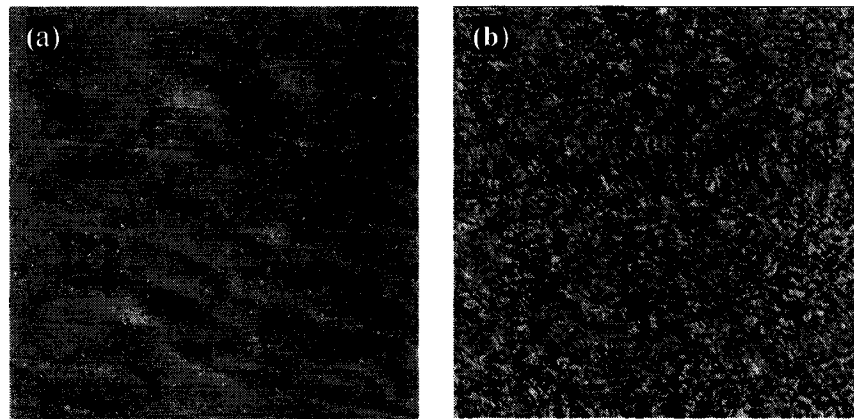


**Fig. 5-13.** (a) Height image of 124 nm thickness PS film (b) Height image of PS film covered by a SEBS layer (scan size:  $10\ \mu\text{m}\times 10\ \mu\text{m}$ , and data scale: (a) 10 nm and (b) 50 nm)

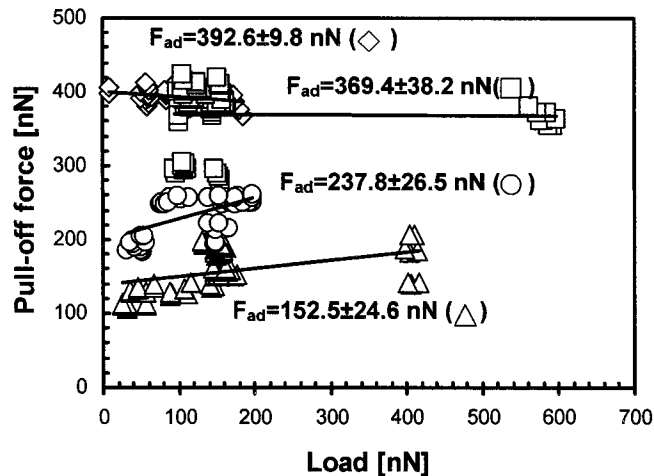
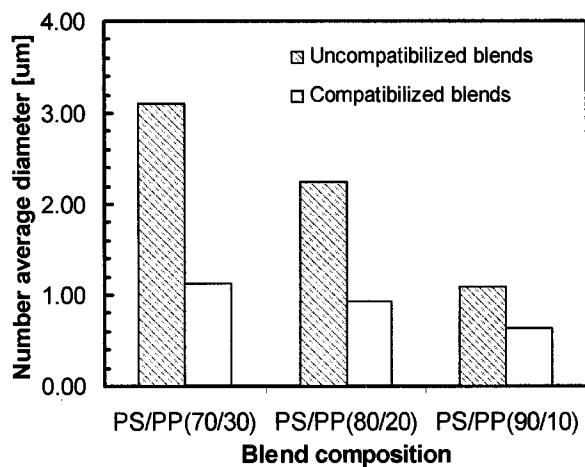


**Fig. 5-14.** Pull-off force vs. applied loading force between a PP particle and the PS surface. ( $\diamond$ : 124 nm thickness PS film with a SEBS layer;  $\square$ : 226 nm thickness PS film with a SEBS layer;  $\circ$ : 226 nm thickness PS film;  $\triangle$ : 124 nm thickness PS film)

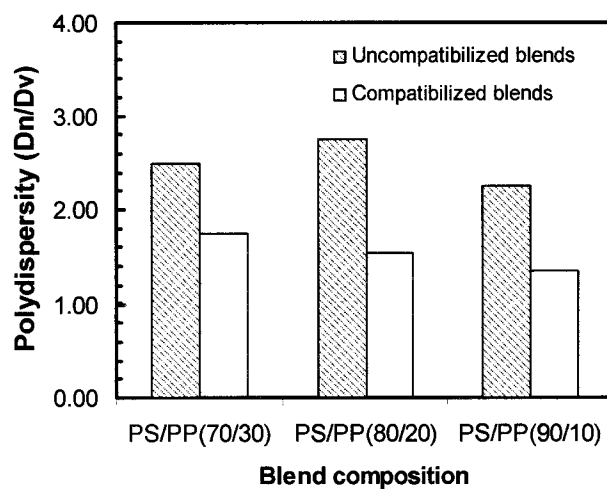
#### 5.4.3.2 Effect of Particle Size on Impact Property in PS/PP Blends

As discussed in the section (5.4.2), PP particle size and the dispersion of particles in the PS matrix are influenced by addition of SEBS. Fig. 5-15 compares the number average diameter ( $D_n$ ) and polydispersity ( $D_w/D_n$ ) of PP particle with different blend compositions. PP particle size decreased by addition of 6.7 wt.% of SEBS in all blends. The decrease particle size is due to increasing of interfacial adhesion and reduction of interfacial tension [10,16,30,31,32,33,34]. It is also due to the coalescence suppression of the blend in the presence of copolymer [18]. In previous section, we found impact absorption in PS/PP (90/10) blend is larger than in PS/PP (70/30) and (80/20) blends. The number average diameter ( $D_n$ ) is 0.63  $\mu\text{m}$ , and the interparticle distance is 0.49  $\mu\text{m}$  in PS/PP (90/10) blend, which is calculated from Wu's percolation model [1]. This interparticle distance value is very close to 0.46  $\mu\text{m}$  in (80/20) PS/PP blend, and less than 0.21  $\mu\text{m}$  in (70/30) PS/PP blend; hence, particle size more importantly affects on impact

property in our investigating PS/PP blends. Compared to the other blends, impact absorption is 1.4 times higher in PS/PP (90/10) blend. Thus, this suggests that impact improvement is efficiently achieved at about 0.6  $\mu\text{m}$  of particle size in the compatibilized PS/PP blends.



(a)



(b)

**Fig. 5-15.** (a) Number average diameter and (b) Polydispersity of PP particle with different blend compositions. The block copolymer (SEBS) used has a molecular weight of 75,000 g/mol.

An estimation of the interfacial area occupied per modifier molecule at the critical concentration is done by following Matos et al. [17]. From previous work, Horák et al. [26] calculated that approximately 2.5 wt.% of SBS copolymer was localized in the interface layer by small angle X- ray scattering (SAXS). On the other hand, Santana and Müller [27] reported the morphology and the size of the dispersed PP particles in the PS/PP blend when PS was a matrix did not change with the addition of 2 wt.% copolymer. This resulted in no improvement of the tensile and impact properties. The estimation of the interfacial area occupied per molecule can be obtained directly from the emulsification curve data (critical concentration).

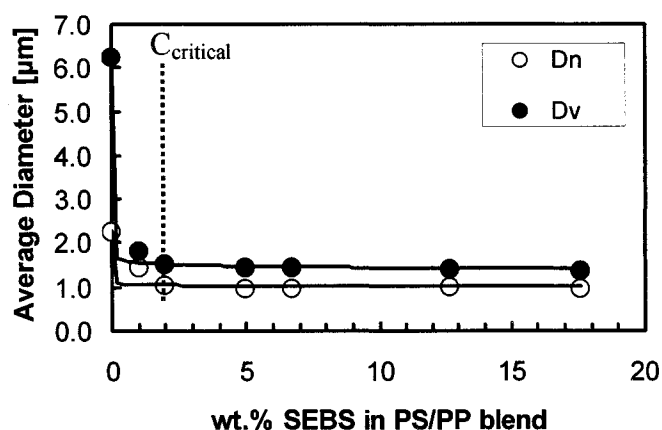


**Fig. 5-16.** Dependence of the dispersed PP particle size for PS/PP (80/20) blend as a function of the wt.% of SEBS

Fig. 5-16 shows the emulsification curve for PS/PP (80/20) blend after addition of triblock copolymer SEBS. The number and volume average diameters of PP decrease with increasing SEBS content sharply when the weight percentage of SEBS is less than 2 % of the blend. Particle size reaches an equilibrium size ( $D_n = 0.95 \mu\text{m}$  and  $D_v = 1.4 \mu\text{m}$ ) when the copolymer content is more than 2 wt.%. Thus, it is inferred that there are a

saturation of copolymer at the interface and formation of micelles in the homopolymer phases at higher copolymer concentration [35].

If we take 2 wt.% as the critical concentration in the emulsification curve, the number of molecules required to saturate the interface is  $8.67 \text{ nm}^2$  per molecule (more detail calculation is presented in Appendix II). This indicates that the saturation concentration for SEBS with  $M_n = 68,000 \text{ g/mol}$  at the interface is  $0.12 \text{ molecule/nm}^2$ . Matos et al. showed the higher the molecular weight of copolymer, the higher the area values [17]. In their work, a value of  $13 \text{ nm}^2$  was obtained for an ethylene-propylene rubber dispersed in a polystyrene matrix compatibilized by a SEBS copolymer. After exceeding the critical concentration of the compatibilizer, the excessive copolymer dispersed in the bulk polymers contributes further to the toughness of materials. Impact absorption improvement in PS/PP blend with 17.6 wt.% SEBS can be considered to be due to the dispersion of the excessive compatibilizer in the blend.

## 5.5 Conclusions

The influence of interfacial adhesion on impact property of polymer blends was studied in this chapter. Before the impact test, the morphology of PS/PP blend was analyzed by the different weight ratios, the addition of compatibilizer, and the content of compatibilizer. The SEM micrographs of uncompatibilized PS/PP blend showed a two-phase morphology with sharp interface, which provides evidence for poor adhesion between the matrix phase (PS) and the dispersed phase particles (PP). This shows PS and PP are immiscible. Compatibilization of PS/PP blend was performed by addition of SEBS triblock copolymer to enhance the interfacial adhesion. The copolymer addition leads to a better distribution and a reduction in the size of the dispersed PP particles in the



blend. A new irregular phase, which tends to envelop small PP particles, formed. The presence of copolymer improves interfacial adhesion and diminishes the coalescence of PP particles. As compatibilizer content increased, excessive copolymer has a tendency to form a mesophase (a reticulate morphology) in the blend in addition to locating at the interface. In some cases, direct evidence of the fibril of SEBS copolymer connecting PS matrix to PP particles was found by means of high magnification SEM micrographs; however, they cannot clearly distinguish the SEBS phase in the blend.

To see the effect of modification on interfacial adhesion and the reduction of dispersed particle size on the impact properties of the blend, the unnotched impact strength of uncompatibilized and compatibilized PS/PP blend was compared using a drop weight impact tester, Dynatup-8250. It was found that using SEBS as a compatibilizer obviously improved the impact properties in all PS/PP blends. The increase of impact absorption changed with the blend composition, and the increase was about 30 % up to 90 %. Increase of total deflection and reduction of deflection at maximum load was observed in compatibilized PS/PP blend. This indicates that the PS/PP blend changes to have more ductile behavior through addition of compatibilizer, meaning that stress applied to the blend can be more easily transferred to the dispersed phase due to improvement in interfacial adhesion. A larger impact absorption was obtained in compatibilized PS/PP (90/10) blend than in PS/PP (70/30) and (80/20) blends. The main reasons for the improved impact behavior in compatibilized PS/PP (90/10) blend are the reduction of particle size and very good dispersion of particles. Various concentrations (6.7 wt.%, 12.5 wt.%, and 17.6 wt.%) were used in the PS/PP blend with fixed weight ratio 80/20 to see the effect of SEBS content. With increasing SEBS concentration, total

deflection was increased and deflection at maximum load was decreased. This result is attributed to the excessive copolymer dispersed in the bulk polymers further toughening the materials and also modifying the interface.

A relative measurement using AFM pull-off force measurement for PP particle on a SEBS/PS double layer film was carried out to prove whether SEBS as a compatibilizer improve interfacial adhesion between PS and PP phases. In the pull-off force measurements, it was found that the pull-off forces were 392.6 nN and 369.4 nN for a PP particle on the SEBS/PS double layer film, which are significantly higher than values determined from the PS/PP system. This suggests the copolymer improves the interfacial adhesion in the PS/PP system.

The improvement of interfacial adhesion is also related to the reduction of dispersed phase particles. PP particle size in all PS/PP blends with addition of SEBS was determined by the number average diameter ( $D_n$ ) and the volume average diameter ( $D_v$ ). PP particle size decreased by addition of 6.7 wt.% of SEBS in all blends. Maximum impact improvement was achieved at about 0.6  $\mu\text{m}$  of particle size and 0.4  $\mu\text{m}$  of interparticle distance in our PS/PP blends. An estimation of the interfacial area occupied per modifier molecule at the critical concentration was done by following previous work. When we take 2 wt.% as the critical concentration in the emulsification curve, the number of molecules required to saturate the interface is 8.67  $\text{nm}^2$  per molecule, meaning that the saturation concentration for SEBS with  $M_n = 68,000$  g/mol at the interface is 0.12 molecule/ $\text{nm}^2$ .

## **REFERENCE**

- [1] S. Wu, *Polymer*, **26**, pp 1855 (1985)
- [2] R. J. Young, and P.A. Lovell, *Introduction to Polymers (2<sup>nd</sup>)*, Stanley Thorne Ltd.: Cheltenham, Chap. 5 (1991)
- [3] P. Behan, A. Thomas, and A. Bevis, *J. of Mater Science*, **11**, pp 1207-1214 (1976)
- [4] D. R. Paul, and S. Newman, *Polymer Blends*, Academic Press: New York (1978)
- [5] C. B. Bucknall, *Comprehensive Polymer Science*, **7**, Pergamon Press:New York (1990)
- [6] D. R. Paul, J.W. Barlow, and H. Keskkula, *Encyclopedia of Polymer Science Engineering*, **12**, pp 399-461 (1988)
- [7] S. Y. Hobbs, *Polymer Eng. Sci.*, **26**, pp 74-81 (1986)
- [8] C. Wortcecki, and R. Wirth, *Proc. 3<sup>rd</sup>. Eur. Symp. Polymer Blends*, Paper E 2/1 (1990)
- [9] J. D. Moore, *Polymer*, **12**, pp 478-486 (1971)
- [10] N. C. Liu and W. E. Baker, *Polymer Eng. Sci.*, **32**, pp 1695-1702 (1992)
- [11] L. E. Nielsen, *Mechanical Properties of Polymers*, Reinhold: New York (1962)
- [12] A. K. Gupta, and S. N. Purwar, *J. Appl. Polym. Sci.*, **30**, pp 1777-1798 (1985)
- [13] R. T. Morison, and R. N. Boyd, *Organic Chemistry*, Allyn and Bacon Inc:New York (1977)
- [14] Retrieved December 04, 2004 from the website:  
[www.instron.com/wa/applications/test\\_types/impact/test\\_types.aspx](http://www.instron.com/wa/applications/test_types/impact/test_types.aspx)
- [15] E. Escudie, and A. Graciaa, and J. Lachaise, *Mater. Chem. Phys.*, **24**, pp 239-246 (1986)

- [16] B. D. Favis and J. P. Chalifoux, *Poly. Eng. Sci.*, **27**, pp 1591-1600 (1987)
- [17] M. Matos and B. D. Favis, *Polymer*, **36**, pp 3899-3907 (1995)
- [18] U. Sundararaj and C. W. Macosko, *Macromolecules*, **28**, pp 2647-2657 (1995)
- [19] L. A. Utracki, *Polymer Alloys and Blends*, Carl Hanser: New York (1989)
- [20] J. Noolandi, *Macromol Chem. Theory Simul.*, **1**, pp 295-298 (1992)
- [21] J. Karger Kocsis, *Polypropylene: Structure Blends and Composites vol. 2*, Chapman and Hall: London (1995)
- [22] Bor Z. Jang, *Advanced Polymer Composites: Principles and Applications*: ASM International: Materials Park, pp169-171 (1994)
- [23] R Sciamanna, C. Albano, and G Arribas, Technical Conference ANTEC vol. 2, pp 3916–3919 (1999)
- [24] D. Hlarata et al., *J. Poly. Sci. Part B: Poly Physics*, **39**, pp 931-942 (2001)
- [25] R. Sciamanna, G. Gribas, C. Albano, and E. Horie, and B. Soto, *Mat. Res. Innovat.* **4**, pp 311-321 (2001)
- [26] Z. Horák, V. Fort, D. Hlavatá, and F. Lednický, *Polymer*, **37**, pp 65-73 (1996)
- [27] O. O Santana and A. J. Müller, *Polym. Bull.*, **32**, pp 471-477 (1994)
- [28] M. C. M. van der Sanden, H. E. H. Meijer, and P. J. Lemstra, *Polymer*, **34**, pp 2148-2156 (1993)
- [29] J. R. Quintana, R. A. Scadazar, I. Katime, *Macromol. Chem. Phys.*, **196**, pp 1625-1634 (1995)
- [30] L. A. Utracki, and J. Can, *J. of Chem. Eng.*, **80**, pp 1008-1016 (2002)
- [31] G. I. Taylor, *Proc. R. Soc. London Ser. A*, **138**, pp 41-48 (1932)
- [32] J. C. Lepers, and B. D. Favis, *AIChE J*, **45**, pp 887-895 (1999)

- [33] H. Liang, B. D. Favis, Y. S. Yu, and A. Eisenberg, *Macromolecules*, **32**, pp 1637-1642 (1999)
- [34] S. Lyu, T. D. Jones, F. S. Bates, and C. W. Macosko, *Macromolecules*, **35**, pp 7845-7855 (2002)
- [35] B. Lin, PhD Thesis, University of Alberta (2005)
- [36] J. R. Quintana, R. A. Salazar, and I. Katime, *Macromol. Chem. Phys.*, **196**, pp 1625-1634 (1995)
- [37] F. Stricker, Y. Thomann, and R. Mülhaupt, *J. of Appl. Polym. Sci.*, **68**, pp 1891-1901 (1998)
- [38] D. W. Van Krevelen, *Properties of Polymers 2<sup>nd</sup> ed.*, Elsevier: Amsterdam (1976)

# CHAPTER 6

## Conclusions and Future Work

### 6.1 General Conclusions

Two different adhesion measurements were studied in this thesis to measure the adhesion in polymer-polymer systems. One is a widely used mechanical test, the DCB test, for the adhesion measurement which determines the strength of an adhesive joint. The other method is using a newly developed technique which is referred to “pull-off force measurement” using atomic force microscopy. Most previous research has been performed using conventional mechanical tests. These conventional techniques are usually applicable only to macroscopic bodies, and they can not properly determine intrinsic adhesion because those values are obtained from the strain energy released by failure of the interface.

In chapter 3, PS/PP system was used to study the adhesion of amorphous-semicrystalline polymers using the double cantilever beam (DCB) test. Adhesion of another polymer system, PS/PMMA, was also measured using DCB test. Most times, the interfacial fracture energy of PS/PP system was zero due to a large difference in thermal expansion coefficient. In PS/PMMA system, fracture energy was found to be about 12-13 J/m<sup>2</sup>. We also found fracture energy does not depend significantly on temperature when the polymers bonded are above their glass transition temperatures. In the temperature range of 110°C to 130°C, the Flory-Huggins interaction parameter,  $\chi$ , is almost constant so that the critical fracture energy is independent in the temperature range investigated. The fracture energy was found to proportionally increase with the square root of the

annealing time at lower time after polymer beams were bonded. Up to 30 minutes annealing time, the fracture energy significantly increases, but it reached at a maximum 30 minutes. The fracture energy for the interface modified by the diblock copolymer (PS-*b*-PMMA) was found to be over 4 times higher than those for the unmodified interface. Hence, block copolymer can be used to reinforce the interface between incompatible polymers. Despite the simplicity of the DCB test, we were not able to find the fracture energy in PS/PP system; in fact, the DCB test cannot be applied to all materials to measure interfacial strength. This is shortening of in using the DCB test.

Another method to measure adhesion was pull-off force measurement using AFM, which is more relevant for interfacial adhesion in polymer blends in chapter 4. In most previous works, polymer adhesion was determined using sharp tips with polymer surfaces. However, we used colloidal probes (polymer particles) since polymer particle-polymer surface system is geometrically closer to adhesion between polymer matrix and polymer drops in polymer blends. Two systems of polymer particle-surface have been investigated to determine the adhesion force using the pull-off force measurement. We found pull-off forces in a range of 70-280 nN for the PP/PS system and 60-180 nN for the PS/PMMA system. The pull-off force value for the PS/PMMA system is similar to 112.8 nN measured by Feldman et al [1]. However, a difference of almost one order of magnitude for the values of the measurement pull-off force was found when compared with the calculated values by JKR model. This discrepancy is attributed to surface roughness (relative to the curvature of the tip), tip shape uniformity, and other factors. For this reason, the effect of roughness of the sample surfaces on the adhesion force has been incorporated using the Rabinovich model. The Rabinovich prediction provides

values closer to experiment than those calculated by the JKR model. Nevertheless, we still found a discrepancy between the theoretical and measured values. A reason for this is that the local deformation of the particle or the surfaces of polymer is ignored. In addition, the Hamaker constants obtained from bulk materials were used for calculating the Rabinovich model. In previous work by Feldman et al. [1], the Hamaker constant measured by the refractive index value for thin polymer films is lower than that of bulk materials from the literature. Thus, a precise Hamaker constant is also required to determine adhesion forces in Rabinovich model.

On the other hand, we noted that the measured pull-off force increases with increasing polymer film thickness in this thesis. In most previous studies, the effect of film thickness on the adhesion force was ignored for polymer particle-polymer surface geometry. However, a variation of thickness of polymer film obtained using different weight concentration solutions was around 200 nm. For deformable polymer particles, a variation in thickness of polymer film might affect the deformation of polymer particle during contact with polymer surface since film is not as stiff as the silicon substrate. When we used a PP particle, the measured pull-off force increased with increasing the film thickness. On the other hand, the measured pull-off force did not have a significant dependence of film thickness when a rigid PS particle was used.

The effect of interfacial adhesion on impact property of polymer blends was studied in chapter 5. The SEM micrographs of PS/PP blend showed a two-phase morphology with sharp interface, which provides evidence for poor adhesion between the matrix phase (PS) and the dispersed phase particles (PP). Due to a weak interfacial adhesion, mechanical properties of PS/PP blend are generally poor. To improve the mechanical



properties, SEBS acting as a compatibilizer was employed in different blend composition PS/PP blends. Unnotched impact test obviously showed the improvement of the impact property in all PS/PP blends. This results in the increase of interfacial adhesion between polymer components in the blends and the reduction of dispersed particle size due to a compatibilizer.

A relative measurement using AFM pull-off force measurement for PP particle on a SEBS/PS double layer film was carried out to prove whether SEBS as a compatibilizer improve interfacial adhesion between PS and PP phases. The measured pull-off force values were significantly higher than values determined from the PS/PP system. We modified two PS surfaces with thickness of about 124 nm and 226 nm using a dilute SEBS solution (0.2 wt.% in  $\text{CH}_2\text{Cl}_2$ ), and found that the pull-off forces were 392.6 nN and 369.4 nN. These values are significantly higher than 132.5 nN and 237.8 nN obtained in chapter 4. Thus, we found SEBS enhances interfacial adhesion between PS and PP phases.

The improvement of interfacial adhesion is also related to the reduction of dispersed phase particles. PP particle size decreased by addition of 6.7 wt.% of SEBS in all blends. Impact improvement was efficiently achieved at about 0.63  $\mu\text{m}$  particle size and 0.49  $\mu\text{m}$  interparticle distance in our PS/PP blends. An estimation of the interfacial area occupied per modifier molecule at the critical concentration was done using the emulsification curve. When we take 2 wt.% as the critical concentration in the emulsification curve, the area occupied per a compatibilizer molecule at the interface is 2.02  $\text{nm}^2$  per molecule with  $M_n = 68,000$  g/mol.

## **6.2 Future Work**

### **6.2.1 Investigation of Effect of Molecular Weight on Polymer Adhesion**

As discussed in chapter 3, the fracture energy depends on the degree of entanglement across the interface between polymers. In general, a narrow region of overlap forms when two polymers are bonded together. In this transition region (an interphase typically has a thickness of 1-5nm), long polymer chains of each type become entangled. In a number of previous studies, the effect of molecular weight on the fracture energy resulting from the degree of entanglement was studied. Dai et al. [2] have showed how polymer fracture behavior depends on the number-average molecular weight  $M_n$ . They observed a transition from chain pullout to chain scission mechanism at a critical molecular weight in PS/PMMA system. An investigation using the AFM pull-off force measurement with various molecular weights of PS/PMMA pairs will give an understanding about the dependence of molecular weight on the critical fracture energy and the determination of the critical entanglement molecular weight for the case of a polymer particle adhering to polymer films. It will also find which fracture mechanism will operate between glassy polymer pairs according to the molecular weight.

### **6.2.2 Measurement of Nanomechanical Properties of Polymer Surfaces Using AFM**

In the pull-off force measurement for polymer-polymer systems, we used spin-cast polymer films in this thesis. Frank et al. [3] revealed that the physical and mechanical properties of thin films can differ substantially from those of corresponding bulk materials. Thus, it is required to measure material properties, i.e. shear modulus and Poisson ratio, for thin polymer films. Contact mode AFM can be used for measuring the nanomechanical properties of polymer films. Lemoine et al. [4] measured nanohardness

and nanowear characterization of polymeric materials from surface indentation with a very stiffness tip ( $k=7.66$  N/m) using AFM in contact mode. AFM probing thin polymer films with very stiff tip such as a diamond indenter can be applied to measure the properties of spin-cast thin polymer films, and this will allow us to calculate accurate values calculated in elastic contact theories.

### **6.2.3 The Effect of Different Compatibilizers on Interfacial Adhesion**

In this thesis, we have studied the improvement of interfacial adhesion in PS/PP blend using SEBS as a compatibilizer with different contents. Other factors besides the content of SEBS are important that allow the styrene-butadiene-styrene triblock copolymer to as a better compatibilizer to modify PS/PP interface. Horák et al. [5] showed the compatibilization of PS/PP (80/20) blend with different structure types of SBS copolymer, di-, tri-, and pentablock. Sciamanna et al. [6] studied the effect of different types of SBS copolymer with different molecular weights and styrene content on the compatibilization of PS/PP (80/20) blend. We will study the effect of different types of compatibilizer on the improvement of interfacial adhesion in PS/PP blend to gain insight about how to achieve better properties of PS/PP blend.

### **6.2.4 Experimental Improvement**

#### **6.2.4.1 The Automated DCB Test**

A major problem with the DCB test was lack of standardization from the manual test, which leads to scattered data. To reduce the uncertainty involved during the manual test, the automated DCB test was be performed using the automated test apparatus such as an Instron Universal Testing Machine [7] . The razor blade should be inserted at the lowest speed possible to minimize any deformation of polymer beams during the DCB

test. It is critical that a razor blade is driven downward into the interface at a constant speed as slowly as possible. The test result is very sensitive to the measurement of the crack lengths, which can be influenced by a loading speed of the razor blade insertion into the interface. Thus, minimization of uncertainty in the test is extremely important. Such an automated test apparatus will consist of following units, (i) the razor blade holder; (ii) the sample holder; (iii) a video recording unit. In addition, a visual analysis for the crack at the interface using a VCR to record the crack propagation will be useful to find time-dependence of crack propagation.

#### **6.2.4.2 Improvement in Polymer Particles Preparation**

In some polymers, spherically shaped particles (powder) are always not commercially available. Due to the immiscibility of most polymer blend, a minor phase forms dispersed spherical particles in a matrix phase with a sharp interface at low minor phase concentrations, (< 20%). Using a polymer particle from polymer blend instead of particles obtained from industry should be more acceptable and suitable to measure the interfacial adhesion between phases consisted of the blend. As mentioned in sample preparation in chapter 4, we attempted to obtain PP particles from the immiscible PS/PP blend because the sharp interface between the two phases in the blend would enable themselves to be easily separated. A sample of the blend was then diluted in CH<sub>2</sub>Cl<sub>2</sub> (methyl chloride) solvent in order to dissolve the PS phase to isolate PP particles. The droplets of the solution were evaporated on the glass substrate in the oven but it was still difficult to pick PP particles up due to remaining PS and solvent on surface. To isolate PP particles from PS matrix, a syringe driven filter unit (Pore size: 0.22 $\mu$ m; Millipore) was also used. However, PP particles were most likely to be embedded in pores of the filter.

This caused that it was difficult to find particles using an optical microscope (the zeiss microscope) for attaching themselves on the AFM cantilever tip. Thus, a better procedure is required for the isolation of dispersed phase particles from the matrix phase.

#### **6.2.4.3 Improvement for Accuracy in Film Thickness Measurement**

In the experiment performed in Chapter 4, we have studied the effect of thickness of polymer film on the pull-off force. First, thickness was determined by scratching the films and performing AFM imaging of the scratch. Although the scratch was performed with circumspection in order to not damage the silicon wafer substrates, there might be an indentation of the substrate due to a manual scratching. To eliminate a possibility of indentation on the surface of silicon wafer, silicon nitride probes with triangular cantilevers was employed. A cantilever with spring constant of 0.58 N/m of the probe was used for scratching PS and PMMA films. To form scratches on the polymer films, the tip was repeatedly scanned back and forth over the same line with high loading forces. However, the scratches on PS and PMMA films were not clearly found due to the lack of stiffness of the tip. Therefore, to better determine the thickness of polymer film using scratch method, a stiffer tip is suggested to make a scratch while at the same time is ensuring this damage to the substrate. This can be a better method to determine more precise thickness of polymer film, and we can find a better correlation between the pull-off force and the film thickness.

#### **6.2.4.4 Improvement in Specimen Preparation for Impact Test**

To prepare specimens of polymer blends for impact testing, the pelletized blends were moulded with an aluminum mold using Carver Model C laboratory press under a high loading pressure to make a uniform thickness of specimens. However, a small

variation of specimen thickness occurred due to the overflow of excessive molten polymer pellets outward the mold. A small increase in specimen thickness is found as outward from the center of the samples. This might lead to a scattered data of the absorbed impact energy since impact absorption depends on specimen thickness. To avoid a variation in specimen thickness, we may want to measure the appropriate amount of polymers to put in the mold or modify the mold by making paths for flow excessive polymer out the mold.

## **REFERENCE**

- [1] K K. Feldman, T. Tervoort, P. Smith, and N.D. Spencer, *Langmuir*, **14**, pp 372-378 (1998)
- [2] C. A. Dai, E. J. Kramer, J. Washiyama, and C. Y. Hui, *Macromolecules*, **29**, pp 7536-7543 (1996)
- [3] C. W. Frank et al., *Science*, **273**, pp 912-915 (1996)
- [4] P. Lemoine and J. Mc Laughlin, *Thin Solid Films*, **339**, pp 258-264 (1999)
- [5] Z. Horák, V. Fort, D. Hlavatá, and F. Lednický, *Polymer*, **37**, No.1, pp 65-73 (1996)
- [6] R. Sciamanna, G. Gribas, C. Albano, E. Horie, and B. Soto, *Mat. Res. Innovat.*, **4**, pp 311-321 (2001)
- [7] M. Lahoti. Msc. Thesis, University of Alberta (1997)

## APPENDIX I

### Comparing Two Means of Measured Adhesion Forces

In Chapter 4, we determined if the difference in measured adhesion force values measured between polymer particle and each different thickness polymer film are statistically significant. To compare two measured pull-off forces, student t-test was performed with 95% confidence using statistical software, MINITAB (Minitab Inc.) [1,2]

(I) For the system for PS particle on PMMA surface

#### Two-Sample T-Test and CI: 0.2% PMMA, 0.5% PMMA

Two-sample T for 0.2% PMMA vs 0.5% PMMA

	N	Mean	StDev	SE Mean
0.2% PMMA	89	91.9	12.8	1.4
0.5% PMMA	87	96.3	13.8	1.5

Difference = mu (0.2% PMMA) - mu (0.5% PMMA)  
Estimate for difference: -4.42666  
95% CI for difference: (-8.38691, -0.46642)  
T-Test of difference = 0 (vs not =): T-Value = -2.21 P-Value = 0.029  
DF = 174  
Both use Pooled StDev = 13.3089

#### Two-Sample T-Test and CI: 0.5% PMMA, 0.8% PMMA

Two-sample T for 0.5% PMMA vs 0.8% PMMA

	N	Mean	StDev	SE Mean
0.5% PMMA	87	96.3	13.8	1.5
0.8% PMMA	79	104.8	10.8	1.2

Difference = mu (0.5% PMMA) - mu (0.8% PMMA)  
Estimate for difference: -8.45687  
95% CI for difference: (-12.28088, -4.63285)  
T-Test of difference = 0 (vs not =): T-Value = -4.37 P-Value = 0.000  
DF = 164  
Both use Pooled StDev = 12.4616

### Two-Sample T-Test and CI: 0.8% PMMA, 1% PMMA

Two-sample T for 0.8% PMMA vs 1% PMMA

	N	Mean	StDev	SE Mean
0.8% PMMA	79	104.8	10.8	1.2
1% PMMA	86	112.6	13.6	1.5

Difference = mu (0.8% PMMA) - mu (1% PMMA)  
Estimate for difference: -7.84054  
95% CI for difference: (-11.63412, -4.04695)  
T-Test of difference = 0 (vs not =): T-Value = -4.08 P-Value = 0.000  
DF = 163  
Both use Pooled StDev = 12.3278

### Two-Sample T-Test and CI: 1% PMMA, 2% PMMA

Two-sample T for 0.8% PMMA vs 1% PMMA

Sample	N	Mean	StDev	SE Mean
1% PMMA	86	112.6	14.5	1.6
2% PMMA	84	116.4	10.7	1.2

Difference = mu (1) - mu (2)  
Estimate for difference: -3.80000  
97.5% CI for difference: (-8.22872, 0.62872)  
T-Test of difference = 0 (vs not =): T-Value = -1.94 P-Value = 0.054  
DF = 168  
Both use Pooled StDev = 12.7648

### (II) For the system for PP particle on PS surface

#### Two-Sample T-Test and CI: 0.2% PS, 0.5% PS

Two-sample T for 0.2% PS vs 0.5% PS

Sample	N	Mean	StDev	SE Mean
0.2% PS	84	105.1	17.3	1.9
0.5% PS	106	110.2	14.2	1.4

Difference = mu (1) - mu (2)  
Estimate for difference: -5.09000  
95% CI for difference: (-9.60817, -0.57183)  
T-Test of difference = 0 (vs not =): T-Value = -2.22 P-Value = 0.027  
DF = 188  
Both use Pooled StDev = 15.6793



### Two-Sample T-Test and CI: 0.5% PS, 0.8% PS

Two-sample T for 0.5% PS vs 0.8% PS

	N	Mean	StDev	SE Mean
0.5% PS	106	110.2	14.3	1.4
0.8% PS	93	145.61	9.33	0.97

Difference = mu (0.5% PS) - mu (0.8% PS)  
Estimate for difference: -35.4115  
95% CI for difference: (-38.8384, -31.9845)  
T-Test of difference = 0 (vs not =): T-Value = -20.38 P-Value = 0.000  
DF = 197  
Both use Pooled StDev = 12.2305

### Two-Sample T-Test and CI: 0.8% PS, 1% PS

Two-sample T for 0.8% PS vs 1% PS

	N	Mean	StDev	SE Mean
0.8% PS	93	145.61	9.33	0.97
1% PS	86	154.7	29.3	3.2

Difference = mu (0.8% PS) - mu (1% PS)  
Estimate for difference: -9.12923  
95% CI for difference: (-15.45263, -2.80584)  
T-Test of difference = 0 (vs not =): T-Value = -2.85 P-Value = 0.005  
DF = 177  
Both use Pooled StDev = 21.4184

### Two-Sample T-Test and CI: 1% PS, 2% PS

Two-sample T for 1% PS vs 2% PS

	N	Mean	StDev	SE Mean
1% PS	86	154.7	29.3	3.2
2% PS	118	237.8	26.1	2.4

Difference = mu (1% PS) - mu (2% PS)  
Estimate for difference: -83.0941  
95% CI for difference: (-90.7827, -75.4055)  
T-Test of difference = 0 (vs not =): T-Value = -21.31 P-Value = 0.000  
DF = 202  
Both use Pooled StDev = 27.5020

Here, if the  $p$ -value is less than  $\alpha$  ( $=0.05$ ), we reject our null hypothesis (difference of means between two data results is zero). The  $p$ -value has such a small value, which means there is strong evidence that the mean difference in the pull-off forces is not zero. However, it was found that there is no data difference between the measured pull-off force values for PS Particle on 114nm thickness (1 wt.%) PMMA film and those for PS particle on 230 nm thickness (2 wt.%) PMMA film.

## **REFERENCE**

- [1] B. F. Ryan, B. L. Joiner, and T. A. Ryan Jr., *Minitab Handbook 2<sup>nd</sup> ed.*, PWS Publishers: Boston (1986)
- [2] D. S. Moore, *The Basic Practice of Statistics*, W. H. Freeman and Company: NewYork (1995)

## APPENDIX II

### Saturation Concentration

An estimation of the critical concentration of copolymer at interface is obtained from the data of the emulsification curve [1]. This critical concentration appears to scale with the interfacial area. The total area occupied by the dispersed phase particles is:

$$A = n \times 4\pi R^2 \quad (\text{III .1})$$

where  $R$  is the radius of the dispersed phase particle, and  $n$  is the number of particles of the minor phase, which can be obtained from following equation:

$$n = \frac{V_d}{\frac{4}{3}\pi R^3} \quad (\text{III .2})$$

where  $V_d$  is the volume of the dispersed phase. The number of molecules of interfacial modifier can be estimated as followed:

$$N = mN_{.AVO} / M_n \quad (\text{III .3})$$

where  $m$  is the mass of interfacial modifier,  $N_{.AVO}$  is the Avogado number.

For PS/PP (80/20 wt.%) blend, we obtained the diameter of dispersed phase particles, 0.94  $\mu\text{m}$  at critical concentration of interfacial modifier, 2 wt.%, from emulsification curve. At 200°C, the density of PS and PP is 1.02  $\text{g}/\text{cm}^3$  and 0.82  $\text{g}/\text{cm}^3$ , respectively, calculated according Van Krevelen [2]. The density of SEBS is estimated

by using the arithmetic average of PS and PEB, 0.92 g/cm<sup>3</sup>. As a result, the interfacial concentration occupied by SEBS with M<sub>n</sub> = 68,000 g/mol is:

$$\frac{A}{N} = \frac{3\phi_d V_d M_n}{mRN_{AVO}} = 8.67 \text{ nm}^2/\text{molecule} \quad (\text{III .4})$$

## **REFERENCE**

- [1] M. Matos and B. D. Favis, *Polymer*, **36**, PP 3899-3907 (1995)
- [2] D. W. Van Krevelen, *Properties of Polymers 2<sup>nd</sup> ed.*, Elsevier: Amsterdam (1976)